UNIVERSITY OF CALIFORNIA,

IRVINE

# Development of 3D conductive wearable sensors

DISSERTATION

submitted in partial satisfaction of the requirements

for the degree of

DOCTOR OF PHILOSOPHY

in Electrical Engineering and Computer Science

by

Somayeh Zanganeh

Dissertation Committee:

Associate Professor Hung Cao, Chair

Professor Fadi Kurdahi

Assistant Professor Hamidreza Aghasi

2024

# DEDICATION

To

my sister, Zeinab, and my beloved parents

in recognition of their worth

# TABLE OF CONTENTS

## LIST OF FIGURES

## LIST OF TABLES

## ACKNOWLEDGEMENTS

I would like to express the deepest appreciation to my advisor, Professor Peter Tseng, who has the attitude and the substance of a genius: he continually and convincingly conveyed a spirit of adventure in regard to research and scholarship, and an excitement in regard to teaching. Without his guidance and persistent help this dissertation would not have been possible.

I would like to thank my committee chair, Professor Hung Cao and committee members, Professor F. Kurdahi and Professor H. Aghasi, whose work demonstrated to me that concern for global affairs supported by an engagement in comparative literature and modern technology should always transcend academia and provide a quest for our times.

Last but not least, I would like to thank my lab mates and everyone who helped me with the projects I conducted during my PhD program.

# VITA

**Somayeh Zanganeh**

2015 B.Sc. in Electrical Engineering and Computer Science, University of Tehran

2017 M.Sc. in BioElectronics, University of Tehran

2018 Research Scholar, UCLA

2024 Ph.D. in Electrical and Computer Science,

University of California, Irvine

PUBLICATIONS

. L. Li, A. Escobar, **S. Zanganeh,** M. Dautta, M. Sajeeb, F. Ye, J. Escobar, P. Tseng, " Mechanically-directed assembly of nanostructured biopolymer with tunable anisotropy, hierarchy, and functionality", ***Next Materials*****, 2024.**

· A. Escobar*****, **S. Zanganeh***, J. Sullivan, L. Li, M. Dautta, J. Lee, P. Tseng, "Fluidic Infiltrative Assembly of Three-Dimensional Hydrogel with Heterogeneous Composition and Function", ***Advanced Functional Materials***, **2021.**

· H. Ko, K. Suthiwanich, H. Mary, **S. Zanganeh**, S. Hu, S. Ahadian, A. Khademhosseini, "A Simple Layer-Stacking Technique to Generate Biomolecular and Mechanical Gradients in Photocrosslinkable Hydrogels," ***Biofabrication***, ***2019***

· **S. Zanganeh** *, M. Abdolahad*, S. A. Hosseini *, M. Dahmardeh, M. Gharooni, H. Abiri, A. Alikhani, S. Mohajerzadeh, O. Mashinchian, "Nanoelectromechanical Chip (NELMEC) Combination of Nanoelectronics and Microfluidics to Diagnose Epithelial and Mesenchymal Circulating Tumor Cells from Leukocytes," ***Small, 2016,*** *DOI: 10.1002/smll.201502808*. (Front Cover Picture of *Small*)

· **S. Zanganeh**, S. Khosravi, N. Namdar, M. Hasanpour, M. Gharooni, M. Abdolahad, "Electrochemical approach for monitoring the effect of anti-tubulin drugs on breast cancer cells based on silicon nanograss electrodes," **Analytical Chemical Acta, 2016***, http://dx.doi.org/10.1016/j.aca.2016.07.042*.

· **S. Zanganeh***, F. Khodadadi*, S. Rafizadeh, M. Abdolahad, "Folic acid functionalized vertically aligned carbon nanotube (FA-VACNT) electrodes for cancer sensing applications; suitable for monitoring in time evolution," **Journal of Materials Science and Technology, 2016,** http://dx.doi.org/10.1016/j.jmst.2016.05.001.

· **S. Zanganeh** *, S. A. Hosseini *, E. Akbarnejad, F. Salehi, M. Abdolahad, "Microfluidic device for label-free quantitation and distinction of bladder cancer cells from the blood cells using micro machined silicon based electrical approach; suitable in urinalysis assays," ***Journal of Pharmaceutical and Biomedical Analysis*****, 134 (2017) 36-42,** https://doi.org/10.1016/j.jpba.2016.11.026.

· S. Rafizadeh-Tafti, M. H. Haqiqatkhah, M. Saviz, M. Janmaleki, R. Faraji Dana, **S. Zanganeh**, M. Abdolahad, "An electrical bio-chip to transfer and detect electromagnetic stimulation on the cells based on vertically aligned carbon nanotubes," **Materials Science and Engineering C, 2017,** https://doi.org/10.1016/j.msec.2016.09.050**.**

· S. Soleimani-Amiri, **S. Zanganeh**, R. Ramzani, R. Talei, S. Mohajerzadeh, S. Azimi, Z. Sanaee, "3D micro- and nano-machining of hydrogenated amorphous silicon films on $SiO_2$/Si and glass substrates," **Journal of Micromechanics and Microengineering, 2015,** doi:10.1088/0960-1317/25/7/074004.

*** indicates equal contributions**

## Conference papers:

· S. A. Hosseini, **S. Zanganeh**, M. Khodaverdian, M. Abdolahad, S. Mohajerzadeh, "Label free detection of epithelial and mesenchymal CTCs by combination of size filtration and impedance measurement in a microfluidic approach," **Oral presentation at Biosensors 2016 Post Congress Symposium, Gothenburg, Sweden, May 2016**.

· S. A. Hosseini, M. Abdolahad, **S. Zanganeh**, S. Mohajerzadeh, "Label free discrimination of CTCs from whole blood by electrically characterization and size filtration of blood cells," **Oral presentation at Sixth International Conference on Nanostructures, Kish, Iran, 2016**.

· S. A. Hosseini, **S. Zanganeh**, M. Abdolahad, S. Mohajerzadeh, "Micro and Nano-machining Suitable for Micro-fluidic Silicon-based Electronic Device Fabrication", **Oral presentation at First national congress on Microfluidics and its application in medicine and engineering, Tehran, Iran, 5-6 March 2016.**

· S. Soleimani-Amiri, **S. Zanganeh**, S. Azimi, Z. Sanaee, S. Mohajerzadeh, H. Taghinejad, "Three dimensional high-order nano-rod formation using a hydrogen-assisted deep reactive ion etching," **TechConnect World 2014 - Nanotech, Microtech, Biotech, Cleantech Joint 2014 Conferences**, **Maryland, U.S.A, June 2014**.

## Patents:

· P. Tseng, A. Escobar, **S. Zanganeh**, "Fluidic infiltrative assembly of 3D hydrogel (nanoporous) materials with heterogeneous composition and function".

. M. Abdolahad, S. A. Hosseini, **S. Zanganeh**, "Nanoelectromechanical Chip (NELMEC)", ***United States Patent,*** **Pub. Date: May 11, 2017.**

## ABSTRACT OF THE DISSERTATION

Development of 3D conductive wearable sensors

by

Somayeh Zanganeh

Doctor of Philosophy in Electrical Engineering and Computer Science

University of California, Irvine, 2024

Professor Hung Cao, Chair

Hydrogels hold immense potential in soft electronics due to their resemblance to biological tissues. However, for applications in fields like tissue engineering and wearable electronics, hydrogels must possess electrical conductivity, stretchability, and implantability. This dissertation explores recent advancements in the development of electrically conductive hydrogel composites with high conductivity and remarkable stretchability. By incorporating conductive particles into hydrogels, such as poly(3,4-ethylenedioxythiophene):poly(styrenesulfonate) (PEDOT:PSS) researchers have enhanced their conductivity. This study presents a synthesis method for creating electrically conductive hydrogel composites by combining PEDOT:PSS with alginate. The hydrogel reveals changes in chemical composition upon treatment with dimethyl sulfoxide (DMSO). Additionally, surface morphology analysis via Field Emission Scanning Electron Microscopy (FESEM) and Atomic Force Microscopy (AFM) demonstrated the impact of DMSO treatment

on PEDOT:PSS Alginate films. Furthermore, electrical conductivity measurements highlighted the effectiveness of the conductive hydrogels in Electromyography (EMG) and human motion detection. This study offers insights into the fabrication and characterization of stretchable, conductive hydrogels, advancing their potential for various biomedical applications.

# Chapter 1: INTRODUCTION

## Importance of Electrical Conductivity, Stretchability, and Implantability in Hydrogels

Hydrogels, as versatile biomaterials, have garnered significant attention in various fields, including biomedicine and soft electronics. Their unique combination of properties, such as high water content, biocompatibility, and tunable mechanical characteristics, makes them promising candidates for a myriad of applications. Among these properties, electrical conductivity, stretchability, and implantability stand out as crucial attributes that significantly impact the functionality and effectiveness of hydrogels in diverse applications. In this section, we delve into the importance of these three key properties and their implications in hydrogel-based systems, supported by relevant literature.

1. Electrical Conductivity

Electrical conductivity stands as a pivotal property in the realm of hydrogel applications, significantly impacting their utility across various domains such as bioelectronics, biosensing, and neural interfaces. Unlike traditional hydrogels, which are typically insulating in nature, conductive hydrogels offer a unique advantage by facilitating the transmission of electrical signals through their three-dimensional network of polymer chains.

This property opens up a plethora of opportunities for innovative applications where seamless interaction with biological systems is paramount.

Conductive hydrogels play a central role in the development of wearable sensors, smart textiles, and flexible electronics designed to monitor physiological signals and biomarkers in real-time. By integrating conductive additives such as PEDOT:PSS into hydrogel matrices, researchers have succeeded in creating soft, biocompatible materials capable of detecting and transmitting electrical signals with high fidelity. These wearable devices enable continuous monitoring of vital signs, such as heart rate, muscle activity, and brain signals, offering invaluable insights into human health and performance.

Moreover, conductive hydrogels find extensive use in biosensing applications, where their ability to transduce biochemical signals into electrical signals allows for sensitive and selective detection of analytes in biological samples. Functionalized hydrogel-based biosensors can selectively bind to target molecules, such as proteins, nucleic acids, or metabolites, triggering a change in electrical conductivity that can be quantitatively measured. This capability has profound implications for medical diagnostics, environmental monitoring, and food safety, enabling rapid and reliable detection of pathogens, toxins, and disease biomarkers. [1]

In neural interfaces and bioelectronic implants, electrical conductivity is critical for establishing seamless communication between artificial devices and the nervous system. Conductive hydrogels serve as electrodes, neural probes, and scaffolds for tissue engineering,

facilitating the integration of implantable devices with neural tissue while minimizing tissue damage and immune response. By modulating the electrical properties of hydrogels, researchers can tailor their performance to suit specific applications, such as deep brain stimulation, spinal cord stimulation, or neuroprosthetics, thereby restoring lost sensory or motor function in patients with neurological disorders. [2]

2. Stretchability

Stretchability stands as a fundamental property that distinguishes hydrogels from conventional materials, rendering them indispensable for a wide array of applications in fields ranging from soft robotics to biomedical engineering. Hydrogels endowed with stretchability possess the remarkable ability to undergo deformation and elongation while maintaining their structural integrity, making them exceptionally well-suited for applications that require compliance with dynamic and irregular surfaces, such as the human body.

Stretchable hydrogels serve as the backbone for the development of actuators, sensors, and artificial muscles that mimic the flexibility and adaptability of biological tissues. By harnessing the inherent stretchability of hydrogels, researchers can create robotic systems capable of performing complex movements and interactions, such as grasping, crawling, and squeezing through confined spaces. These soft robotic devices find applications in diverse fields, including healthcare, manufacturing, and environmental monitoring, where their ability to navigate complex environments with precision and dexterity is indispensable.

Furthermore, in the domain of wearable electronics, stretchable hydrogels play a pivotal role in the design and fabrication of conformable sensors, smart textiles, and flexible

circuits that seamlessly integrate with the human body. Unlike rigid electronic materials, stretchable hydrogels offer superior comfort, mobility, and biointegration, allowing for continuous monitoring of physiological signals and activities without causing discomfort or restriction of movement. Wearable devices based on stretchable hydrogels enable applications such as health monitoring, fitness tracking, and assistive technologies, empowering users to manage their health and well-being proactively.

In tissue engineering and regenerative medicine, the stretchability of hydrogels is essential for creating scaffolds and matrices that mimic the mechanical properties of native tissues and organs. By engineering hydrogels with tunable mechanical properties, researchers can tailor their stiffness, elasticity, and resilience to match the mechanical environment of target tissues, promoting cell adhesion, proliferation, and differentiation. Stretchable hydrogel scaffolds facilitate tissue regeneration and wound healing by providing a supportive microenvironment that guides cellular behavior and promotes functional tissue formation. [3]

Moreover, stretchable hydrogels find applications in drug delivery systems, where their ability to deform and conform to physiological surfaces enables targeted and controlled release of therapeutic agents. Stretchable hydrogel-based drug delivery devices can adapt to dynamic changes in tissue geometry and mechanical stress, ensuring precise delivery of drugs to the desired site of action while minimizing systemic side effects. This targeted drug delivery approach holds promise for improving the efficacy and safety of therapeutics in various disease conditions, including cancer, inflammation, and chronic pain. [4]

3. Implantability

Implantability stands as a defining attribute of hydrogels, delineating their applicability in a diverse array of biomedical interventions, including tissue engineering, drug delivery, and regenerative medicine. Implantable hydrogels offer a unique advantage by providing a supportive matrix for cell growth and tissue regeneration within the physiological environment, thereby facilitating therapeutic interventions with minimal invasiveness and optimal biocompatibility.

In tissue engineering, implantable hydrogels serve as scaffolds for the regeneration and repair of damaged or diseased tissues, offering a conducive microenvironment for cellular infiltration, proliferation, and differentiation. Engineered hydrogel matrices can mimic the extracellular matrix (ECM) of native tissues, providing structural support and biochemical cues that guide tissue morphogenesis and functional integration. These implantable constructs find applications in a wide range of tissue engineering strategies, including bone regeneration, cartilage repair, and organ transplantation, where they facilitate the development of functional tissue substitutes with the potential to restore physiological function and improve patient outcomes.

Moreover, in drug delivery systems, implantable hydrogels offer a versatile platform for localized and sustained release of therapeutic agents, enabling targeted delivery to specific anatomical sites while minimizing systemic exposure and off-target effects. By encapsulating drugs within implantable hydrogel matrices, researchers can achieve controlled release kinetics, prolonging drug residence time and enhancing therapeutic efficacy. Implantable drug delivery devices based on hydrogels find applications in the treatment of various disease

conditions, including cancer, diabetes, and cardiovascular disorders, where precise control over drug delivery is critical for achieving therapeutic outcomes.

In regenerative medicine, implantable hydrogels play a pivotal role in promoting tissue repair and wound healing by creating a supportive microenvironment that stimulates endogenous repair mechanisms and accelerates tissue regeneration. Hydrogel-based wound dressings and scaffolds facilitate the recruitment and migration of endogenous cells to the site of injury, promoting angiogenesis, epithelialization, and collagen deposition. These implantable constructs provide a barrier against infection, maintain a moist wound environment, and promote granulation tissue formation, thereby facilitating the healing process and minimizing scar formation. [5]

Furthermore, implantable hydrogels find applications in the development of bioelectronic implants and neural interfaces, where they serve as biocompatible substrates for the integration of electronic components with neural tissue. Implantable hydrogel electrodes and neural probes enable seamless interfacing with the nervous system, facilitating the recording and modulation of neural activity for applications such as deep brain stimulation, spinal cord injury, and prosthetic control. These implantable devices offer the potential to restore lost sensory or motor function in patients with neurological disorders, improving their quality of life and functional independence. [6]

## 4. Integration of Electrical Conductivity, Stretchability, and Implantability

The convergence of electrical conductivity, stretchability, and implantability represents a transformative paradigm in the design and development of hydrogels for advanced biomedical applications. By seamlessly integrating these three key properties, researchers are

poised to unlock new frontiers in tissue engineering, bioelectronics, drug delivery, and regenerative medicine, offering unprecedented opportunities for addressing complex biomedical challenges and improving patient outcomes.

1. Synergistic Enhancement of Properties

The integration of electrical conductivity, stretchability, and implantability in hydrogels results in a synergistic enhancement of their overall performance and functionality. Conductive hydrogels with embedded nanomaterials exhibit high electrical conductivity, enabling the transmission of electrical signals for applications such as neural interfaces, biosensors, and bioelectronic implants. Simultaneously, the stretchability of these hydrogels allows them to conform to dynamic and irregular surfaces, facilitating seamless integration with biological tissues and organs. Furthermore, their implantability ensures compatibility with the physiological environment, promoting tissue regeneration, and minimizing inflammatory response upon implantation.

2. Applications in Biomedical Engineering

The integration of electrical conductivity, stretchability, and implantability in hydrogels opens up a plethora of opportunities for innovative applications in biomedical engineering. For instance, conductive hydrogels with tunable mechanical properties can serve as electrodes and neural interfaces for interfacing with the nervous system, enabling precise control of neural activity for applications such as brain-computer interfaces and neuroprosthetics. Additionally, implantable hydrogel scaffolds with controlled release capabilities can deliver therapeutic agents to specific anatomical sites, promoting tissue regeneration and wound

healing while minimizing systemic side effects. Moreover, stretchable hydrogel-based sensors and actuators find applications in wearable robotics, soft exoskeletons, and assistive devices, where their flexibility and adaptability enable natural and intuitive interactions with the human body.

## 3. Challenges and Future Directions

Despite the promising potential of integrating electrical conductivity, stretchability, and implantability in hydrogels, several challenges remain to be addressed. One major challenge is achieving a balance between these properties while maintaining biocompatibility and long-term stability. Additionally, optimizing the fabrication processes and scaling up production to meet clinical demands are critical considerations for translating these technologies from the lab to the clinic. Furthermore, elucidating the biophysical and biochemical interactions between hydrogels and biological systems is essential for understanding their in vivo behavior and optimizing their performance for specific applications. [7]

The integration of electrical conductivity, stretchability, and implantability represents a groundbreaking approach in the design and development of hydrogels for advanced biomedical applications. By harnessing the synergistic interactions between these properties, researchers are pioneering new therapeutic strategies and interventions that hold promise for revolutionizing healthcare and improving patient outcomes. Continued advancements in materials science, bioengineering, and translational research are expected to accelerate the translation of these technologies from bench to bedside, shaping the future of biomedicine and healthcare. [8]

**Overview of Hydrogels in Soft Electronics and Biomedical Applications**

Hydrogels, three-dimensional networks of hydrophilic polymer chains capable of absorbing and retaining large amounts of water, have emerged as versatile materials with extensive applications in soft electronics and biomedical engineering. Their unique properties, such as high water content, biocompatibility, and tunable mechanical properties, make them highly attractive for a wide range of applications, particularly in fields where interaction with biological systems is required. [9] [10] This section provides an overview of the role of hydrogels in soft electronics and biomedical applications, highlighting their significance, key properties, and recent advancements. [11]

1. Biomedical Applications of Hydrogels

Hydrogels have revolutionized various aspects of biomedical engineering, owing to their ability to mimic the physiological environment and interact seamlessly with biological systems. Some of the notable biomedical applications of hydrogels include:

a. Tissue Engineering:

Hydrogels serve as scaffolds for tissue regeneration and repair due to their biocompatibility and ability to support cell growth. They provide a conducive microenvironment for cells to proliferate and differentiate, making them invaluable in tissue engineering strategies aimed at developing replacement tissues and organs. [12] [13]

b. Drug Delivery Systems:

Hydrogels have been extensively explored as drug delivery vehicles owing to their capacity to encapsulate and release therapeutic agents in a controlled manner. [14] [15] By modifying the chemical composition and structure of hydrogels, researchers can tailor drug release kinetics, improving efficacy and minimizing side effects. [16] [17]

c. Wound Healing:

Hydrogels are employed in wound dressings and bandages for promoting wound healing and tissue regeneration. [18] They create a moist environment conducive to cell migration and proliferation, while also protecting the wound from external contaminants. [19]

d. Biosensing and Diagnostics:

Hydrogels are utilized in biosensors and diagnostic devices for detecting biomolecules and analytes in biological fluids. [20] Functionalized hydrogels can selectively bind to target molecules, enabling sensitive and specific detection, with applications ranging from glucose monitoring to pathogen detection. [21]

2. Soft Electronics Applications of Hydrogels

In recent years, hydrogels have gained significant traction in the field of soft electronics, where flexibility, stretchability, and bio integration are paramount. [22] [23] By incorporating conductive additives into hydrogel matrices, researchers have developed novel materials with electrical conductivity, enabling applications such as:

a. Wearable Electronics:

Hydrogel-based wearable sensors and electronics offer comfort and conformability to the human body, facilitating continuous monitoring of physiological parameters such as heart rate, temperature, and motion. [24] These devices are particularly well-suited for healthcare monitoring, sports performance analysis, and personalized medicine. [25]

b. Human-Machine Interfaces:

Hydrogel-based electrodes and interfaces play a crucial role in interfacing with biological systems for applications such as brain-computer interfaces (BCIs) and prosthetic control. [26] Their soft and conformable nature reduces discomfort and tissue damage, enhancing the user experience and functionality of these devices. [27]

c. Soft Robotics:

Hydrogel actuators and sensors are integral components of soft robotic systems designed to mimic the flexibility and dexterity of biological organisms. [28] These robots find applications in medical devices, rehabilitation robotics, and human-robot interaction scenarios where safety and adaptability are paramount. [29]

3. Recent Advancements and Future Directions

Recent advancements in hydrogel research have focused on enhancing their mechanical, electrical, and biochemical properties to broaden their scope of applications in soft electronics and biomedical engineering. Strategies such as nanocomposite reinforcement, molecular functionalization, and additive manufacturing techniques have been employed to tailor hydrogel properties for specific applications. [30] [31] Additionally, efforts are

underway to develop bioactive hydrogels capable of responding to external stimuli or interacting dynamically with biological systems for therapeutic and diagnostic purposes. [32] [33]

Hydrogels represent a versatile class of materials with immense potential in soft electronics and biomedical applications. Their unique combination of properties makes them ideal candidates for a wide range of applications, from tissue engineering and drug delivery to wearable electronics and soft robotics. [34] Continued research and innovation in hydrogel science are expected to unlock new possibilities and pave the way for transformative advancements in healthcare, biotechnology, and beyond. [35]

## Chapter 2: Research gap and objectives of the dissertation

### Research gap and significance of improving conductivity in hydrogels

The development of hydrogel composites with enhanced electrical conductivity represents a critical area of research with significant implications for various biomedical and soft electronic applications. [36] While hydrogels offer unique advantages such as biocompatibility and tunable mechanical properties, their inherently insulating nature limits their utility in applications that require electrical conductivity. [37] Addressing this research gap by improving the conductivity of hydrogel composites holds immense significance for advancing fields such as tissue engineering, biosensing, and wearable electronics. [38] [39] This section explores the research gap and the importance of enhancing conductivity in hydrogel composites, highlighting its potential impact on various biomedical processes. [40]

1. Research gap

Hydrogels, owing to their biocompatibility and versatility, have found widespread applications in various biomedical fields, ranging from tissue engineering to drug delivery. However, a critical limitation hindering their broader utility is their inherently low electrical conductivity. [41] Traditional hydrogels composed of hydrophilic polymers lack the ability to efficiently conduct electrical signals, which restricts their applicability in bioelectronics, biosensing, and neural interfacing. [42] This research gap poses a significant challenge to the development of hydrogel-based systems that require electrical conductivity for functionality. In this section, we delve into the underlying factors contributing to the limited electrical conductivity of hydrogels and explore strategies to address this research gap.

The limited electrical conductivity of hydrogels arises from several intrinsic factors:

a. Insulating Nature of Hydrophilic Polymers:

Hydrogels predominantly consist of hydrophilic polymers such as polyacrylamide, polyethylene glycol, and alginate, which are inherently insulating materials. The lack of conjugated π-electron systems within these polymers inhibits the efficient flow of electrons, resulting in poor electrical conductivity. [43]

b. Sparse Interchain Contacts:

In traditional hydrogels, polymer chains are sparsely crosslinked, resulting in limited interchain contacts and reduced pathways for electron transport. This sparse network

structure hinders the formation of continuous pathways for electron conduction, further compromising electrical conductivity. [44]

c. Presence of Water:

The high water content of hydrogels, while imparting biocompatibility and swelling properties, also acts as a barrier to electron transport. Water molecules create hydration layers around polymer chains, increasing the distance between them and impeding electron mobility.

d. Absence of Conductive Fillers:

Unlike conductive polymers or carbon-based materials, traditional hydrogels lack conductive fillers or additives that can enhance electrical conductivity. Incorporating conductive additives into hydrogel matrices presents challenges related to maintaining biocompatibility, mechanical properties, and long-term stability. [45]

2. Strategies to Address the Research Gap

Several strategies have been proposed to address the research gap and improve the electrical conductivity of hydrogels:

a. Incorporation of Conductive Nanomaterials:

Nanomaterials such as carbon nanotubes, graphene, and conductive polymers have shown promise as additives for enhancing the electrical conductivity of hydrogels. These nanomaterials can form conductive networks within the hydrogel matrix, facilitating electron transport and improving overall conductivity. [46] [47]

b. Surface Modification Techniques:

Surface modification techniques, such as chemical functionalization or plasma treatment, can be employed to introduce conductive functional groups onto the surface of hydrogel particles. These functional groups promote interparticle interactions and enhance electrical conductivity without compromising biocompatibility. [48]

c. Hybrid Composite Approaches:

Hybrid composite approaches involve combining hydrogels with other conductive materials, such as metals or metal oxides, to create composite materials with enhanced electrical conductivity. [49] By optimizing the composition and morphology of these hybrid composites, researchers can tailor their electrical properties to suit specific applications.

d. Conductive Hydrogel Synthesis Methods:

Novel synthesis methods, such as in situ polymerization or electrochemical deposition, enable the direct fabrication of conductive hydrogels with predefined structures and properties. [50] These methods offer precise control over the composition, morphology, and conductivity of hydrogel composites, opening up new avenues for enhancing their electrical performance.

The limited electrical conductivity of hydrogels poses a significant research gap that hinders their broader utility in biomedical applications. [51] Addressing this gap requires interdisciplinary efforts to develop novel materials, fabrication techniques, and characterization methods. By enhancing the electrical conductivity of hydrogels, researchers can unlock new opportunities for developing advanced bioelectronics, biosensors, neural interfaces, and drug delivery systems with improved performance and functionality. [52] [53] Continued research and innovation in this area are essential for realizing the full potential of hydrogels in biomedical engineering and soft electronics.

## 3. Future Directions and Challenges

Despite the significant progress in enhancing the conductivity of hydrogel composites, several challenges remain to be addressed. Achieving high conductivity levels while maintaining biocompatibility, mechanical properties, and long-term stability remains a formidable task. Furthermore, optimizing the fabrication processes and scaling up production to meet the demands of clinical translation represent significant challenges. Future research efforts should focus on developing novel materials, fabrication techniques, and characterization methods to overcome these challenges and unlock the full potential of conductive hydrogel composites in biomedical and soft electronic applications.

Improving the conductivity of hydrogel composites represents a critical research area with profound implications for biomedical engineering and soft electronics. Addressing the

research gap by enhancing conductivity levels holds immense significance for advancing fields such as neural interfaces, biosensing, tissue engineering, and wearable electronics. By developing highly conductive hydrogel composites with tailored properties, researchers can unlock new opportunities for diagnosing, treating, and monitoring various health conditions, ultimately improving patient outcomes and quality of life. Continued research efforts and interdisciplinary collaboration are essential for overcoming existing challenges and realizing the full potential of conductive hydrogel composites in biomedical and soft electronic applications.

**Objectives of the dissertation**

This dissertation aims to address the research gap surrounding the limited electrical conductivity of hydrogels by focusing on the development of innovative strategies to enhance their electrical performance. Through comprehensive experimental investigations and theoretical analyses, the following objectives have been outlined:

1. Synthesis and Characterization of Conductive Hydrogels

The primary objective of the dissertation is to develop novel methods for synthesizing conductive hydrogel composites with enhanced electrical conductivity, stretchability, and biocompatibility. This involves the incorporation of conductive nanomaterials, such as carbon nanotubes, graphene, or conductive polymers, into hydrogel matrices using various fabrication techniques. The synthesized hydrogel composites will be systematically characterized to evaluate their electrical, mechanical, and morphological properties, providing insights into the structure-property relationships governing their performance.

2. Optimization of Conductive Hydrogel Formulations:

Another objective is to optimize the formulation parameters, such as the type and concentration of conductive additives, crosslinking density, and solvent composition, to achieve the desired balance between electrical conductivity, stretchability, and biocompatibility. By systematically varying these parameters and analyzing their effects on the properties of conductive hydrogel composites, the dissertation aims to identify optimal formulations that meet the requirements of specific biomedical applications, such as tissue engineering, biosensing, and drug delivery.

3. Evaluation of Biomedical Applications:

The dissertation seeks to explore the biomedical applications of conductive hydrogel composites, with a focus on tissue engineering, biosensing, and neural interfacing. This involves conducting in vitro and in vivo studies to assess the biocompatibility, cell response, and tissue integration of conductive hydrogel scaffolds. Furthermore, the dissertation aims to demonstrate the feasibility of using conductive hydrogel composites for real-time monitoring of physiological signals, drug release kinetics, and neural activity, showcasing their potential for transformative advancements in healthcare.

4. Development of One-Pot Synthesis Methods:

Additionally, the dissertation aims to develop one-pot synthesis methods for creating conductive hydrogel composites, simplifying the fabrication process and improving scalability. By integrating multiple synthesis steps into a single reaction vessel, the dissertation seeks to

streamline the production of conductive hydrogel composites while minimizing the use of toxic solvents and reducing production costs. The developed one-pot synthesis methods will be evaluated for their effectiveness, reproducibility, and scalability, offering practical solutions for translating laboratory research into industrial applications.

5. Contribution to Advancements in Biomedical Engineering:

Ultimately, the dissertation aims to contribute to advancements in biomedical engineering by addressing the research gap surrounding the limited electrical conductivity of hydrogels. By developing innovative strategies to enhance the electrical performance of hydrogel composites, the dissertation seeks to pave the way for the development of next-generation biomaterials with improved functionality and effectiveness in diverse biomedical applications. Through collaborative efforts with researchers, clinicians, and industry partners, the dissertation aims to accelerate the translation of research findings into practical solutions that have a positive impact on healthcare and patient outcomes.

The objectives of this dissertation encompass synthesizing and characterizing conductive hydrogel composites, optimizing their formulation parameters, evaluating their biomedical applications, developing one-pot synthesis methods, and contributing to advancements in biomedical engineering. By addressing these objectives, the dissertation seeks to bridge the research gap and facilitate the development of innovative hydrogel-based solutions for a range of biomedical challenges.

# Chapter 3: Developing 3D multifunctional hydrogel material/systems

## Hydrogel Formation and Characteristics

Hydrogels, a class of polymeric materials with high water content, have emerged as a cornerstone in the realm of biomaterials owing to their unique properties and diverse applications in various fields, particularly in medicine. These three-dimensional networks of hydrophilic polymers possess remarkable biocompatibility, tunable mechanical properties, and the ability to absorb and retain large amounts of water while maintaining their structural integrity. The versatility of hydrogels arises from their ability to mimic the extracellular matrix, providing an ideal environment for cell growth and tissue regeneration.

In medical devices, hydrogels have sparked considerable interest due to their potential to revolutionize diagnostics, drug delivery, and tissue engineering. One notable application lies in the development of smart hydrogel-based sensors capable of detecting various biomarkers in real-time, offering a non-invasive approach for disease diagnosis and monitoring. Additionally, hydrogel-based drug delivery systems exhibit precise control over drug release kinetics, ensuring optimal therapeutic efficacy while minimizing side effects. Furthermore, hydrogel scaffolds have shown promise in tissue engineering, providing a supportive matrix for cell proliferation and differentiation, thus facilitating the regeneration of damaged tissues and organs. Overall, the unique properties of hydrogels position them as a cornerstone in the design and development of next-generation medical devices, offering tailored solutions to address a myriad of healthcare challenges.

Mechanisms and Crosslinking Strategies:

Hydrogels, three-dimensional networks of hydrophilic polymers, have garnered significant attention across various scientific disciplines, particularly in biomedical and pharmaceutical fields, owing to their unique properties and diverse applications. The formation of hydrogels typically involves the crosslinking of polymer chains to create a network structure capable of retaining large amounts of water while maintaining structural integrity. Understanding the mechanisms of hydrogel formation and the various strategies employed for crosslinking is crucial for tailoring hydrogel properties to specific applications.

Hydrogel formation can occur through several mechanisms, including physical, chemical, and biological processes.

1. Physical Crosslinking: Physical hydrogels form through non-covalent interactions, such as hydrogen bonding, hydrophobic interactions, and electrostatic interactions, between polymer chains. These interactions are reversible, allowing for dynamic and stimuli-responsive properties. Physical hydrogels are often formed by sol-gel transition, where the polymer solution undergoes a phase transition from a sol state (liquid) to a gel state (solid) upon exposure to external stimuli such as temperature, pH, or ionic strength.

2. Chemical Crosslinking: Chemical hydrogels are formed through covalent bonds between polymer chains, resulting in a stable network structure. Common chemical crosslinking methods include free radical polymerization, Michael addition, Schiff base formation, and click chemistry. Chemical crosslinking offers precise control over hydrogel

properties such as mechanical strength, swelling behavior, and degradation rate. However, excessive crosslinking can hinder biodegradability and biocompatibility.

3. Biological Crosslinking: Biological hydrogels are formed through enzymatic or biological reactions, where specific enzymes or biomolecules catalyze the crosslinking of polymer chains. Examples include enzymatic crosslinking using transglutaminase or tyrosinase enzymes and biomolecule-mediated crosslinking via peptide self-assembly or protein-protein interactions. Biological hydrogels offer excellent biocompatibility and bioactivity, making them suitable for tissue engineering and regenerative medicine applications.

Types of Crosslinking:

Crosslinking plays a pivotal role in determining the properties and performance of hydrogels. Various crosslinking strategies can be employed based on the desired characteristics and applications of the hydrogel.

1. Physical Crosslinking:

- Hydrogen Bonding: Hydrogen bonding between polymer chains, typically involving hydrophilic groups such as hydroxyl (-OH) or amine (-NH2) groups, leads to the formation of physical hydrogels. Examples include polyvinyl alcohol (PVA) and polyethylene glycol (PEG) hydrogels.

- Ionic Interactions: Electrostatic interactions between charged polymer chains or ions in solution result in ionic hydrogels. For instance, alginate hydrogels form crosslinks with divalent cations (e.g., calcium ions) through ionic interactions.

- Hydrophobic Interactions: Hydrophobic interactions between hydrophobic segments of polymer chains contribute to physical crosslinking in hydrogels. Amphiphilic polymers, such as Pluronics or block copolymers, form hydrogels through hydrophobic interactions.

2. Chemical Crosslinking:

- Free Radical Polymerization: Initiators such as azobisisobutyronitrile (AIBN) or photoinitiators initiate polymerization reactions, leading to the formation of covalent bonds between polymer chains. Crosslinking agents such as N,N'-methylenebisacrylamide (MBAA) or ethylene glycol dimethacrylate (EGDMA) are commonly used to facilitate crosslinking.

- Michael Addition: Functional groups such as thiols (-SH) react with Michael acceptors (e.g., maleimide groups) to form covalent bonds via nucleophilic addition reactions.

- Click Chemistry: Highly selective and efficient reactions such as copper-catalyzed azide-alkyne cycloaddition (CuAAC) or strain-promoted azide-alkyne cycloaddition (SPAAC) enable the formation of hydrogels with well-defined structures and properties.

3. Biological Crosslinking:

- Enzymatic Crosslinking: Enzymes such as transglutaminase, tyrosinase, or horseradish peroxidase catalyze the formation of covalent bonds between specific amino acid

residues or functional groups within polymer chains, resulting in biocompatible and enzymatically degradable hydrogels.

- Biomolecule-Mediated Crosslinking: Peptide sequences or biomolecules capable of self-assembly or specific molecular recognition events can be incorporated into hydrogel formulations to induce crosslinking via non-covalent interactions, offering precise control over hydrogel structure and function.

Characteristics of Hydrogels

1. Swelling Behavior:

One of the defining characteristics of hydrogels is their ability to absorb and retain large amounts of water while maintaining their structural integrity. This swelling behavior is governed by the polymer composition, crosslinking density, and environmental conditions such as pH, temperature, and ionic strength. Hydrogels swell in response to the presence of water molecules, leading to an increase in volume and a corresponding decrease in polymer chain density. The extent of swelling is influenced by the degree of crosslinking and the affinity of the polymer chains for water molecules, with highly crosslinked hydrogels typically exhibiting lower swelling ratios.

2. Mechanical Properties:

The mechanical properties of hydrogels play a crucial role in determining their suitability for specific applications, ranging from soft and compliant to stiff and robust materials. These properties are influenced by factors such as polymer chain flexibility,

crosslinking density, and network architecture. While hydrogels generally exhibit lower mechanical strength compared to conventional engineering materials, their mechanical properties can be tailored through the selection of appropriate polymers and crosslinking strategies. For instance, physically crosslinked hydrogels tend to be more elastic and compliant, whereas chemically crosslinked hydrogels offer higher stiffness and strength.

3. Biodegradability:

Biodegradability is an important characteristic of hydrogels for many biomedical applications, particularly in tissue engineering and drug delivery, where the transient presence of the scaffold or carrier is desired. Biodegradable hydrogels undergo degradation either through enzymatic or hydrolytic cleavage of polymer chains, resulting in the gradual breakdown of the material into biocompatible byproducts that can be metabolized or excreted from the body. The degradation rate of hydrogels can be tailored by adjusting parameters such as polymer composition, crosslinking density, and degradation mechanism, allowing for precise control over the release kinetics of encapsulated drugs or the remodeling of tissue scaffolds.

**Optimizing hydrogel parameters for mold degradation protocol**

Materials

Materials used in this study are listed as below:

Acrylamide (AAm), n-isopropylacrylamide (NIPAAm), methylene bisacrylamide (MBAAm), ammonium persulfate (APS), N,N,N',N'-tetramethylethylenediamine (TEMED), calcium

carbonate (CaCO3), D-(+)-gluconic acid δ-lactone (GDL), fluorescein o-acrylate (FOA), trisodium citrate dihydrate, gold (III) chloride trihydrate (HAuCl4), sodium chloride (NaCl), dimethyl sulfoxide (DMSO), and iron (III) chloride hexahydrate (FeCl3) were purchased from Millipore Sigma. Isopropanol (IPA) and acetone (ACE) were purchased from Fisher Scientific. Sodium alginate (Na-ALG, viscosity 80 – 120 cp) was purchased from FUJIFILM Wako Pure Chemical Corporation, 1,1,1,3,3,3- hexafluoro-2-propanol (HFIP) from Matrix Scientific, rhodamine methacrylate (RHO) from Polysciences, Inc., and 3DM-ABS resin from 3DM Inc. All chemicals were purchased and used without further purification. All aqueous solutions were prepared using deionized water (DI) unless otherwise stated.

## Methods

### Preparation of Hydrogel Stock Solutions

Stock solutions of the hydrogel monomers were made in DI and stored at 4 °C until needed. PAAm precursor: 20% (w/w) AAm (10.16 g), 6% (w/w) MBAAm relative to AAm (0.6 g), 40 mL DI. PNIPAAm precursor: 20% (w/v) NIPAAm (8 g), 0.7% (w/v) MBAAm (0.28 g), 40 mL DI. ALG precursor: X% (w/v) Na-ALG, 40 mL DI. X refers to a value between 0.5 and 1.5 as these percentages were used. PAAm-ALG precursor: 15% (w/w) AAm (4.514 g), 1.875 % (w/w) Na-ALG (0.564 g), 0.35% (w/w) MBAAm relative to AAm (0.0158 g), 25 mL DI. Solutions containing Na-ALG were sonicated until the powders were completely dissolved.

### Hydrogel Synthesis

PAAm Hydrogels: 10% (w/w) PAAm hydrogel: PAAm stock (500 µL), DI (470 µL), and TEMED (5 µL) were added to a microcentrifuge tube and mixed. 10% APS (25 µL) was added and quickly mixed into the solution via tube inversion. 10% (w/w) PAAm-co-FOA hydrogel: PAAm stock (500 µL), DI (465 µL), TEMED (5 µL), and FOA solution (5 µL, 100 mg/mL in DMSO) were added to a microcentrifuge tube and mixed. 10% APS (25 µL) was added and quickly mixed into the solution via tube inversion. 10% (w/w) PAAmco-RHO hydrogel: PAAm stock (500 µL), DI (445 µL), TEMED (5 µL), DMSO (5 µL), and RHO solution (20 µL, 100 mg/mL in DI) were added to a microcentrifuge tube and mixed. 10% APS (25 µL) was added and quickly mixed into the solution via tube inversion. For a 10% (w/v) PNIPAAm hydrogel: PNIPAAm stock (500 µL), DI (455 µL), and TEMED (5 µL) were added to a microcentrifuge tube and mixed. 10% APS (40 µL) was added and quickly mixed into the solution via tube inversion.

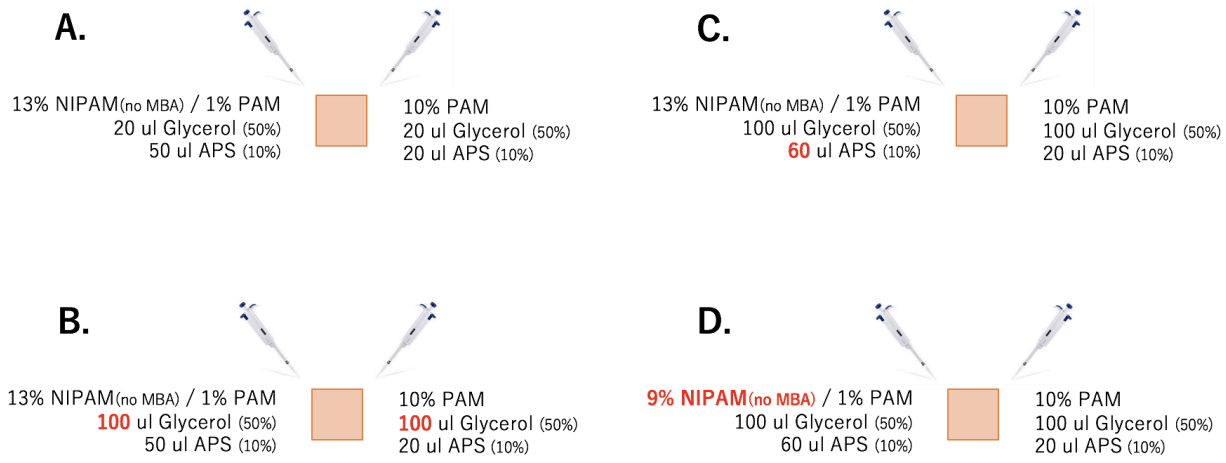


- Different amount of TEMED:
  - NIPAM/PAM: 10-14 ul
  - PAM: 6-12 ul
- Keep Prepolymer in fridge: Fixed temp

**Figure 1. Preparation of Hydrogels**

At room temperature, these volumes of TEMED and APS yield an initial gel within five minutes and was used upon mixing. For a 1.5% (w/v) Ca-ALG hydrogel: Na-ALG stock (1 mL) was added to a microcentrifuge tube. To the tube, $CaCO_3$ (0.0045 g, 45 mM final concentration) and GDL (0.016 g, 90 mM final concentration) were added sequentially, mixing vigorously after each addition. The solution was used immediately upon mixing.

At room temperature, these amounts of $CaCO_3$ and GDL take 24 hours to form a complete gel but the viscosity of the solution begins to increase rapidly within 10 minutes as the initial gel begins to form. For a 12.9% (w/w) PAAm/1.6% (w/w) ALG PAAm-co-Ca-ALG hydrogel: PAAm-ALG stock (2.58 mL), DI (282 µL), 50% glycerol (60 µL), and TEMED (0.3 µL) were added to a microcentrifuge tube and mixed by tube inversion. To the tube, $CaCO_3$ (0.0039 g) and GDL (0.0138 g) were added sequentially to initiate, mixing vigorously after each addition. Working quickly, 10% APS (75 µL) was added to the solution and mixed via tube inversion. The solution was used immediately. For 13% (w/v) PNIPAAm/1% PAAm (w/v) PNIPAAm-co-PAAm hydrogel: PNIPAAm stock (650 µL), PAAm stock (50 µL), 50% glycerol (50 µL), ethanol (50 µL), DI (145 µL), and TEMED (5 µL) were added to a microcentrifuge tube and mixed. 10% APS (50 µL) was added and quickly mixed into the solution via tube inversion. At room temperature, these volumes of TEMED and APS yield an initial gel within five minutes and was used upon mixing. All hydrogel solutions prior to gelation are referred to as precursor solutions.

Gold Nanoparticle (GNP) Synthesis

Gold nanoparticles were synthesized following an established protocol [70]. Briefly, HAuCl4 (20 mL, 1.0 mM) was brought to a rolling boil in a flask on a stirring hot plate. To the rapidly stirred boiling solution, trisodium citrate dihydrate (2 mL, 1% in DI) was added to initiate nanoparticle formation through the reduction of the gold (III) in solution. Once the solution turned a deep red, it was removed from the hot plate and allowed to cool. An approximation of the GNP concentration was made by measuring the difference between an empty weighing boat and the weighing boat with an air-dried aliquot of the GNP solution then dividing by the volume of the aliquot.

Mold Preparation, Infiltration, and Degradation

UV-cured molds were filled with 100% EtOH followed by DI and a 10% Tween 20 (BioRad) solution. The molds were left with the Tween 20 solution for a minimum of one hour before being rinsed with DI and used immediately. Prepped molds were filled with the hydrogel precursor solution of choice and allowed to gel completely before transferring into DI for 24 hours.

The gel-containing molds were transferred to a conical tube with DI and placed in a heated water bath (PAAm/ALG/PAAm-ALG: 70 °C; PNIPAAm: 50 °C). A conical tube of an HFIP solution was also placed in the water bath to warm prior to degradation (PAAm/ALG/PAAmALG: 50% HFIP diluted with DI; PNIPAAm: 100% HFIP). Once heated, a mold was transferred to separate conicals along with enough HFIP solution to cover. Mold degradation was carefully supervised until the gel was mostly released as the degradation time varied depending on mold complexity. The tube was removed from the water bath and the HFIP solution was replaced with DI a minimum of three times to remove the gels from the

HFIP environment and to remove remaining mold pieces. Over the course of 24 hours, the DI in the tube was exchanged with clean DI minimum of three times to leech any remaining HFIP from the solution. After 24 hours, the 3D gel was ready to use.

Three-Dimensional (3D) Printing and Post-Processing

3D Computer Aided Design (CAD) models of a fluidic mold were made in SolidWorks® (Dassault Systèmes) and outputted as a standard tessellation file (STL). Support structures were added manually in Meshmixer (Autodesk) to avoid auto-generating supports within the mold itself. The modified STL was oriented and duplicated in Autodesk Netfabb (Autodesk) with the build volume of the program matching the build volume of the 3D printer. The file was uploaded, sliced, and printed in a liquid crystal display stereolithography (LCD-SLA) 3D printer (Phrozen) with an XY-resolution of 47 μm and a user-defined Z-resolution. After printing, the molds were removed from the build platform and placed in an IPA bath for 15 minutes. Resin remaining in the molds were removed by vigorous shaking in paper towels or forcing the resin out with an air gun. Molds with resin cured in the internal area were discarded. The molds were placed in a UV-curing box (Spierce Technologies) for 15 minutes, after which they were ready to use.

Print Resolution and Hydrogel Fidelity

Two-and-a-half dimensional (2.5D) molds with cubic indentations of variable side length were made to test the accuracy of the 3D printer against the intended CAD design and the fidelity of PAAm hydrogels against the printed mold. The indentation side lengths varied between 200 μm and 1000 μm at 200 μm intervals. To better visualize the print resolution and

hydrogel fidelity, a 3D “donut” with 16 equally spaced, circular ridges present on the donut’s surface. The ridges were 500 μm in width and were 22.5° apart.

Gel Functionality After Solvent

Treatment PAAm, PNIPAAm, and Ca-ALG gels were qualitatively gauged for retained functionality (mechanical strength, thermosensitivity, secondary crosslinking respectively) following degradation and DI equilibration. PAAm hydrogel: A square pyramid-like, tubular mold was filled with PAAm precursor, allowed to gel and equilibrate in DI, and was degraded according to the PAAm-specific, mold degradation protocol. The resulting gel was equilibrated in DI before being pressed with a finger. PNIPAAm hydrogel: A cube-like, tubular mold was filled with PNIPAAm precursor, allowed to gel and equilibrate in DI, and was degraded according to the PNIPAAm-specific, mold degradation protocol. The resulting gel was equilibrated in DI before being heated past the lower critical solution temperature (LCST) of PNIPAAm in a water bath. Ca-ALG hydrogel: A sphere-like, tubular mold was filled with ALG precursor, allowed to gel and equilibrate in DI, and was degraded according to the ALG-specific, mold degradation protocol. The resulting gel was equilibrated in DI before undergoing secondary crosslinking by a multivalent cation ($Fe^{3+}$) of a higher alginic affinity than $Ca^{2+}$ .

Fluidic Operations in 2.5D

A simple 2.5D, Y-shaped mold was made to characterize different methods of mold infiltration and their resulting hydrogels using the technique. Co-flow: PAAm-co-FOA

precursor and PAAm-co-RHO precursor solutions were simultaneously infiltrated into the mold at equivalent flow rates and gelled completely after the flows inside the mold stabilized.

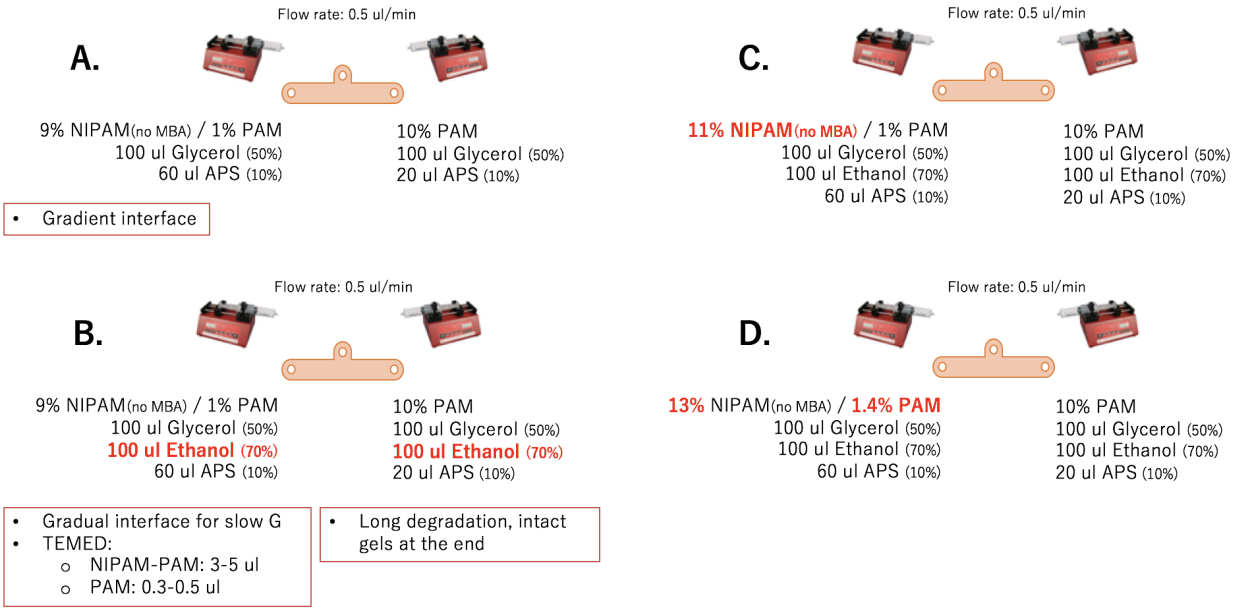


**Figure 2. Preparation of hydrogels for fluidic operations in 2D.**

Sequential: PAAm-co-FOA precursor was infiltrated into one inlet of the mold at a defined flow rate until the mold was filled with solution. A known volume of PAAmco-RHO precursor was infiltrated into the other inlet of the mold at the same flow rate after the flow of the PAAm-co-FOA was stopped. Once the volume had fully entered the mold, the solution gelled completely. The volumes of PAAm-co-RHO were varied to create different sized regions of PAAm-co-RHO in the final gel. Consecutive: PAAm-coFOA precursor was infiltrated into one inlet of the mold at a defined flow rate until the mold was filled with solution. A known volume of PAAm-co-RHO precursor was infiltrated into the other inlet of the mold at the same flow rate immediately after the flow of the PAAm-co-FOA was stopped. A known volume of PAAm-co-FOA precursor was infiltrated into the same inlet as PAAm-co-RHO to push the PAAm-co-RHO precursor deeper into the mold and encase the PAAm-co-RHO in

PAAm-co-FOA. Once the volume had fully entered the mold, the solution gelled completely. The volumes of PAAm-co-RHO were varied to create different sized regions of PAAm-co-RHO in the final gel. Diffusion: PAAm-co-FOA precursor was infiltrated into one inlet of the mold at a defined flow rate until the mold was filled with solution. A known volume of PAAm-coRHO precursor was added to the other inlet of the mold and mixed using a micropipette (Eppendorf) for 0 s, 3 s, and 6 s, respectively, after which the solution gelled completely.

Microfluidic Operations

2.5D molds of a microfluidic herringbone mixer and gravity separator were 3D printed to gauge the compatibility of this technique with microfluidic operations. Mixer: PAAm-coFOA precursor and PAAm-co-RHO precursor were co-infiltrated into a 2.5D, pseudomicrofluidic mixer with dual herringbone-shaped protrusions on the top and bottom of the mold at equivalent flow rates (< 0.5 mL/min) and allowed to gel completely after the flows stabilized. The experiment was repeated in a mold without the herringbone-like protrusions to obtain control samples. Particle Separator: PAAm precursor doped with blue polyethylene microspheres (47 – 53 μm) was infiltrated into a 2.5D mold containing an array of square-pyramidal indentations on the bottom of the mold. Precursor flow was allowed to stabilize before letting the solution gel completely.

Dynamic Mechanical Analysis (DMA)

PAAm, Ca-ALG, and PAAm-co-Ca-ALG type IV dumbbells conforming to the American Standards for Testing and Materials (ASTM) International standards for tensile testing were made by casting precursor solutions in 3D printed molds of the dumbbell structure. Stress/strain curves for each hydrogel were obtained using a DMA Q800 (TA Instruments)

equipped with a tensile clamp and set with a strain rate of 0.2 mm/min. The following hydrogel compositions were tested: 5% (w/w) PAAm, 7.5% (w/w) PAAm, and 10% (w/w) PAAm; 0.5% (w/v) ALG, 1% (w/v) ALG, and 1.5% (w/v) ALG; 10%/0.5% PAM-co-Ca-ALG. For each hydrogel composition, a subset of the gels was subjected to a 50% HFIP solution diluted in DI for 11 minutes before being allowed to equilibrate in DI for 24 hours. After DI equilibration, these solvent-treated gels were tested alongside their control counterparts. All tensile experiments were taken to failure.

Thermally Induced Water Loss in PNIPAAm

10% (w/v) PNIPAAm blocks (10 mm x 10 mm x 4 mm) were made in polydimethylsiloxane (PDMS) molds and placed in a DI bath set to temperatures between 25 °C and 50 °C with 5 °C steps to quantify the water loss percentage at each temperature. The blocks spent 10 minutes equilibrating at each temperature before measuring the mass of each block using a NewClassic ME Analytical Balance (Mettler Toledo™). The blocks were returned to the water bath, the temperature was increased, and the cycle repeated until the final measurements at 50 °C were taken. Two subsets (n = 6 each) of the tested blocks were subjected to 100% HFIP for four and eight minutes respectively before being retested for their water loss percentage.

Hydrogel Transparency

The transparencies of hydrogel samples (L: 2 cm; W: 2 cm; H: 2 mm) made of PAAm, Ca-ALG, and PNIPAAm were characterized before and after solvent exposure. A small circuit comprised of a linear DC voltage regulator, a 9-volt (V) battery, and a white light emitting diode (LED) was made to provide a consistent light source for the experiment. The samples were placed in a semi-dark chamber on a glass slide a minimal distance (touching) away from

the LED with another glass slide placed on top to reduce light reflection and scattering. The light illuminance passing through the hydrogels were measured using a REED R8140 LED Light Meter (REED Instruments) and analyzed in MATLAB (MathWorks®).

Functionality Gradients

2.5D molds designed around a 20 mm x 4 mm x 2 mm bar-like space were 3D-printed to characterize simple gradients in stiffness, material constituency, dopant concentration, and chemical moiety concentration created from the collision of opposing inflows. Stiffness: Opposing flows of 10% PAAm precursor and 5% PAAm precursor (stiff and soft respectively) were infiltrated into modified molds with dumbbell-like grips and hemispherical indentations resulting in dumbbell like hydrogels with hemispherical protrusions down the length of the gel. The gels were placed in a 3D printed stretching fixture and imaged under a microscope in an unstretched state and a stretched state. The displacement between the hemispherical protrusions before and after stretching were calculated in ImageJ (ImageJ) and plotted using MATLAB. Material: Opposing flows of 10% PAAm precursor and 13%/1% PNIPAAm-co-PAAm precursor were infiltrated into the 2.5D molds and allowed to gel completely. The gels were placed between two glass slides with spacers on each end and submerged in a water bath above 40 °C. Images taken with a digital single-lens reflex (DSLR) camera (Nikon D3400, Nikon) were quantified for changes in gray value in ImageJ. Dopant Concentration: Opposing flows of 10% PAAm precursor and 10% PAAm with GNP precursor were infiltrated into the 2.5D molds and allowed to gel completely. Images taken under a binocular microscope (AMScope™) with a DSLR camera and a microscope camera adapter (AMScope) were quantified for changes in gray value in ImageJ. Chemical Moiety: Opposing flows of 10%

PAAm-co-FOA precursor and 10% PAAm-co-RHO precursor were infiltrated into the 2.5D molds and allowed to gel completely. Images taken with a fluorescent microscope (Olympus BX-53, Olympus) were quantified for changes in intensity in ImageJ.

Hydrogel Functionality in 3D

3D fluidic molds were 3D printed to showcase hydrogel creations made using a combination of the infiltration methods and gradient schemes established in this work. Table: A four-legged table with a geometric flower design on the top, inlets above each leg, and an outlet in the center was 3D printed to highlight stiffness variance within a single structure and 3.5% PAAm precursor was infiltrated into two legs to represent “soft legs” and, before the “soft legs” gelled, 10% PAAm precursor was infiltrated into the other two of the legs as “stiff legs” and the table-top before gelling completely. OctetTruss Lattice: An octet lattice mold comprised of seven repeating octet units and two tensile “grips” was carefully infiltrated with PAAm-co-Ca-ALG precursor and allowed to gel completely before removal of the mold. Flower: A flower mold with an inlet from the top, an inlet from the bottom, and outlets on each “petal” was made to create an environmentally responsive, hydrogel flower. PAAm-co-FOA precursor was infiltrated from the top at a flow rate (0.3 mL/min) twice that of the PAAm-co-RHO precursor flowing in from the bottom inlet (0.15 mL/min). After the flow within the mold stabilized, the solution gelled completely prior to mold removal. Egg: An egg mold with a large inlet encasing a smaller inlet within it was made to create an egg-shaped hydrogel with an encapsulated, GNP center. 10% PAAm precursor was infiltrated from the larger inlet until approximately 1/3 of the egg was filled. A known volume of GNP-doped 10% PAAm precursor was then co-infiltrated alongside the PAAm precursor at an equivalent flow rate until the flow

of this solution stopped. The flow of the PAAm precursor continued until the GNP-doped PAAm region within the mold was fully encapsulated in PAAm. After this occurred, the solution within the egg gelled completely prior to mold removal.

## Results

### Fluidic sculpting and release of 3-dimensional hydrogel

The infiltrative assembly process studied herein can be generally simplified into three main steps: (1) 3D-printing of the fluidic mold; (2) infiltration with a hydrogel precursor solution and in-situ gelation; followed by (3) release of the hydrogel by dissolution of the encompassing mold (Figure 1a and 1b). Steps (1) and (3) are primarily responsible for determining the efficacy of the hydrogel sculpting process while step (2) gives users the ability to impart multifunctional attributes to their final construct through the modulation of precursor solutions infiltrated into inlets defined in the mold.

In step (1), the effective print resolution of the 3D printer and the fidelity of the hydrogel material to its printed shape determines the resolution of the resultant material. In published research, SLA printers can readily print complex geometries down to nano-scale resolution, and we focused on such platforms to synthesize our molds [43]–[45]. This enables significantly finer structural features (and enables smooth or rounded walls) than those achievable in wax or sugar printing in existing hydrogel sacrificial templating studies [35]–[40]. In this research we utilized a low-cost, commercially available 3D printer (Phrozen), alongside a commercially available resin (3DM-ABS) to print our molds. Factors such as the properties of the printing resin, the printing parameters, and the orientation of the mold while printing can cause the dimensions of the mold (and subsequently the hydrogel) to

differ from the intended design (Supp. Figure 1). Commercially available, low-cost SLA printers can print at a putative resolution of down below 50 μm, however in practice it is difficult to generate structural features at these sizes. For our low-cost setup we printed well-defined ridge-openings down to 200 um, however more weakly defined openings could be achieved down towards 150 μm. The fidelity of the hydrogel precursor to the mold also affects the final synthesized material as the precursor solution, depending on its surface tension, can trap air within the small, enclosed areas of a mold rendering a particular feature absent or malformed on the hydrogel (Figure 1c). We studied several techniques to eliminate this issue, primarily involving pretreatment of the mold with low surface tension solutions (mixed with surfactant or solvent) prior to infiltration of the prepolymer. Proper characterization of a 3D printer's effective resolution, the resin, and the properties of a hydrogel precursor solution are necessary to obtain a high-quality, 3D hydrogel (Figure 1d and 1e).

Step (3) is critical in determining whether the process is viable for a particular application as the cured SLA resin must be dissolvable and the hydrogel must survive the degradation. In this publication we focused on a commercial ABS (acrylonitrile butadiene styrene)-like resin. Most SLA resins are robust against solvent attack, however we surmised that the ABS-like resin could be more easily degraded in solvent (ABS printed from extrusion printers can be etched in acetone). We tested ethanol (EtOH), isopropanol (IPA), acetone (ACE), and 1,1,1,3,3,3-hexafluoro-2-propanol (HFIP) as potential water-miscible solvents for the printed material. Results of the testing revealed that HFIP was the only solvent capable of dissolving the cured resin (Supp. Figure 2a and 2b). HFIP is used in lieu of water during the synthesis of some hydrogels, and due to its polarity and water miscibility is compatible with a

variety of polymerized hydrogel [46]–[48]. Subsequent testing of the survivability and behavior of polyacrylamide (PAAm), poly(n-isopropylacrylamide) (PNIPAAm), and calcium alginate (Ca-ALG) hydrogels was performed to determine an optimum degradation scheme for three types of hydrogels that represented natural and synthetic sources, different crosslinking mechanisms, and unique functionalities (Supp. Figure 3a and 3b).

Optimization of the degradation process on a hydrogel-specific basis allows for the creation of small, 3D hydrogel structures that retain their unique functionality and reflect the resolution of the SLA printer (Figure 1f - 1n). Degradation schemes were developed to minimize the time hydrogels spent in the solvent and the concentration of HFIP, while maximizing the rate of mold degradation as excessive time spent in high concentrations of HFIP led to the gel becoming more brittle and potentially broken as the resin shell deformed and degraded. We found that by increasing the temperature of the degradation reaction, we could minimize the concentration of the HFIP and the solvent exposure time while achieving a satisfactory mold degradation rate (Supp. Figure 2c). For PAAm and Ca-ALG hydrogels, the degradation process was performed at a temperature of 70 °C in 50% HFIP (determined empirically to provide a good degradation rate without exceeding the boiling point of the HFIP mixture). For PNIPAAm hydrogels, 100% HFIP at 50 °C was used since an HFIP mixture could induce co-nonsolvancy effects that would deswell the gel structure [49]. Due to the more volatile nature of PNIPAAm (which swells and unswells aggressively depending on environment), these gels sometimes require additional tweezer-assisted mold-bit removal after initial solvent treatment. The more brittle behavior of hydrogel in HFIP could be improved by introduction of glycerol to the precursor solution--this acts both as a plasticizer and substitutes for water molecules that enhances hydrogel performance during its

short-term exposure to solvent. In the future, alternative SLA resins that degrade in milder conditions (such as alkaline water solutions) could improve the versatility of this approach.

Infiltrative assembly of hydrogel with gradient composition

The infiltration step of the process allows for the creation of heterogeneous hydrogel constructs. This occurs through control of infiltrated precursor solutions alongside their gelation rate. Inlet flow rates, infiltrated volumes, and flow stabilization time can be programmed to modify the local characteristics of the final hydrogel. Additionally, controlling the magnitude of inlet flow rates and the bulk gelation rate of the hydrogel precursor solutions (through crosslinker concentration) enables control over the gradient interfaces that occur between different sections of hydrogel. Slower flow rates encourage near laminar flows that can yield more defined interfacial boundaries, whereas faster flow rates encourage turbulent flows that can stimulate the formation of interfacial gradients. Inversely, slower bulk gelation rates translate to longer time frames over which diffusion can occur between separate regions (facilitating gradient formation), while faster gelation rates reduce such time frames and encourage more defined boundaries between regions . Furthermore, control over the infiltrated volumes yields regions of varying size that add further complexity to the final gel structures.

Simple 3D-printed fluidic molds with two inlets and one outlet were used to characterize how four basic methods of fluidic infiltration (co-flow, sequential flow, consecutive flow, and diffusion) can be modulated to yield structurally-complex 3D hydrogels (Figure 2ai – di). In this simplified scenario, we studied how the infiltration of 2 precursor

solutions (one doped with fluorescein-modified and the other with rhodamine-modified monomer) could be uniquely coordinated.

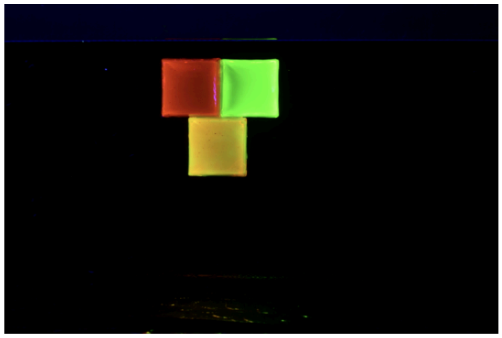

20ul Rhodemine in 1ml solution
10 ul Fluorescein in 1ml solution

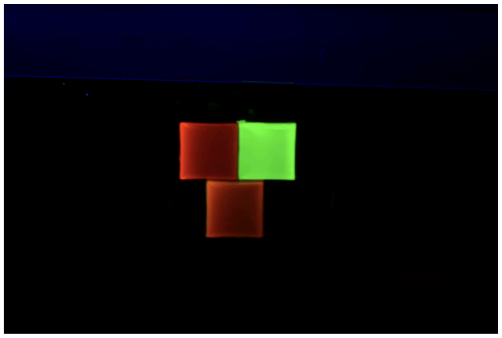

40ul Rhodemine in 1ml solution
10 ul Fluorescein in 1ml solution

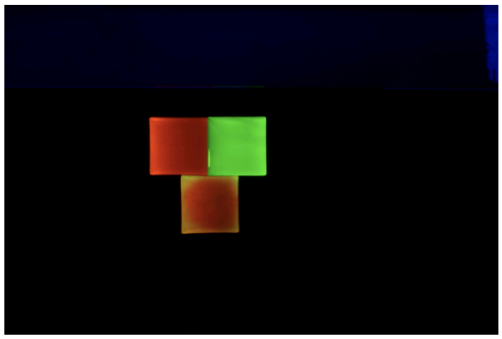

20ul Rhodemine in 1ml solution
5 ul Fluorescein in 1ml solution

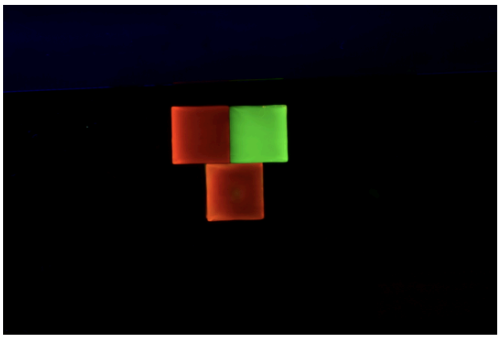

40ul Rhodemine in 1ml solution
5 ul Fluorescein in 1ml solution

**Figure 3. Different percentage of Rhodemine/Fluorencein for mixer analysis**

When flowing two precursor solutions at the same time through a mold (co-flow), differences in inlet flow rates yielded hydrogel regions of different sizes within a single gel (Figure 2aii). Sequential flow through alternate inlets could be used to modulate the shape and size of a secondary region within a main hydrogel (Figure 2bii).

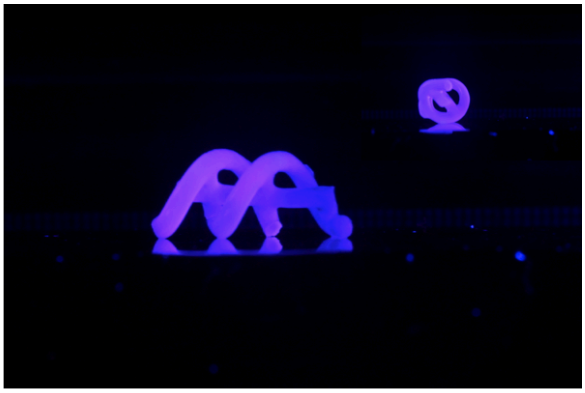


**Figure 4. Co-infiltration showcase**

Here the second infiltrated precursor displaces a portion of the initially infiltrated precursor, the volume of which controls the size of the new region. Consecutive flow operates in a manner like sequential flow, however, occurs through the same inlet. This enables the creation of multiple, secondary hydrogel regions within a primary hydrogel (Figure 2cii). The size and shape of these regions are defined by the infiltrated volumes and inlet flow rates, respectively. Lastly, diffuse regions of another precursor solution can be incorporated into a gel via passive or active diffusion (Figure 2dii). For such experiments, the equalization of precursor solution densities improved the reliability of the final synthesized material.

These infiltration and fluidic manipulation strategies can be readily applied to create 3D hydrogels with localized structural and functional characteristics. Examples of such structures are shown in Figure 2aiii – diii with fluorescent PAAm-co-FOA and PAAm-co-RHO as the gel constituents. An alternating, three-layer serpentine structure was made to highlight co-flow-mediated generation of a hydrogel with dual regions of fluorescent polymer that traverse the entire length of the mold (Figure 2aiii – iv). PAAm-co-FOA precursor solution and PAAm-co-RHO precursor were infiltrated at equal flow rates (0.3 mL/min) to maintain

approximately the same space within the molds. The resultant gel maintained separate regions of PAAm-co-FOA and PAAm-co-RHO with slight diffusion throughout the winding 3-dimensional interface within the material. To highlight sequential flow generation, a multilayer UCI mold was made where the U and the I were made out of PAAm-co-FOA and the C was made out of PAAm-co-RHO (Figure 2biii – iv). To make this gel, the U was first filled in with PAAm-co-FOA precursor, then the C was filled in with PAAm-co-RHO precursor before the U fully gelled, and, lastly, the I was filled with PAAm-co-FOA precursor before the C fully gelled. Slight diffusion between the U, C, and I sections of the mold clearly indicate that the resulting structure is a single gel rather than three gelled on top of each other.

To illustrate consecutive flow generation, a fish mold with a single inlet/outlet was 3D printed with the intent of creating a striped hydrogel fish (Figure 2ciii – iv). Using a micropipette, alternating aliquots of PAAm-co-FOA and PAAm-co-RHO precursor solutions were gently infiltrated into the mold until the mold was filled. We chose to approximate the thickness of the layers visually, leveraging the distinct colors of the precursor solutions and the transparency of the mold to our advantage. Lastly, to show how diffusion could be used to add complexity to a 3D hydrogel, a capillary-like mold with a large inlet and several 3D interleaving, vessel-like branched outlets was made (Figure 2diii – div). The mold was first fully infiltrated with a PAAm precursor solution before small aliquots of PAAm-co-FOA were added to each outlet and allowed to diffuse into the vessel tips. The aliquot volumes added to the outlets were dependent on their height from their support--this is because vessels above others in height experienced gravity-mediated diffusion that reduced the amount of PAAm-co-FOA needed to achieve the same diffusion as lower vessels.

Microfluidic operators can also be built-in to the sacrificial 3D-printed shell to further facilitate control over the resultant hydrogel. As a demonstration of this, two molds inspired by microfluidic operations--a mixer and a gravity separator--were developed. The mixer mold was inspired by a staggered herringbone mixer and has dual herringbone shaped protrusions on the top and bottom of the molds inner surface down the length of the mold to facilitate mixing between PAAm-co-FOA and PAAm-co-RHO (Figure 2e) [50]. Control and mixer-integrated molds were co-infiltrated with fluorescing precursor solutions and allowed to gel. Control molds yielding materials with highly distinct fluorescent regions, whereas mixer-integrated molds generated more intermixed constructs--particularly at the middle and end of the channel (Figure 2f). The separator mold was inspired by microfluidic gravity separators and synthesizes a 3D needle-like array with square pyramidal indentations on the bottom. This structure allowed for the sedimentation of stiff blue polystyrene microspheres from a PAAm precursor solution (Figure 2g) [43]. When the mold was removed, the bulk of the resulting gel remained clear but the tips of the square pyramid array were bright blue, demonstrating that the mold was successful in separating the microspheres from the precursor solution to form a hydrogel with stiff needle-like tips (Figure 2h).

Synthesis of 2.5-dimensional hydrogel systems

a. Co-flow
b. sequential flow
c. Consecutive flow
d. Diffusion

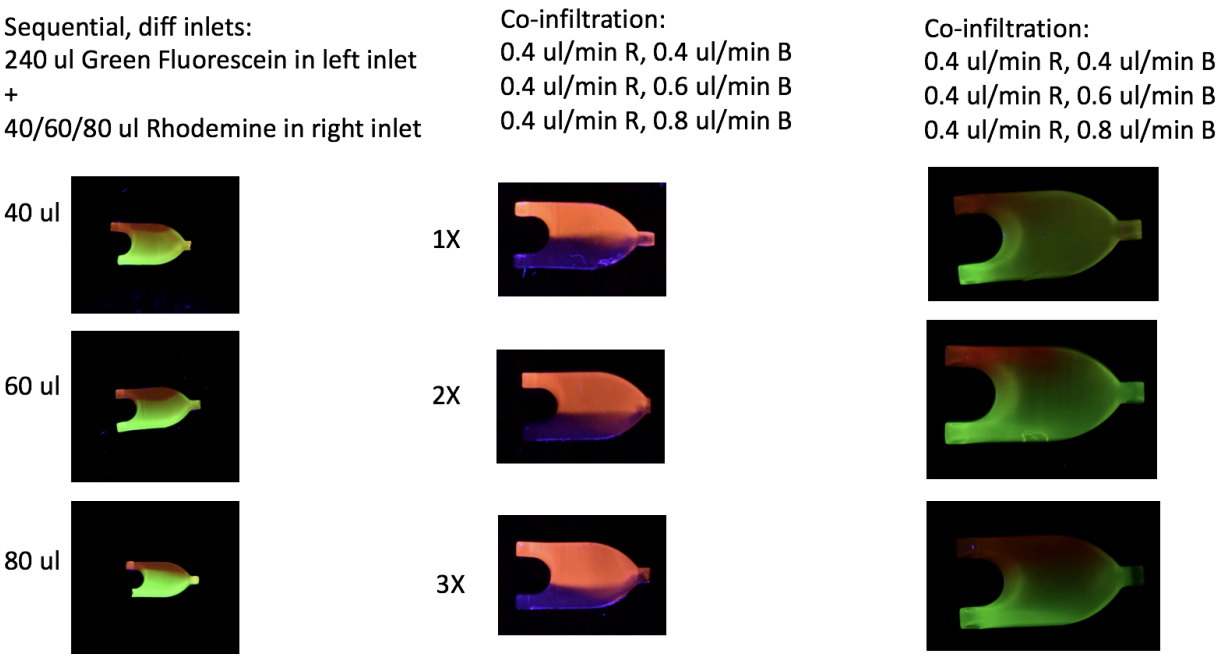


**Figure 5. Sequential and co-infiltration mechanism**

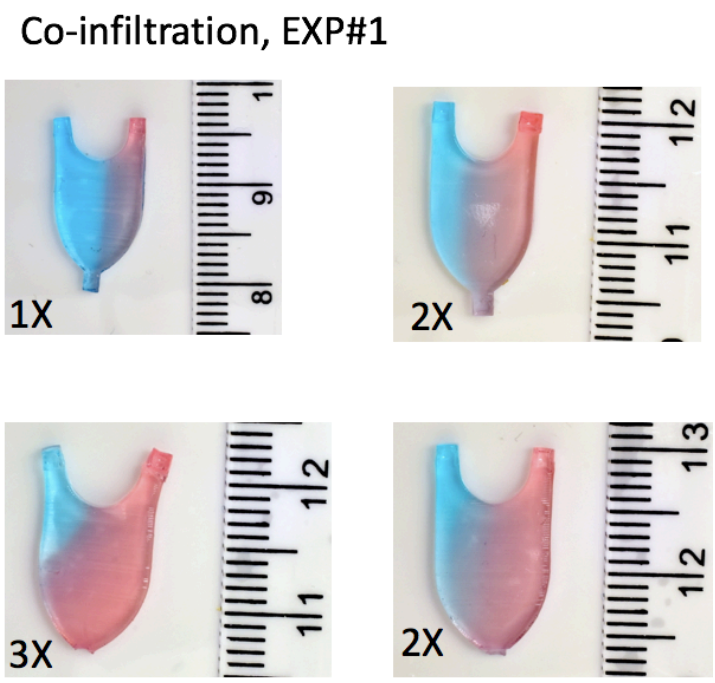


**Figure 6. Co-infiltration with different fluid flow**

| Diffusion<br>300 ul clear PAM + ⋯ | 3 sec agitation | 6 sec agitation | 9 sec agitation |
|---|---|---|---|
| ⋯ +10ul Pink Fluorescent Poly bead from source | 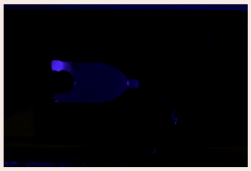 |  | 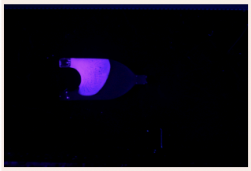 |
| ⋯ +10ul (Pink Fluorescent Poly bead from source +DI water + TEMED) |  |  | 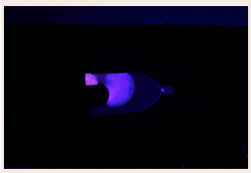 |

**Figure 7. Diffusion operation over time**

Microfluidic Operation

a. Mixer

we tested ”Y-shape” microfluidic channel as a mixer. Using the same percentage of PAM as before, best flow rate is achieved at 0.3 ml/min. Flow long enough to reach steady state.

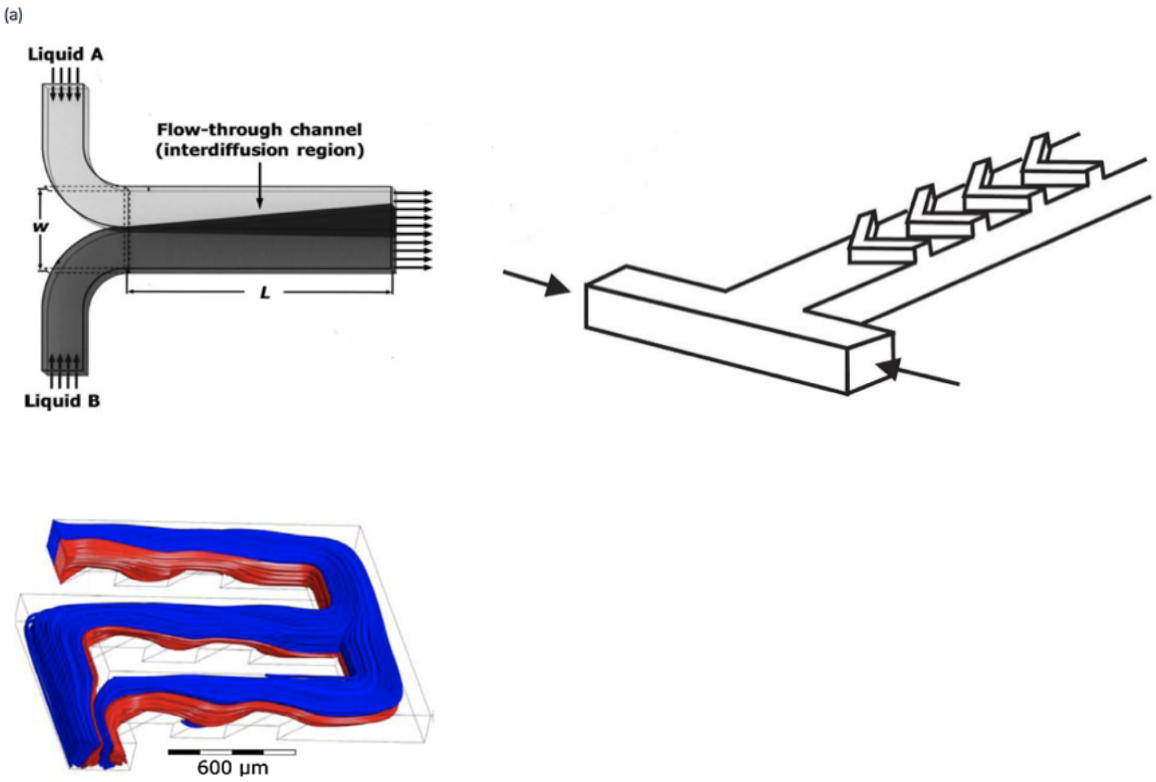


**Figure 8. Schematic and Simulation of mixer**

Last picture is a simulation that shows the liquids go on top of each other after they rotate 90 degrees.

3 different designs have been used so far:

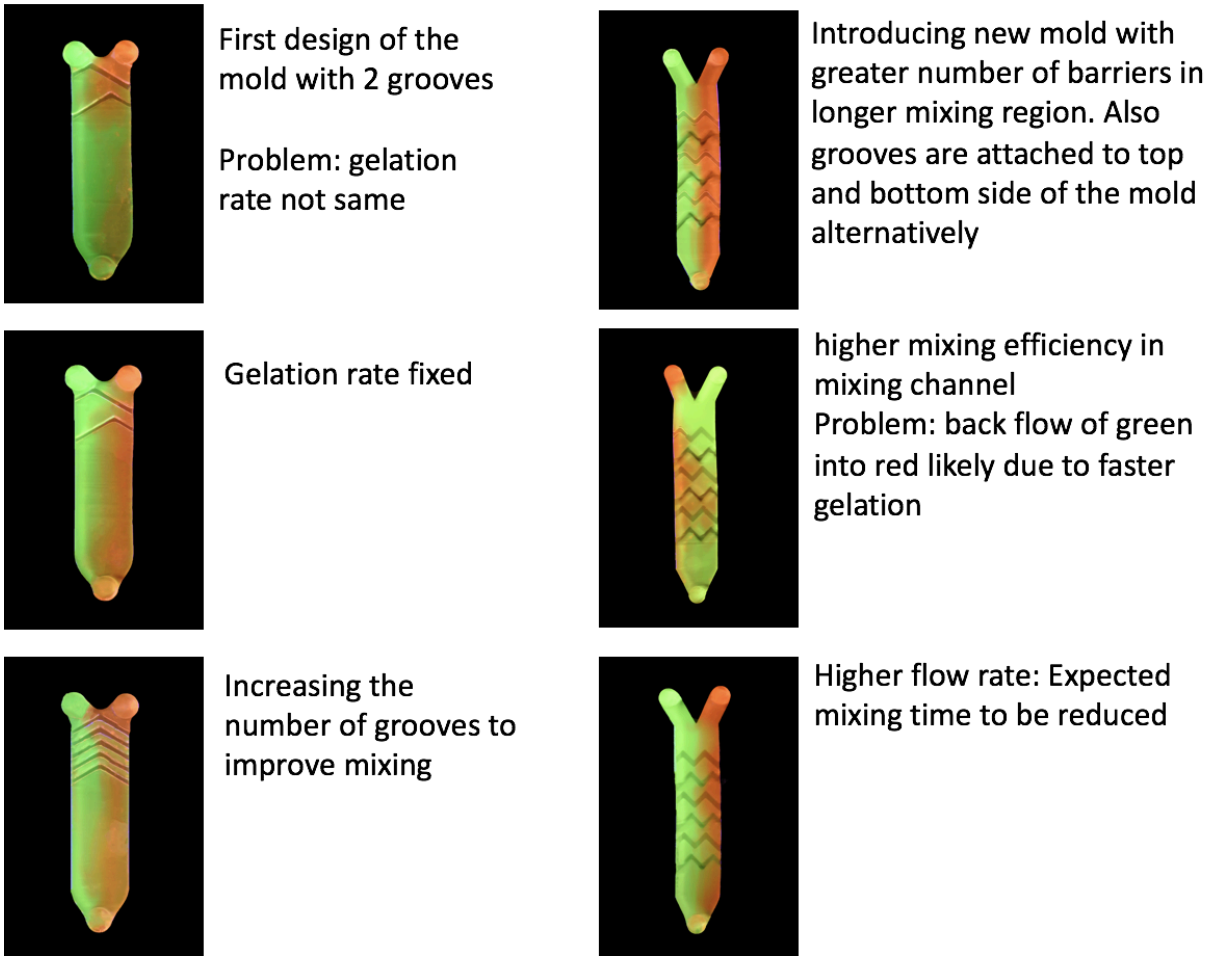


**Figure 9. Enhancing mixer functionality by adding grooves**

After optimizing the design and the flow rate of each side the best results shown below, didn't completely meet the expectation. so longer mixing region was designed to tackle this issue.


**Figure 10. Enhancing mixer functionality by increasing the length**

Many of the molds destroyed in oven >> blow dry molds OR leave in room temp.

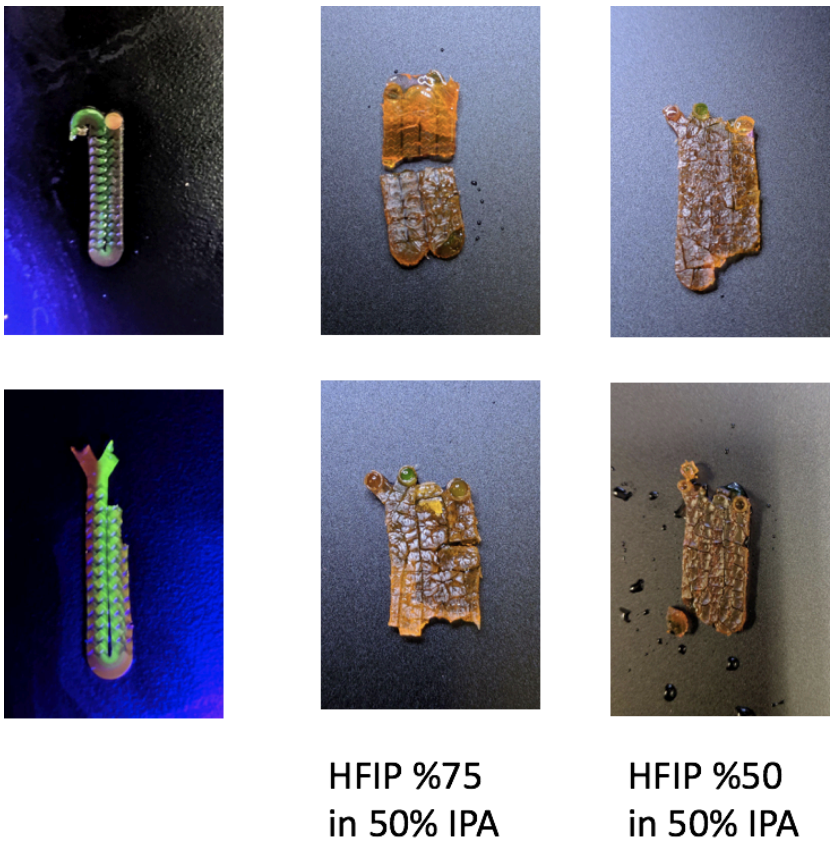

**Figure 11. Mold degradation for mixer**

In the figure below the difference between mixers with and without groove have been demonstrated. Arrows show:

a.Diffusion at the entrance of main channel

b.Different flow pattern in the channel

c.Mixing in outlet

Several papers have used similar mold as a mixer and the fact that they mix with each other (even without any barrier in the channel) has been shown in either experiment or simulation.

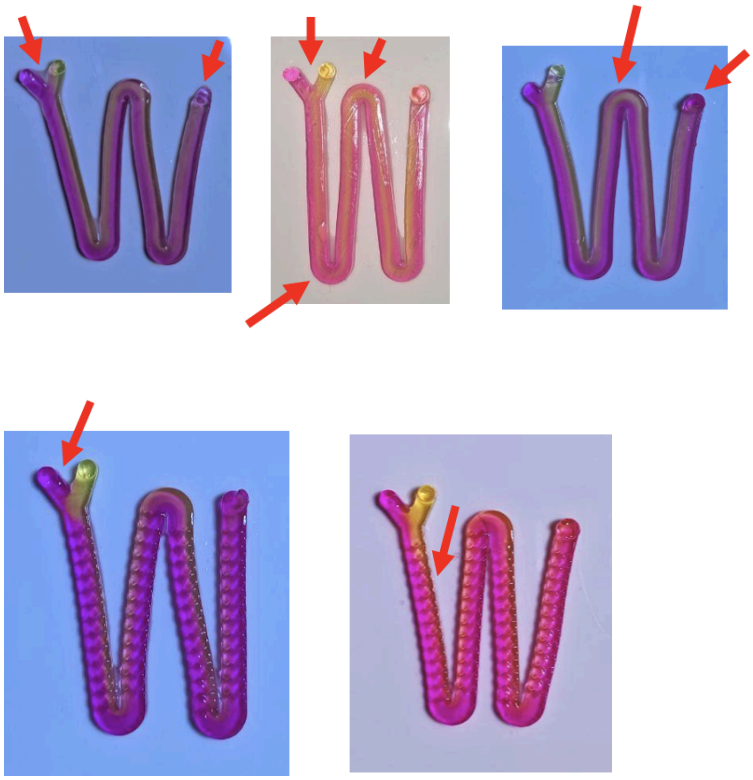

MIXER: 3-D structure: Using tweezers to take out the mold particles. Some results after degrading mold in HFIP 75% and 50% (~ 12 samples):

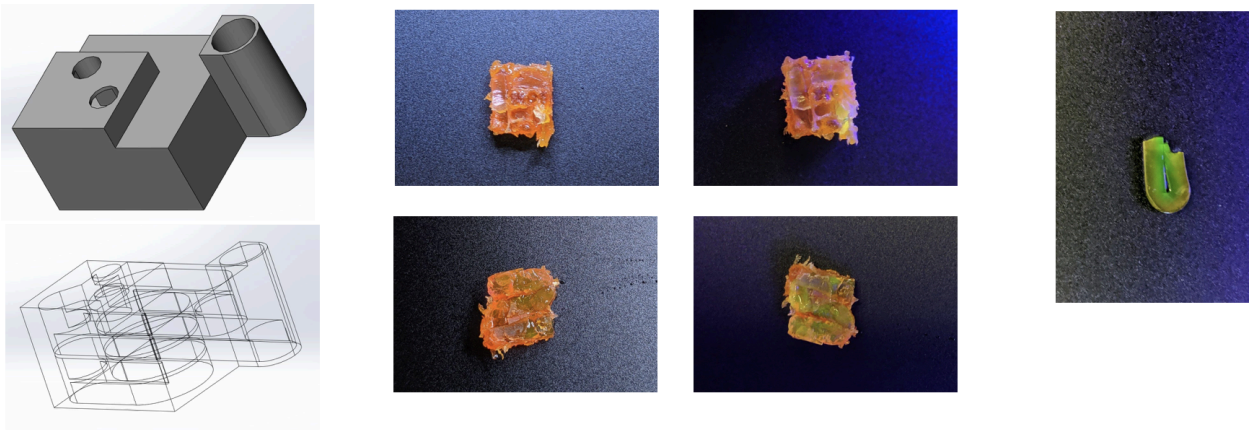

Schematic of the design with 3 layer

**Figure 12. 3-D structure of mixer**

Some advantages of the new design is first less ABS on corners and second Inlets and outlet close to each other to better see the contrast of colors after mixing.

This has been demonstrated below:

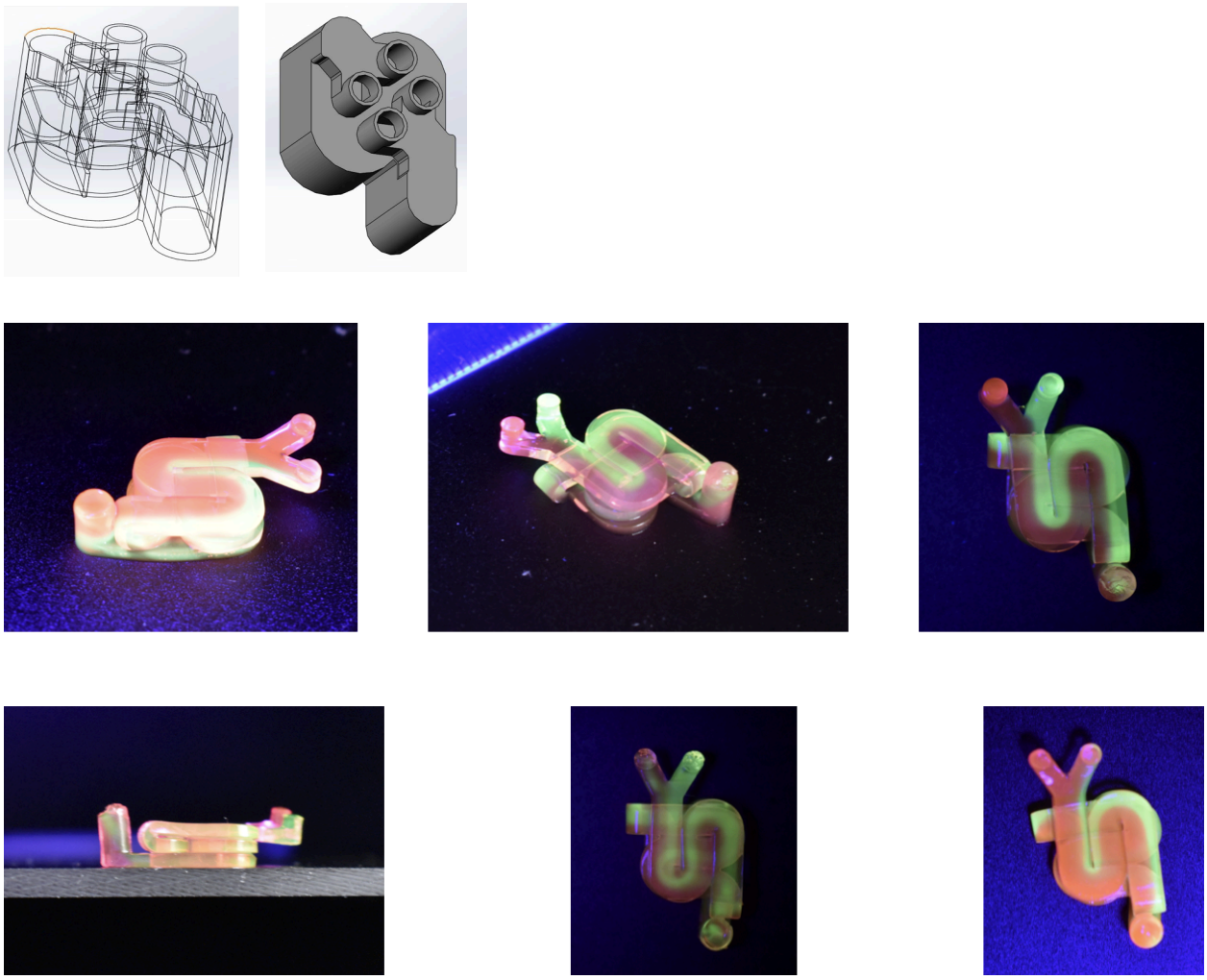

**Figure 13. 3D mixer after mold degradation in 2 layers**

And in three layers:

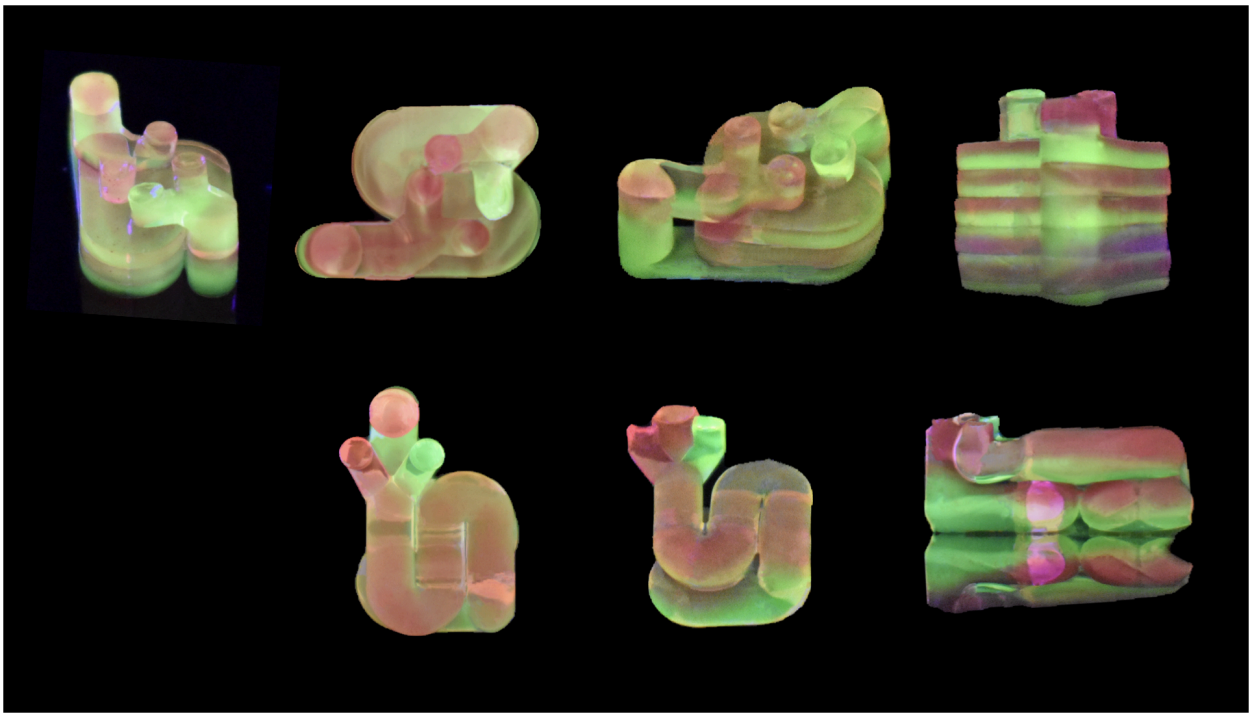

**Figure 14. 3D mixer after mold degradation in 3 layers**

b. Particle Separator

The purpose of this study is To build a gradient generator for separation of μbeads from PAM based on their density difference.

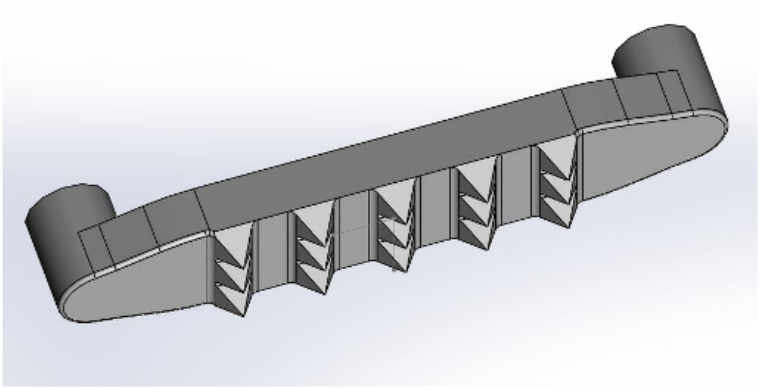

**Figure 15. Schematic of separator design**

Using 100um and 200um glass microparticles the designed separator works as shown in figure.

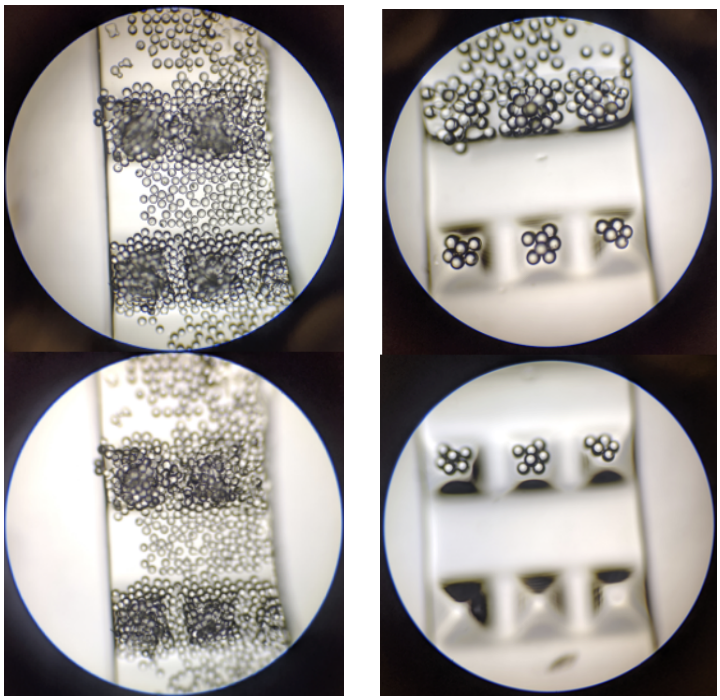

**Figure 16. Separator using glass microparticles**

In order to better understand the functionality of the separator in the pictures, we used 25um and 50um blue beads and used them in gravity separator.

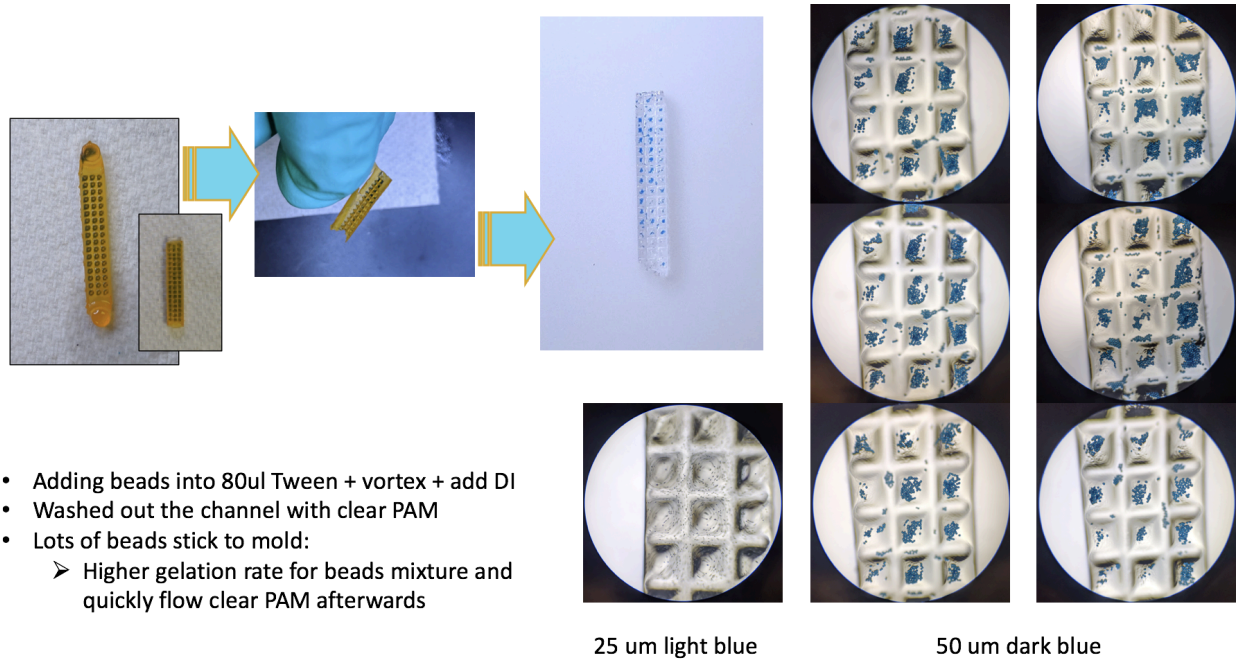


**Figure 17. Separator using beads**

No difference in the number of beads inside each well was observed. So the possible cause could be either particles never sediment or flow take out the particles again. In order to troubleshoot we studied three cases: Case 1, High Flow Rate. Case 2, Fast gelation: Not enough time to sediment. Case 3, High concentration of PAM.

Case 1 study:

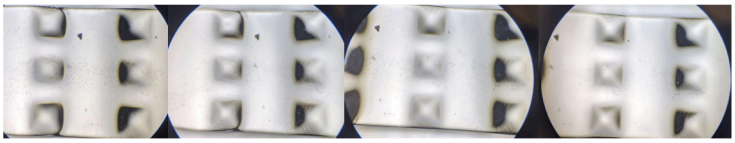

S1: Pipette 5ul PS + Pipette [T+10% PAM]

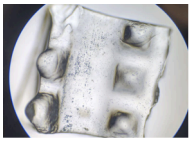

S4: Pipette 10ul PS + Pump at flow rate: 0.4 ml/min [T+10% PAM]

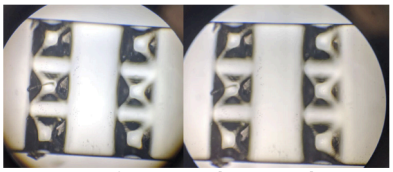

S2: Pipette 10ul PS + Pipette [T+10% PAM]

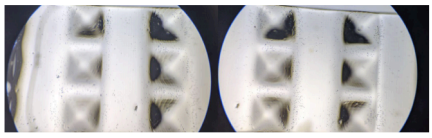

S5: Pipette 50ul PS + Pump at flow rate: 0.2 ml/min [T+ 10% PAM]

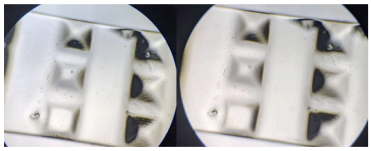

S3: Pipette 10ul PS + Pump at flow rate: 0.4 ml/min [T+10% PAM]

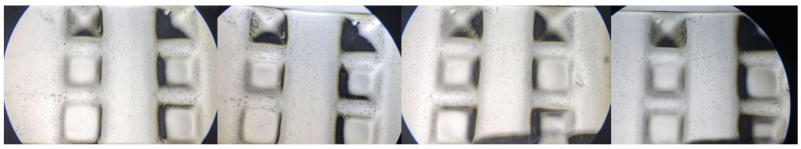

S6: Pipette 50ul PS + Pump at flow rate: 0.3 ml/min [ T+10% PAM]

## Case 2 study:

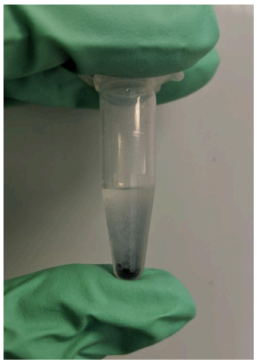

PS beads in 10%PAM after 3 days

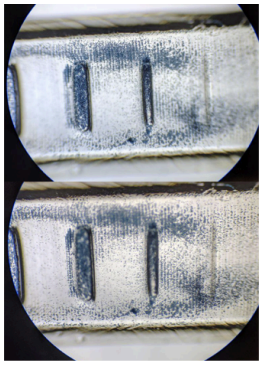

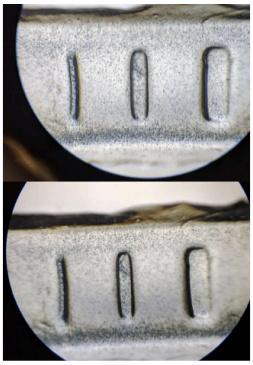

**EXP#1:**
At t=0, t=10s, t=20s, t=30s, t=1min, t=2min, t=3min, t=10min
pipette [10ul PS in PAM%10] in mold At t=15 min added TEMED

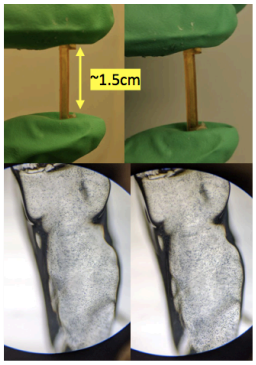


**EXP#2:**
Fill up a mold and fix it to the wall vertically
Wait for: 10 min

## Case 3 study:

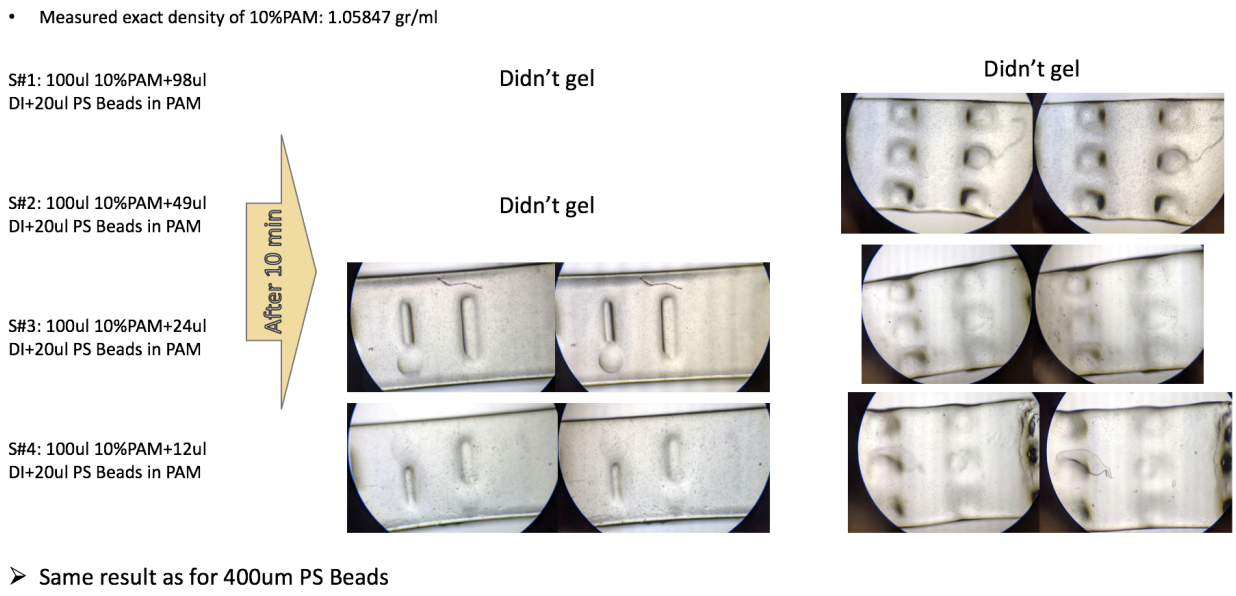


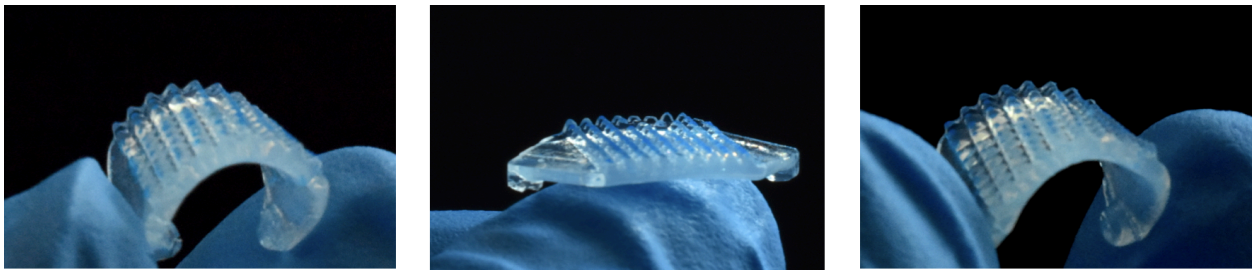

**Figure 18. Three case studies to achieve best separator functionality in 3D**

Synthesis of 3-dimensional hydrogel systems

Through proper material selection and creative infiltration, unique multi-material structures with region-specific functionality can be easily built. As demonstration, four 3D structures were synthesized that represent the structural tunability, synergy between material choice and geometric constraint, and multimaterial functionality that can be achieved via this process.

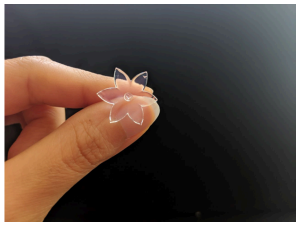

A flower-like mold was fabricated to highlight environmental-responsiveness of 3D multimaterial constructs. This mold consisted of two inlets entering above and below the central point (flowing red, fluorescent PAAm and green, fluorescent PNIPAM-co-PAAm respectively), and six petals with outlets on their tips. This forms a fluorescing, thermo-responsive hydrogel bilayer with a graduated interfacial boundary (Figure 4ci) that can be synthesized in-situ.

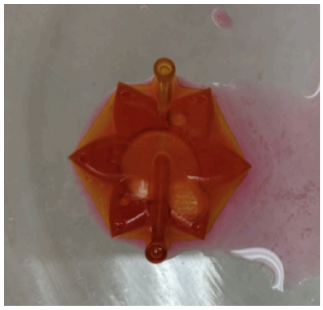

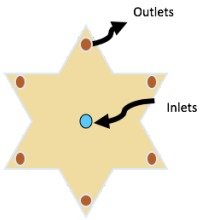


Top view

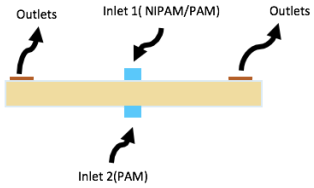


Side view

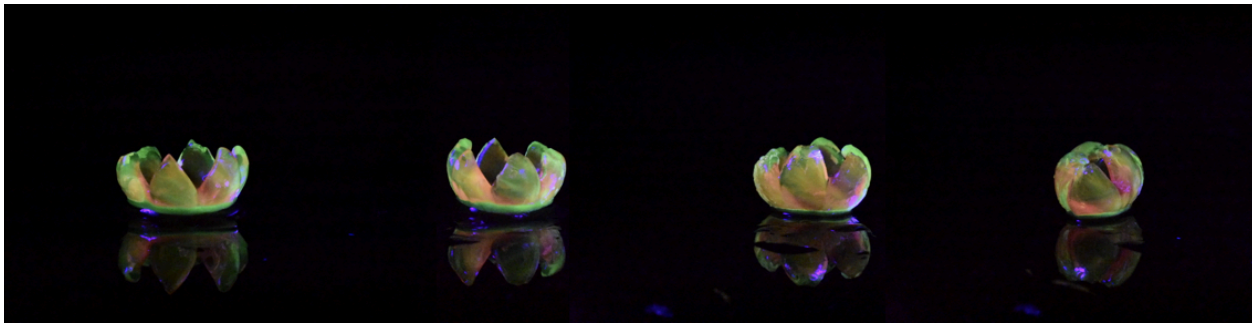

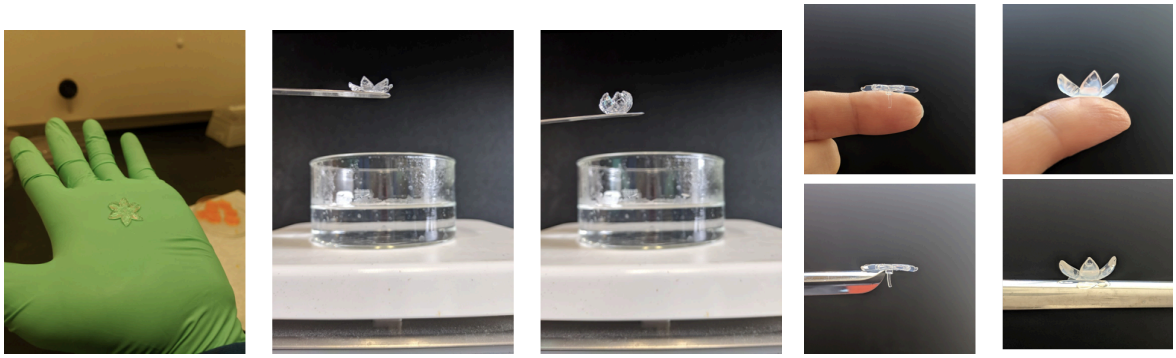

**Figure 19. Environmental-responsiveness of 3D multimaterial constructs**

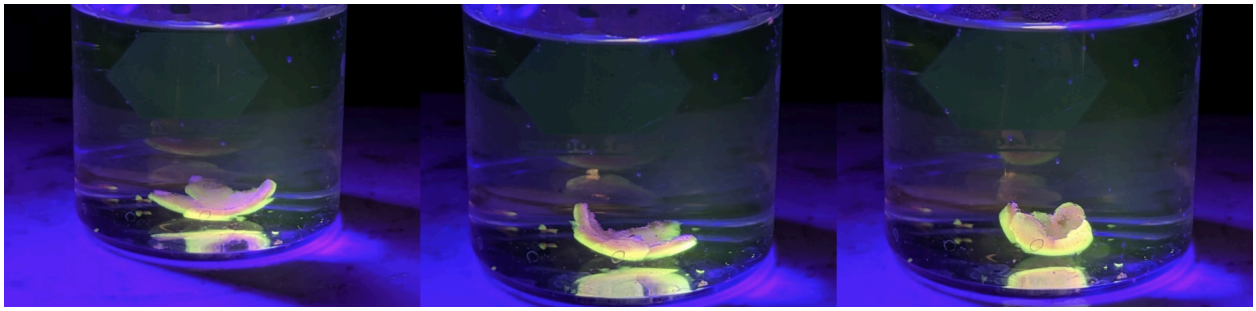

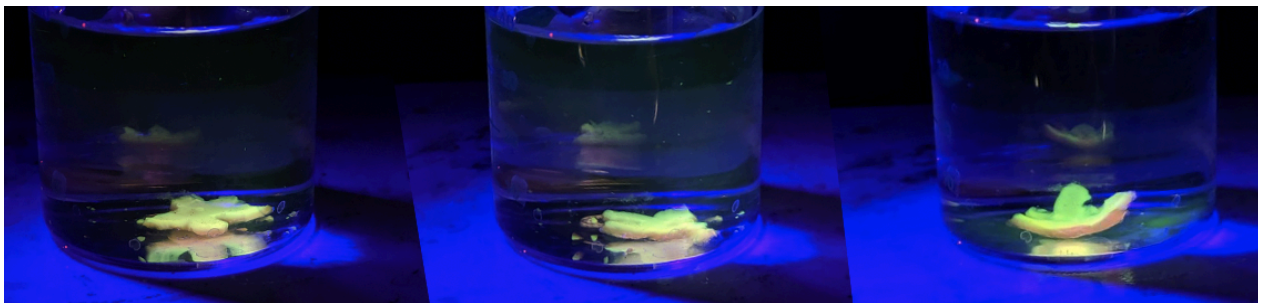

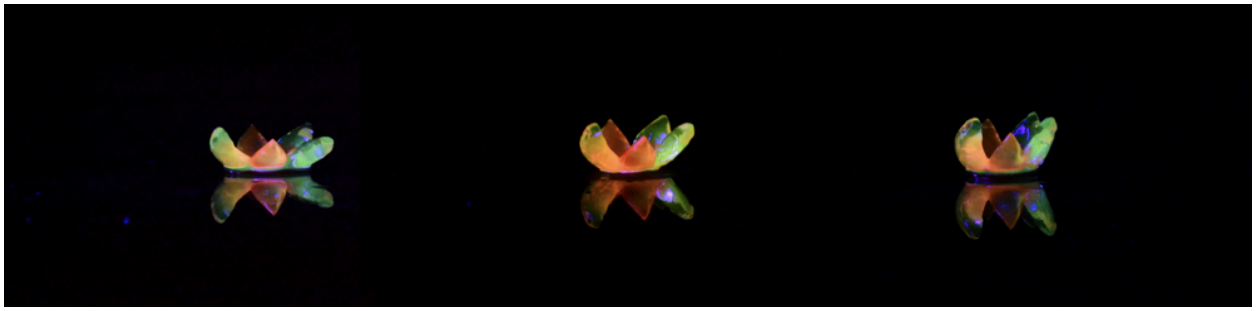

**Figure 20. Functionality of flower mold in hot and room temperature water**

Note that such fluorescent structures are difficult to synthesize using direct laser printing due to bleaching in UV light. Thermo-responsive hydrogel bilayers incorporating PNIPAAm as its thermosensitive element have been previously reported in literature and are generated by either forming one layer on top of another after complete gelation of the former or by adhering two layers together using an adhesive [69]–[73]. These bilayers are often employed as actuators in solutions that bend as the temperature exceeds the LCST of PNIPAAm. The PNIPAAm-co-PAAm-co-RHO precursor had a lower density than the PAAm-co-FOA precursor so we designed the mold such that the less dense precursor could enter from above and the denser precursor could enter from below (Figure 4cii). The resulting gel was a green and red hydrogel bilayer that closes like a flower when exposed to temperatures exceeding the top layers LCST, and additionally possessed a graduated interfacial boundary linking the two materials together (Figure 4ciii, Supp. Movie 2). By modifying the inlet flow rates of the precursors, we changed the thickness of the layers and modulated the contractile behavior of the resulting gel to our specification. Gels with greater complexity and functionality could be easily fabricated by modifying the mold geometry, the precursors, or the infiltration strategy.

Velocity Profile of a Particle Flowing in a Viscous Fluid using MATLAB

The objective of this section is to address numerical and computational tools in 3D Bioprinting. This way first, 3D printing can be used to validate the complex simulations and second, the flow models can be used to improve designs.

Investigated Analysis:

1.Microfluidic Gravity Separator Analysis in MATLAB

- Diffusivity
- Length of diffusion
- Drop rate of the particles

2.Microfluidic Y-Shaped Mixer Analysis in COMSOL

- Streamline/Flowline
- Velocity distribution
- Concentration gradient

What do we learn from other systems? A summary of previously reported papers are shown below:

**Table 1. Previously reported papers**

| Title of Journal | Parameters | Computational Methods |
|---|---|---|
| "Biomimetic shark skin: design, fabrication and hydrodynamic function" | surface roughness | SEM, Solidworks, Digital particle image velocimetry, Mimics 3D modeling software |

| | | |
|---|---|---|
| “Computational Fluid Dynamics and Additive Manufacturing to Diagnose and Treat Cardiovascular Disease” | Tensile stress and Wall shear stress (WSS) | Computational Fluid Dynamics |
| “Preferred interparticle spacings in trains of particles in inertial microchannel flows Y-shape channel “ | probability density function, relative motion of particles, steady-state separation | lattice Boltzman method in MATLAB |
| “Size-tunable microvortex capture of rare cells” | streamline and velocity distribution of the microvortex flow | COMSOL |

We have shown so far:

•Novel 3D printing method using multi-materials based on hydrogel

•Focusing on dynamics of fluid transfer on macro scale

•Co-infiltration, Sequential (same and different inlets), Diffusion methods

•Mechanical, Temperature, Transparency properties of gels

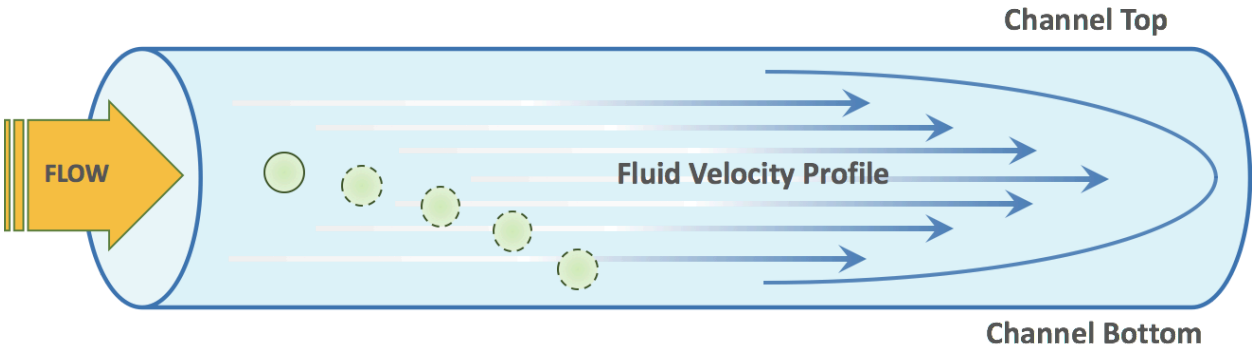


How long does it take the particle to fall the bottom?

Assumptions:

- •Laminar Flow (No Turbulence)
- •Incompressible fluid
- •Static viscosity
- •Constant pressure difference ΔP over length of channel
- •Constant circular cross-sectional area

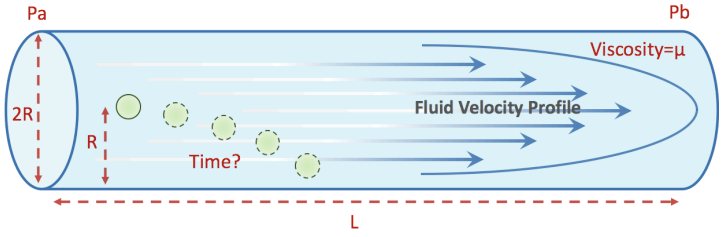


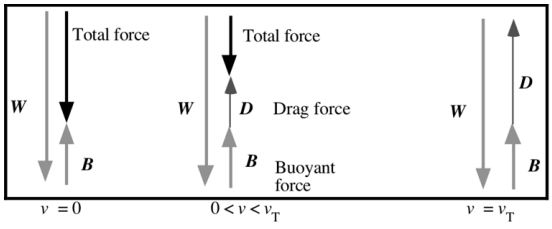


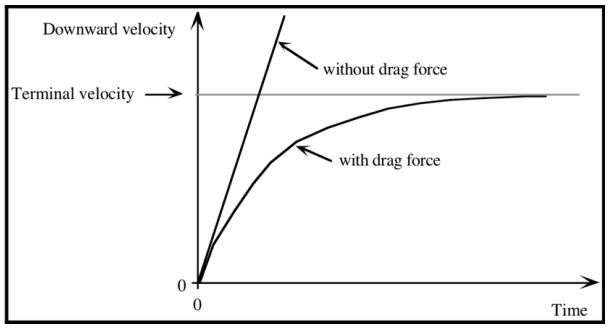

Motion Equation in Vertical Direction

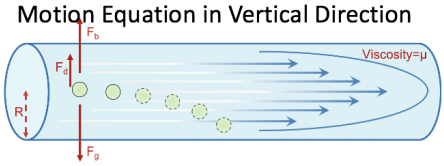


| | |
|---|---|
| Buoyant Force | $F_b = \rho_l g \frac{\pi dp^3}{6}$ |
| Drag Force | $F_d = 3\pi\mu dpup$ |
| Gravitational Force | $F_g = \rho_p g \frac{\pi dp^3}{6}$ |

$$Newton's\ 2^{nd}\ Law: \sum F = F_{gb} + Fd = ma$$

$$\frac{\pi dp^3}{6}(\rho_p - \rho_l) + 3\pi\mu dpup = m_p \frac{du_p}{dt}$$

$X = Vt \Rightarrow$

**Total Time:** $T \cong \frac{R}{u_{p0}}$

*(Effective acceleration period is generally of short duration for very small particles)*

Motion Equation in Horizontal Direction

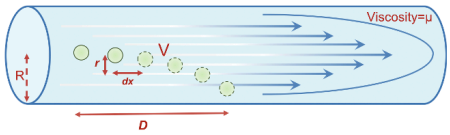


$Vmax = \frac{Q}{\pi R^2}$ Q is constant as we use syringe pump

$V = Vmax\ (1 - \frac{r2}{R^2}) \Rightarrow$ *Velocity is* ***not*** *dependent to Viscosity*

$$For\ each\quad r = \frac{2R}{N-1} \quad \Rightarrow \quad t = \frac{r}{u_{0p}}$$

$$dx = V * t \quad \Rightarrow$$

**Horizontal Displacement:** $D \cong \sum dx$

Dividing the problem into 2 parts:

1.Without the particle:

- What's the velocity at each point? -Poiseuille's Law

1.

$0 = \mu\nabla 2[vx(y,z)] - \nabla P$

$\Rightarrow \mu[\partial y2 + \partial z2]\ vx(y,z) = \partial xP(x)$

.

.

$$Q = \frac{\Delta P}{2\mu L} * \frac{A^2}{P^2} = \frac{\Delta P\ \pi R\text{^}4}{8\mu L}$$

$$Q = VS = V\pi R^2$$

$$V = \frac{\Delta PR\text{^}2}{8\mu L}$$

2.Adding the particle:

- Based on the velocity at each point, how long does it take to hit the bottom?

2.

$$\Delta h = \frac{g}{2} t2 + V(i-1)t$$
$$\Sigma h = R$$

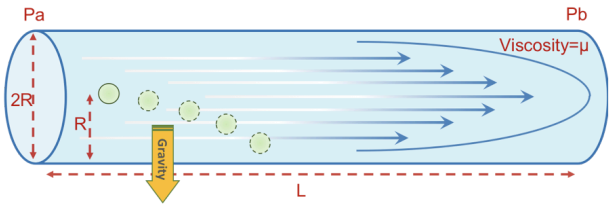


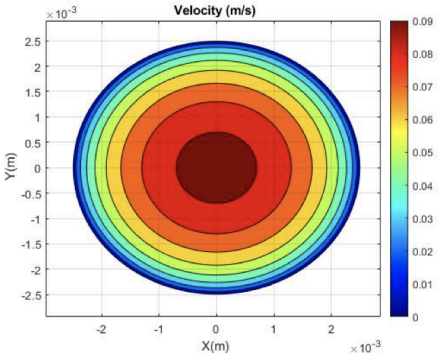


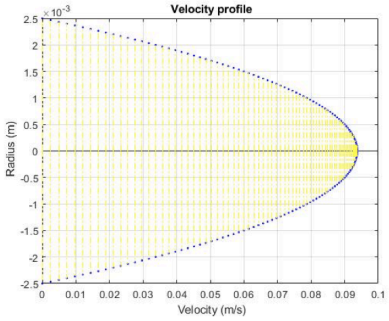


Constant Values:

| | |
|---|---|
| μ= 25m Pa.s; | (Viscosity of 10%PAM at room temperature)[1*] |
| R=2.5 mm | (2R=5mm) |
| Qa=0.5 ml/min; | (flow rate at the inlet) |
| Qb=0.1 ml/min; | (flow rate at the outlet) |
| Pa= μ/2 (Qa/A)^2; | (Bernoulli's Equation: Pressure at inlet) |
| Pb= μ/2 (Qb/A)^2; | (Bernoulli's Equation: Pressure at outlet) |
| L=2 cm; | (channel length) |
| g=9.8 m/s$^2$ ; | (acceleration of gravity) |
| $V_{particle}(0)=0$; | (velocity of particle at time=0) |

Total Time: 0.8071 s

For the parameters below the results are shown in figure 3.9.

| | |
|---|---|
| R=2.5 mm | (Diameter of the Channel) |
| d=390 μm | (Average diameter of PS spheres) |
| $\rho_F$= 1 g/ml | (Density of Fluid) |
| $\rho_p$= 1.05 g/ml | (Density of Polystyrene) |
| Q=0.5 ml/min; | (Volumetric Flow Rate) |

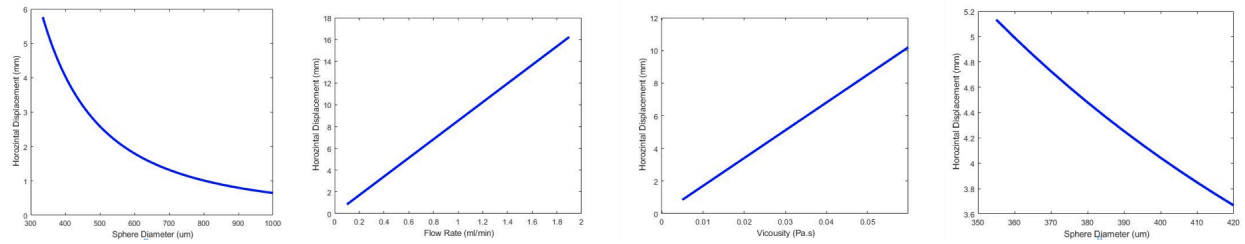


The simulation results of horizontal displacement are as below:

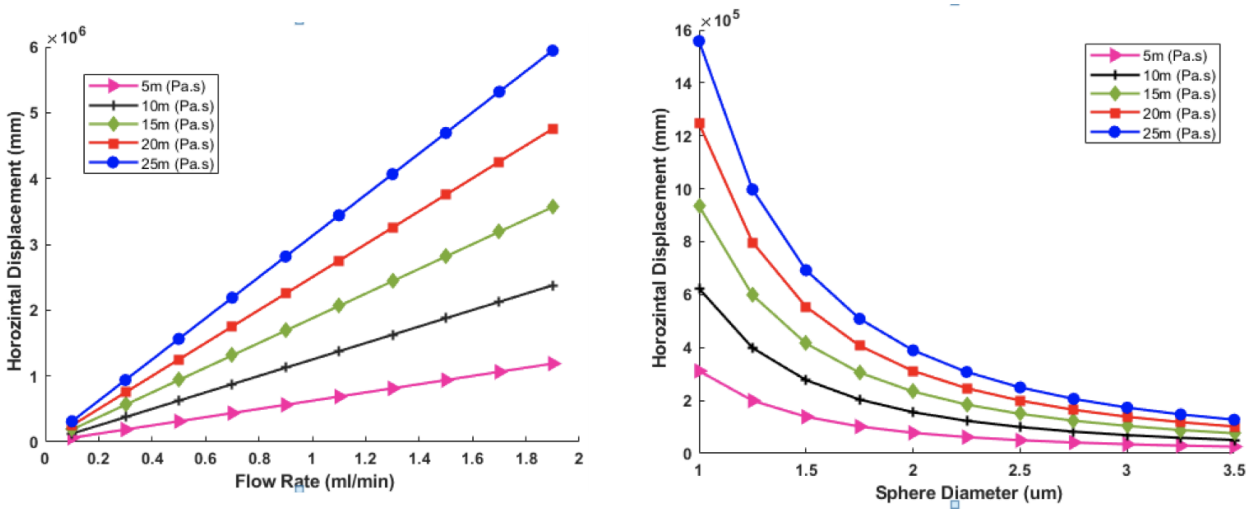


**Figure 21. simulation results of horizontal displacement**

For Y-shape mixer analysis in COMSOL we made few assumptions as listed: constant properties, no gravitational forces, incompressible fluid, and constant initial concentration in the system.

The initial conditions are defined as: initial concentration across the system = 0 T=300 K, P = 0 Pa, u = 0 m/s and for boundary conditions the inlet velocity is set as 10-6 and 10-5 m/s. The outlet pressure is set at p = 0 Pa since the pressure at the outlet is equal to atmospheric pressure. Additionally, the walls have the ideal no-slip condition. For the transport of diluted species profile, the inlet concentration is set at 1 mol/m3. The outflow area is also set where

diffusion is zero. The diffusion coefficient of the system is set at 1 ∗ 10- 9 m2/s. The concentration at inlet 1 is considered as 1 mol/m3 and at inlet 2 as 0. The parameters along with the values are listed in table 2.

**Table 2. Values of each parameter in separator simulation**

| Parameters | Value |
|---|---|
| Width of the channel | 1mm |
| Depth of the channel | 0.5 mm |
| Number of Loops | 3 |
| Flow Rate | 0.5 ml/min |

Transport of Diluted Species is chosen due to the flux and concentration gradients in the fluids. 1 mol/m3 and 0 mol/m3 concentration and single outlet is based on the design with best experimental results. We see effective mixing happened with 0.5 mol/m3 concentration. Navier–Stokes equations, fixed mean velocity and zero pressure at outlet with no backflow is considered during this study.

Results are shown in Figure.

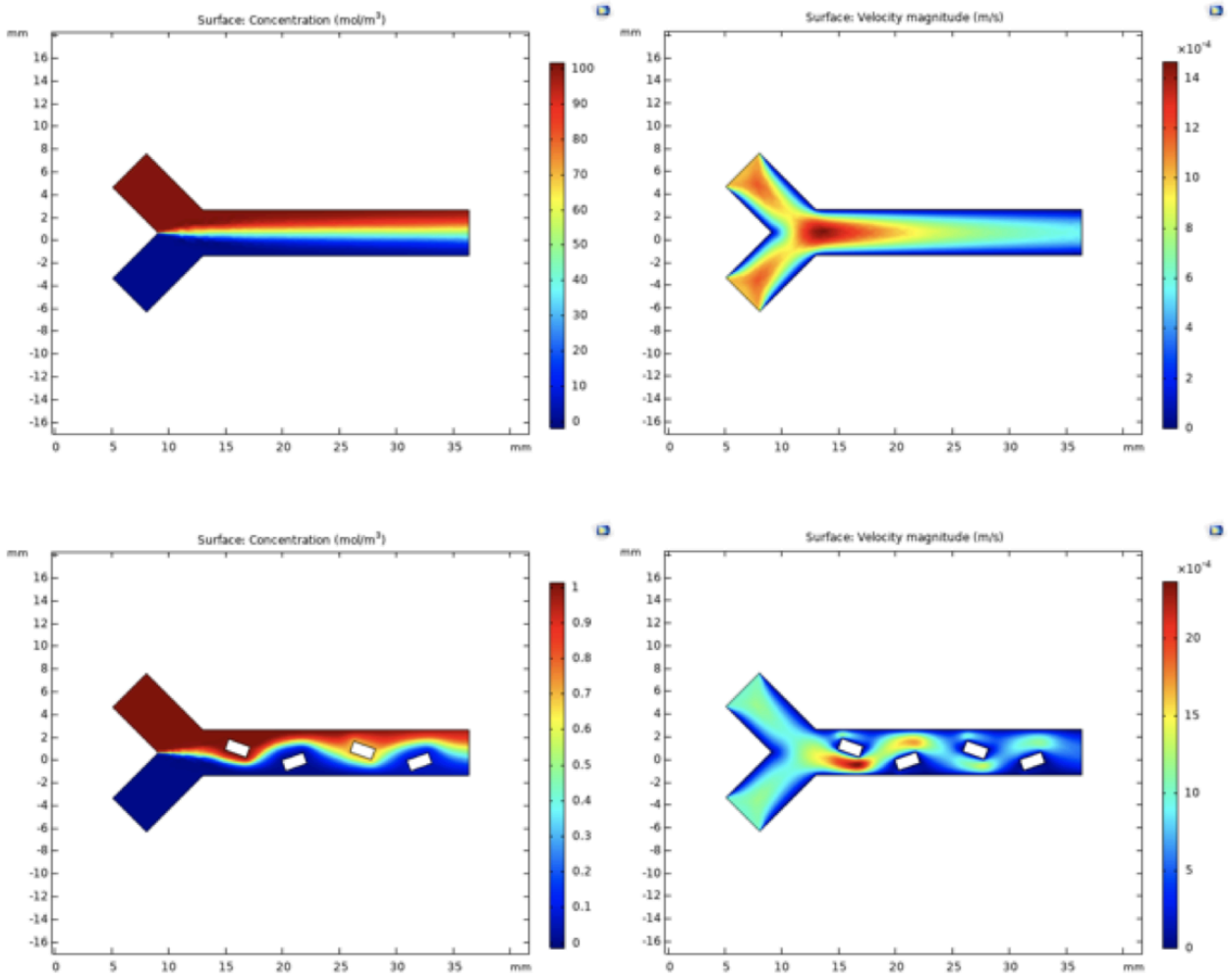


Modeling is done by considering fluid as an incompressible Newtonian liquid in a microchannel. For longer mixer the results are shown in figure 22 .

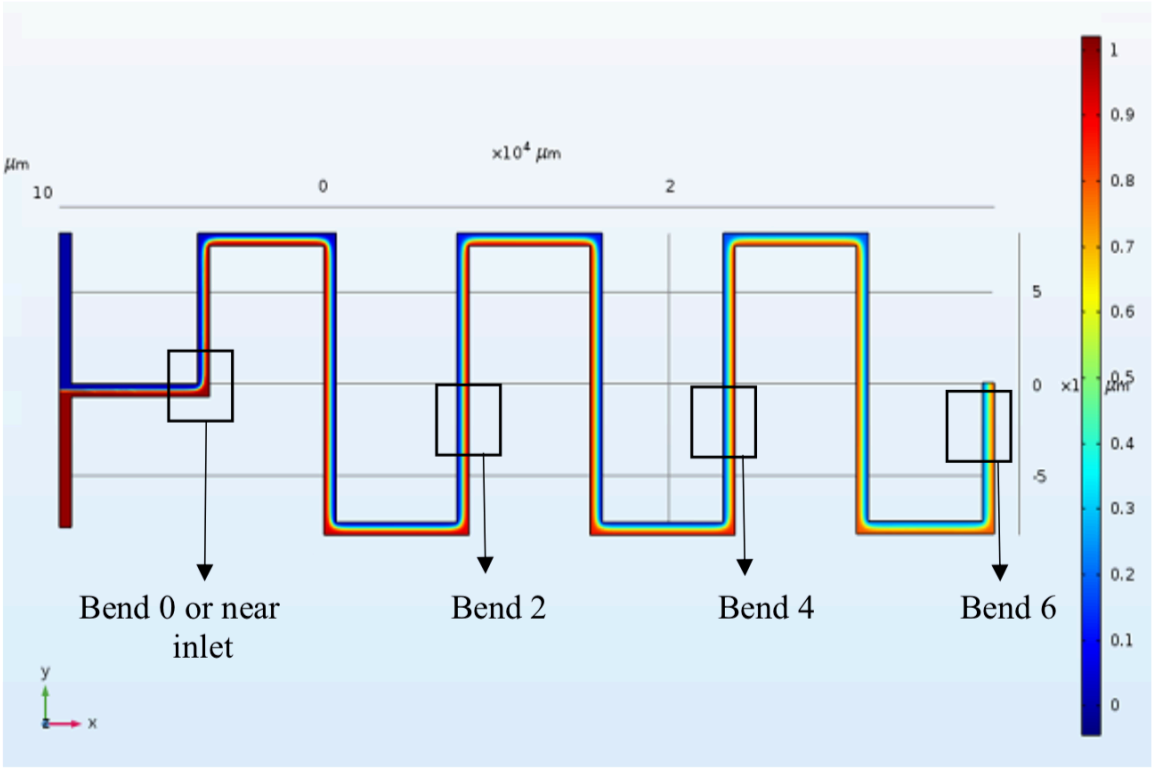
μm
10
0
×10⁴ μm
2
5
0
-5
×1
μm
1
0.9
0.8
0.7
0.6
0.5
0.4
0.3
0.2
0.1
0
Bend 0 or near inlet
Bend 2
Bend 4
Bend 6
y
x

**Table 3. Concentration and intensity of each corner in COMSOL**

| Width of the channel(X-axis×100µm) | Concentration value from COMSOL | Intensity Value from Experiment |
|---|---|---|
| 0 | 0.90593 | 0.90322 |
| 1 | 0.90592 | 0.90848 |
| 2 | 0.83562 | 0.79463 |
| 3 | 0.6419 | 0.59172 |
| 4 | 0.38193 | 0.30512 |
| 5 | 0.12488 | 0.15514 |
| 6 | 0.05039 | 0.0448 |
| 7 | 0.05026 | 0.01487 |

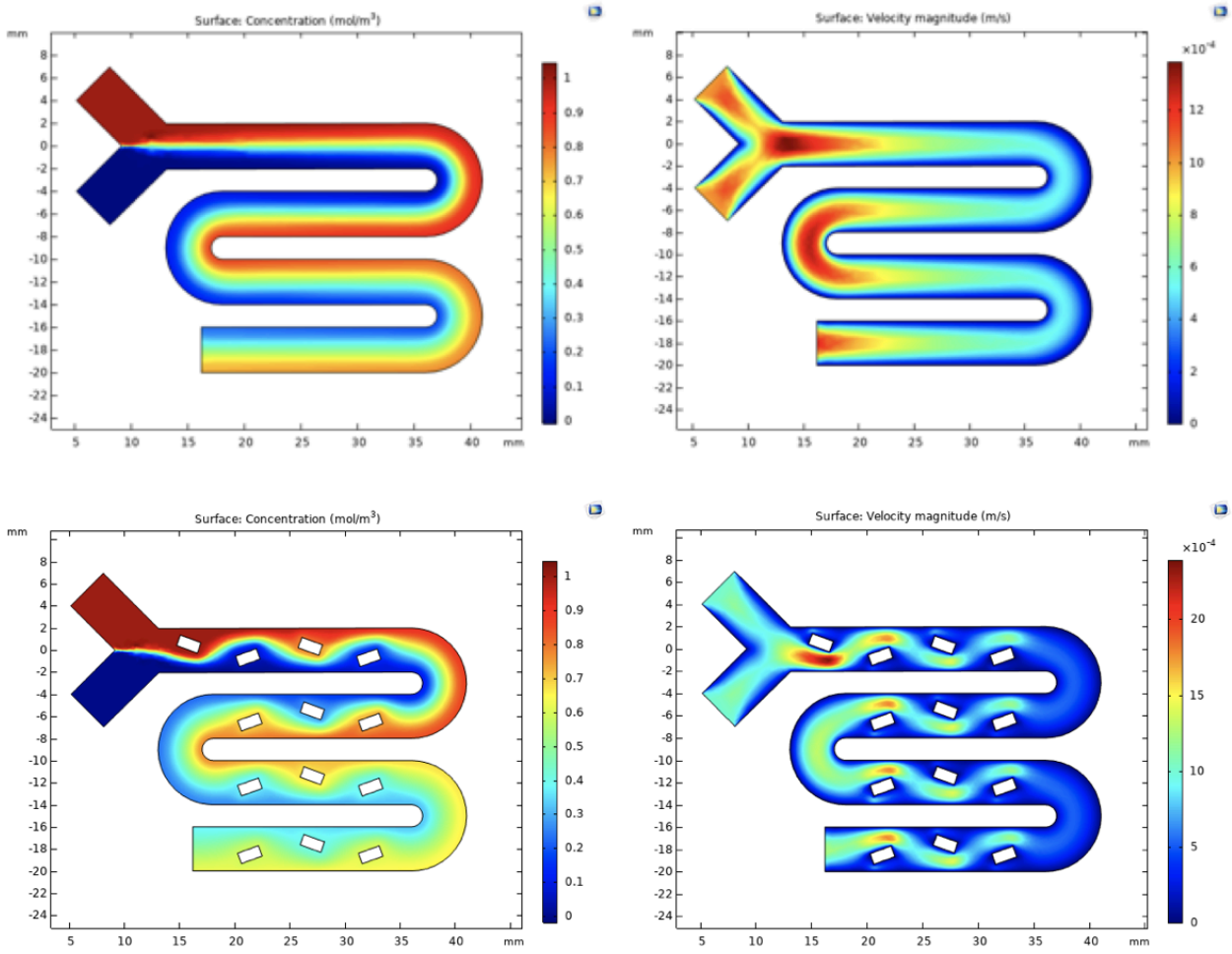


**Figure 22. Simulation result of longer mixer**

Streamline of a Particle Flowing in a Viscous Fluid using COMSOL

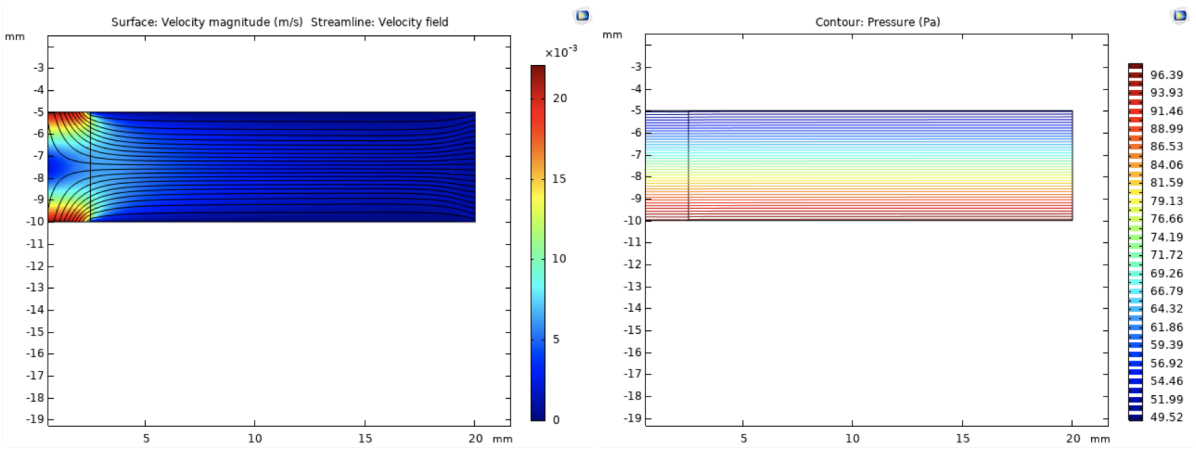


- Left side of triangle can't be defined as an inlet/outlet
- No PAM in material library: used **water**
- ✓ Drag, Gravity and Lift forces

| Name | Expression | Value | Description |
|---|---|---|---|
| u0 | 4.227155288520741e... | 4.2272E-4 m/s | Max_inlet velocity |
| H | 5[mm] | 0.005 m | Channel Height |
| L | 2[cm] | 0.02 m | Channel Length |
| rho_P | 1100[kg/m^3] | 1100 kg/m³ | Density of Particle |

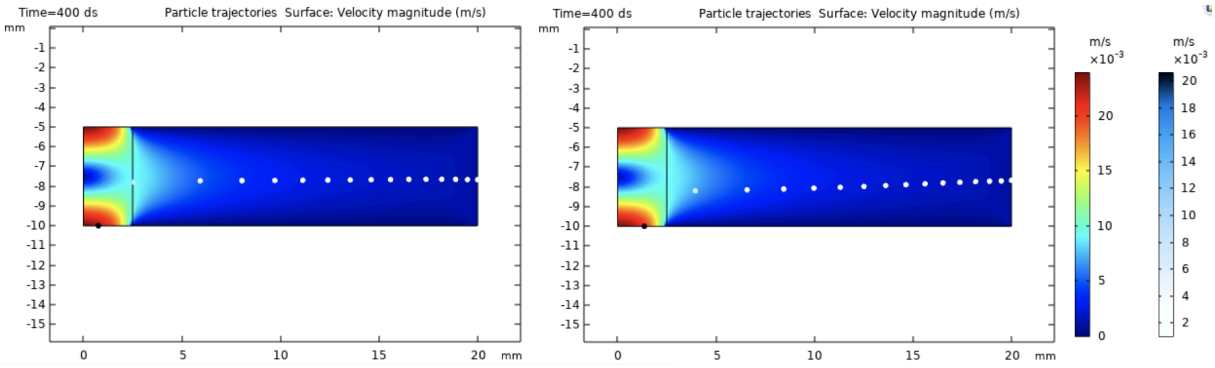


- Results for **PAM**
  - ➢ For small particles we should use longer/thinner channel

| Name | Expression | Value | Description |
|---|---|---|---|
| u0 | 4.227155288520741e... | 4.2272E-4 m/s | Max_inlet velocity |
| H | 5[mm] | 0.005 m | Channel Height |
| L | 2[cm] | 0.02 m | Channel Length |
| rho_F | 1000[kg/m^3] | 1000 kg/m³ | Density of Fluid |
| rho_P | 1100[kg/m^3] | 1100 kg/m³ | Density of Particle |
| mu0 | 0.025[Pa*s] | 0.025 Pa·s | Fluid Viscosity |
| | | | |

# Chapter 4: Developing conductive hydrogel film and bioelectric interfaces

## Materials

PEDOT:PSS aqueous solution (PH1000, Heraeus Clevios) was purchased from Heraeus, Germany. Dimethyl sulfoxide (DMSO) (purity ≥98%), D-(+)-gluconic acid δ-lactone (GDL) and calcium carbonate (CaCO3) were obtained from Sigma Aldrich. Sodium alginate (Na-ALG, viscosity 80 – 120 cp) was purchased from FUJIFILM Wako Pure Chemical Corporation. All chemicals were purchased and used without further purification. All aqueous solutions were prepared using deionized water (DI) unless otherwise stated.

## Methods

PEDOT/ALG Hydrogel Film Preparation

In order to make hydrogels with various mechanical and electrical properties, three different PEDOT:PSS/Alg precursor solutions were prepared at room temperature. The schematic of PEDOT/ALG hydrogel film preparation is shown in Figure 23 .

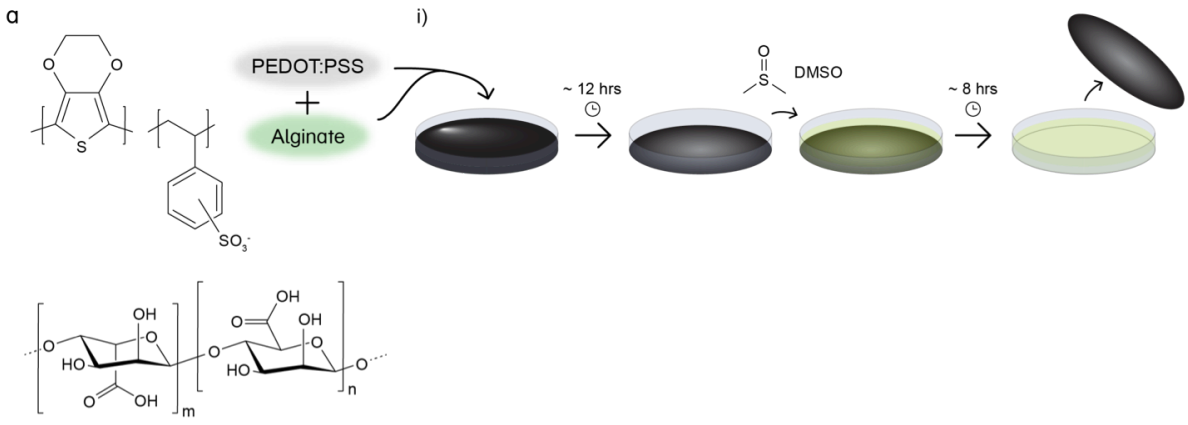

**Figure 23. Schematic of PEDOT/ALG hydrogel film preparation**

First, Alginate (Alg) 10 % was made by vigorously mixing 4 grams of Sodium Alginate in 40 mL deionized water using a magnetic stirrer until it completely dissolves.

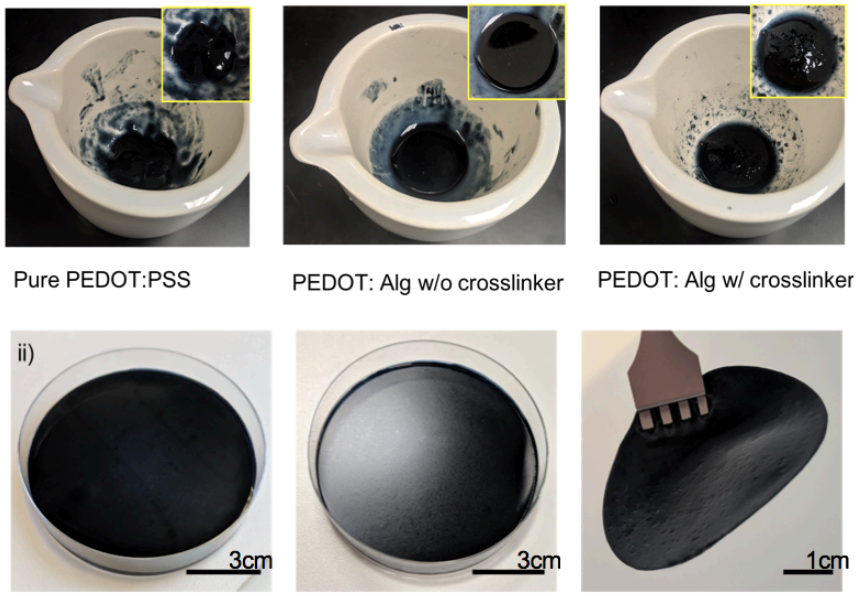


This Alginate was used in all samples and the remaining has been kept in the fridge 4 degree Celsius.

To Prepare PEDOT:PSS films, we added the pristine aqueous PEDOT:PSS solution into the Alginate precursor solution. To investigate the properties of the whole range of PEDOT:PSS/Alg compositions, we prepared three different concentrations of Alg. We made PEDOT:PSS/Alg 1:1 by mixing equal volumes of 1.3 wt% PEDOT:PSS and 1.3 wt% Alginate, PEDOT:PSS/Alg 1:3 by mixing equal volumes of 1.3 wt% PEDOT:PSS and 3.9 wt% Alginate, and PEDOT:PSS/Alg 3:1 by mixing three times the volume of 1.3 wt% PEDOT:PSS with respect to that of 1.3 wt% Alginate. We then added 16 mg/ml Gluconic acid and 4.5mg/ml Calcium Carbonate to accelerate the gelation of films. The solutions have then been strongly mixed

using vortex. Stirring the solutions between each step assures proper chemical bonding. The precursor solutions were then transferred into a substrate, usually petri dishes, and were kept under fume hood for minimum 12 hours at room temperature.

The petri dishes were left open to accelerate the drying sequence. Hydrogel films made with this method are referred to as 3:1, 1:1, or 1:3 PEDOT/Alg. Fig1 .a depicts this procedure.

Post-treatment

In order to form a conductive and mechanically stable film using secondary doping method, DMSO >99% was poured on the dried 1:3, 1:1 and 3:1 PEDOT:PSS and the thoroughly submerged films together with the petri dishes were left at room temperature for 8 hours after sealing the cap using parafilm to avoid the solution from evaporating. The films then easily detach from the substrate and can be kept in DMSO for over two months without any change in their mechanical and/or electrical properties for further characterization and analysis.


Fourier-Transform Infrared Spectroscopy (FTIR)

Fourier Transform Infrared Spectroscopy (FTIR) was used to characterize the presence of specific chemical groups in the materials. PEDOT/Alg films (control samples) and PEDOT/Alg films exposed in DMSO were obtained as 1–2 mm thick films and analyzed by FTIR using Transmittance Mode. FTIR spectra were obtained in the range of wavenumber from 400 to 4000 cm− 1 and normalized to show major vibration bands associated with chemical groups.

ALG Film Patterning

The patterning process begins with the preparation of a clean substrate, typically glass slides, onto which a uniform layer of PEDOT:Alg solution is deposited using standard coating

techniques. After drying, the desired pattern is visualized directly onto the PEDOT:Alg film, either through freehand sketching or with the aid of pictures being put underneath the glass slides. Subsequently, a sharp razor blade is employed to meticulously cut through the film along the outlined pattern. Careful attention is paid to ensure clean cuts without compromising the integrity of the substrate. Following the initial cutting, finer tools such as precision knives or micro-needles are utilized for pattern refinement, enhancing the accuracy and detail of the final pattern.

The samples were put in humidity chamber for 1 day, then in Ethanol 50% and 100% overnight .Degraded in HFIP 75% at T=70. Resistance right after was for 10% PAM: S1=3.6k, S2=15k. In Ethanol 50% and 100% overnight was examined and noticed that they are mechanically more stable than Alg.

- Stability over time for PEDOT:Alg 1:1 W/ DMSO

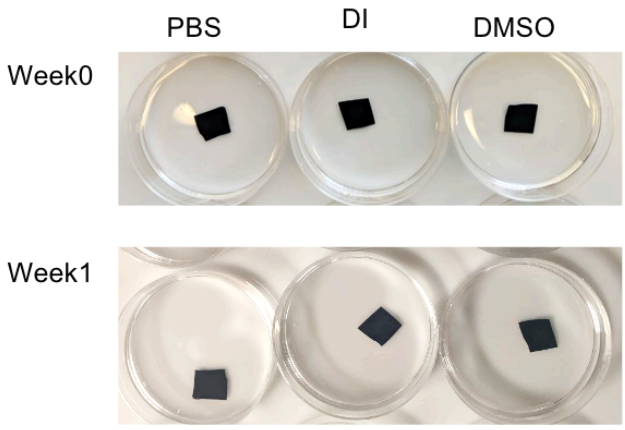


Scanning Electron Microscopy (SEM)

Scanning electron microscopy (SEM) was performed using an FEI Magellan 400 XHR Scanning Electron Microscope (Field Electron and Ion Company). Samples were mounted onto SEM-compatible stubs using conductive adhesive tape. The samples were then sputter-coated with a thin layer of Ir to enhance conductivity and minimize charging effects during imaging. Once coated, the samples were transferred to the microscope's vacuum chamber and secured to the stage. During imaging, the SEM was operated in high-vacuum mode to maintain optimal imaging conditions and prevent contamination of the electron column. Image acquisition and processing were carried out using integrated software, enabling real-time adjustments to focus, magnification, and contrast.

AFM was conducted using Tosca 400 AFM from Anton Paar Tapping mode, with arrow NCR cantilever, Typical resonant frequency ~285 kHz ✧Scan size: 500 nm x 500 nm Scan rate: 1 line/s.

Resistance Measurements

PEDOT/ALG films were cut into 1 x 2 cm2 rectangles and left to dry completely under ambient conditions (~10 minutes). Copper wires were attached to each end of the rectangles using conductive silver glue (epoxy adhesive (8331D, MG Chemicals)). A low resistivity meter (Loresta-GP MCP-T600, Mitsubishi) was used to measure the electrical conductivity of the films with the probes attached to the copper wires.

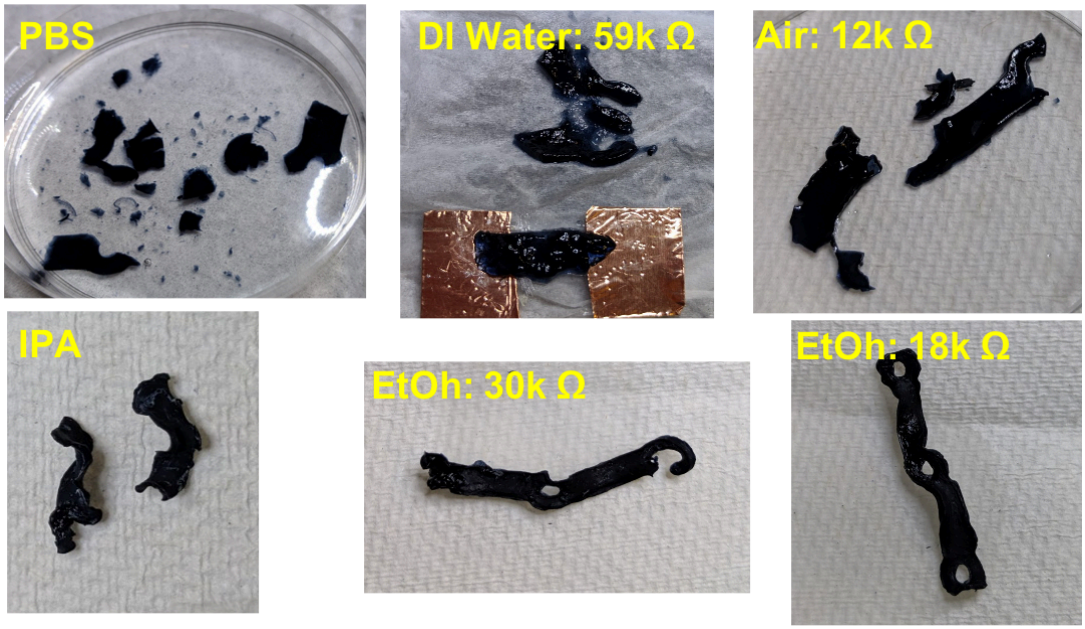


**Figure 24. Resistance in different solvents**

Dynamic Mechanical Analysis (DMA)

Uniform rectangular sections of 1:3, 1:1, and 3:1 PEDOT/ALG films were cut from larger films for tensile testing. For each PEDOT/ALG ratio, two conditions were tested: a control condition without DMSO treatment and an experimental condition with DMSO

treatment. Since the control films disintegrate when in contact with water, they were strained as dry films. The experimental samples were lightly dried using a delicate task wipe (Kimwipes, Kimtech™) before straining. Stress/strain curves for each film were obtained using a DMA Q800 (TA Instruments) equipped with a tensile clamp set to perform a force ramp at 0.1 N/min until sample failure.

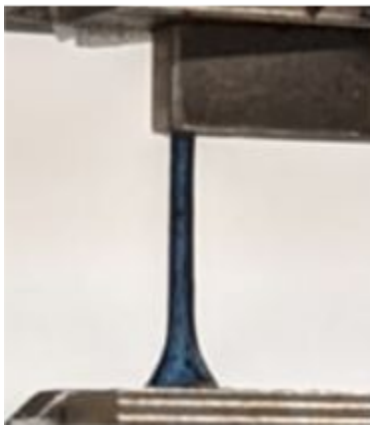

**Figure 25. Tensile set up**

Electromyography (EMG)

One of the main applications of conductive films is in electronic circuits and EMG. Firstly, a simplified circuit model was utilized to characterize the RC time constant of the material, as illustrated in Fig. 1a. The schematic of the parallel plate capacitor, featuring planar copper plates separated by a PEDOT:PSS conductive film, was employed to understand the electrical behavior of the material. The fabricated conductive films were placed in between two copper layers to make a capacitor (Figure 4.a. ) and then connected to a voltage source.

## Results

Drying ratio used to optimize the time where the samples are left in the fume hood to dry.

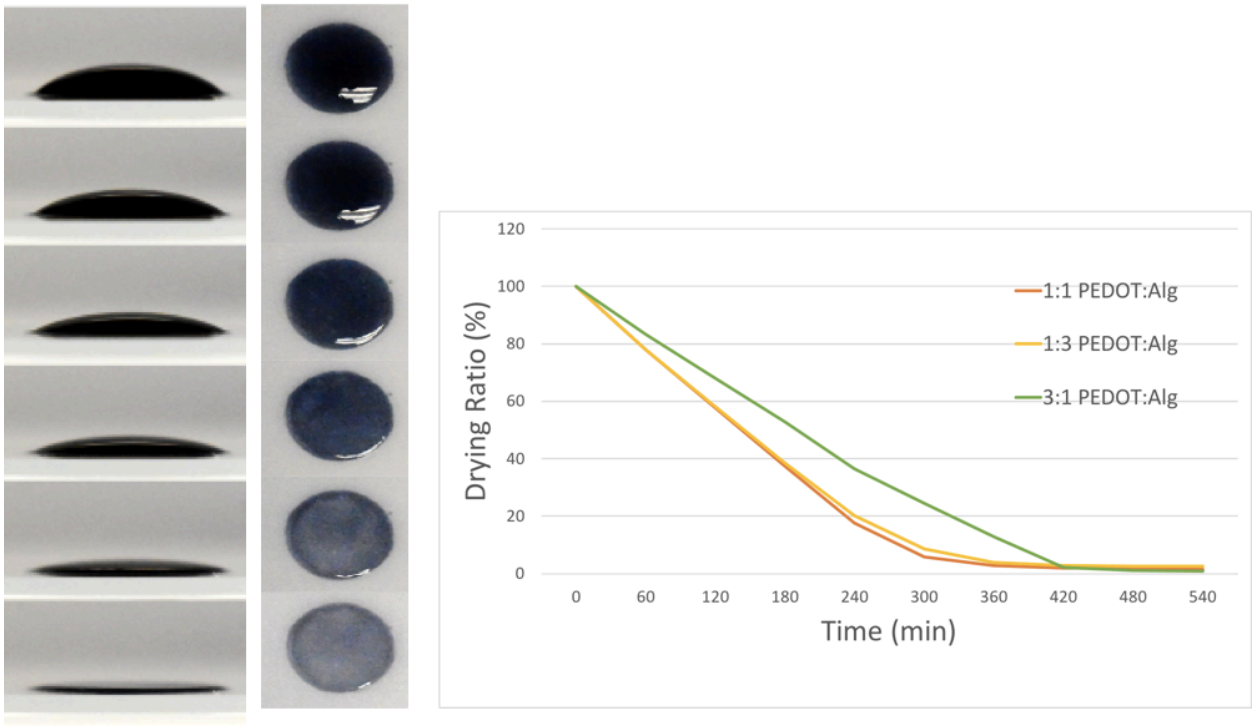


**Figure 26. Drying ratio**

Fourier-Transform Infrared Spectroscopy (FTIR)

Several methods, such as conductivity measurements, spectroscopy, microscopy, and mechanical testing, may be used to examine the obtained films. Figure 1b shows the Fourier Transform InfraRed (FTIR) spectra of 1:1 PEDOT:Alg as the control and 1:1 PEDOT:Alg with DMSO treatment using a FTIR spectrometer. As well as the absorption bands at 1564 cm-1 for the C=C stretching in the thiophene ring, at 1270 and 1122 cm-1 for the vibrations of the fused dioxane ring, and at 862 cm-1 for the stretching of the C–S bond in the thiophene ring [JMC] associated with PEDOT:PSS in both spectra, the absorption bands at 980, 2900 and

3000 confirms the presence of DMSO in films after post treatment with DMSO while in the control sample before adding DMSO those peaks are disappeared. Based on the FTIR spectra, adding DMSO does not damage the PEDOT:Alg chains and it allows re-orientation of the carboxylate groups and maintains the mechanical stability of the film.

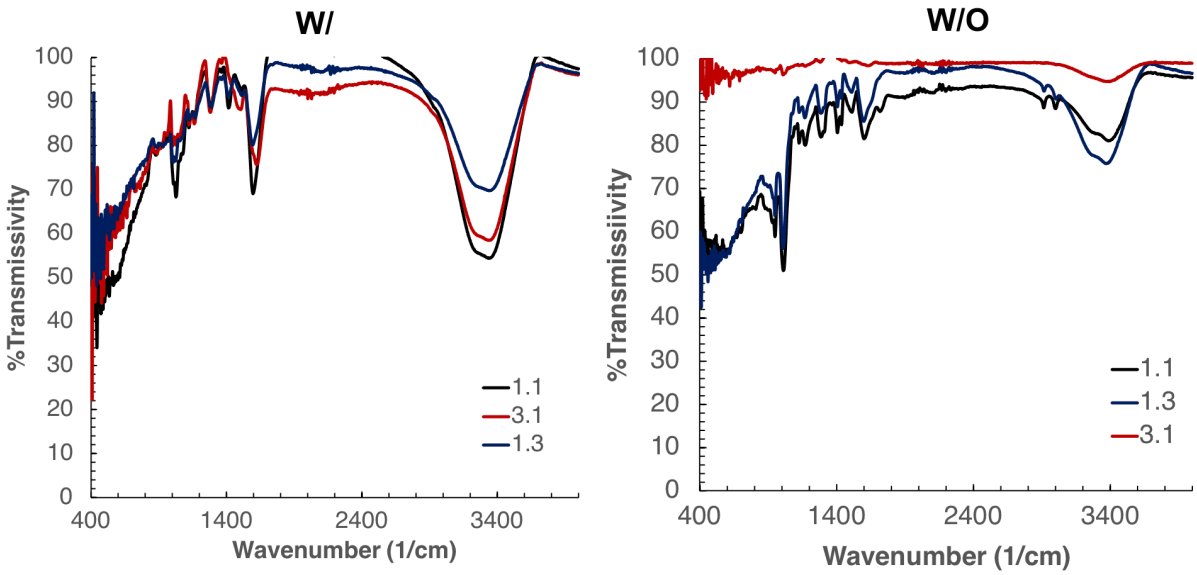


**Figure 27. FTIR spectra of different PEDOT:Alg with and without DMSO**

PEDOT/ALG Film Patterning

Patterning of conductive hydrogels is an important step in making bioelectronic. Due to their water content it is challenging to pattern hydrogel based films. Fig.1.c shows different pattering of our stretchable and conductive hydrogel films in different shapes including honeycomb, snowflake and Christmas tree to confirm the stability, patternability and homogeneity of the films, making them perfect applicants for use in a wide spectrum of applications in flexible sensors and actuators. These films are stable in different media and no

change in their physical condition has been noticed in DI water, PBS and ethanol after 6 months.


**Figure 28. Different 2D patterning of PEDOT:Alg films**

The honeycomb pattern, with its hexagonal symmetry, evokes the efficiency of natural architectures while enhancing the film's conductivity. Meanwhile, the branching structure of a tree highlights the adaptability of PEDOT:Alg to form intricate yet robust frameworks, mirroring the resilience found in nature. Lastly, the delicate symmetry of a snowflake demonstrates the potential for intricate patterning, opening avenues for applications in microelectronics and biosensing. This simple yet elegant approach to patterning PEDOT:Alg films not only showcases their aesthetic appeal but also underscores their potential for diverse functional applications.

Scanning Electron Microscopy (SEM)

In order to study the morphology of the PEDOT:PSS films, field emission scanning electron microscope (FESEM) images were used. Fig 2.a. shows the surface morphology of all films with different ratios of PEDOT to Alg and before and after emerging in DMSO. SEM images for PEDOT:Alg 3:1 samples are as below:

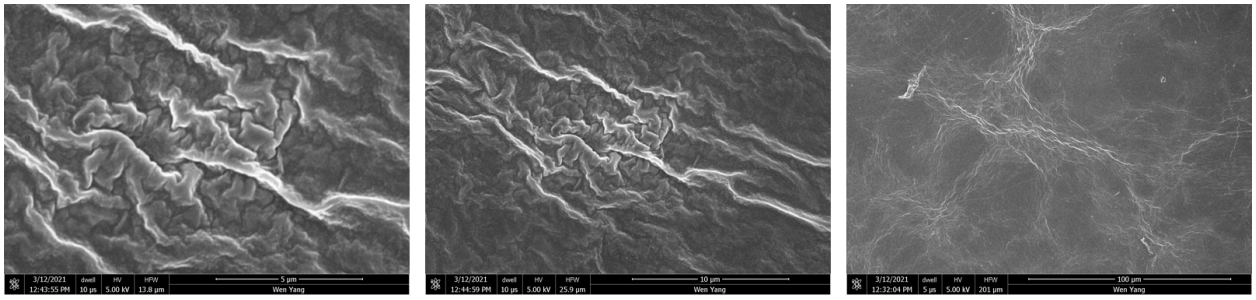

The control samples (before adding DMSO) show a homogeneous structure with irregular structure and variable pore size. On the other hand, FESEM pictures of the films that were submerged in DMSO exhibit a uniform interconnected structure due to the creation of long chains on the surface across the films. These long chains accelerate electron transfer and hence increase the conductivity which also have improved the mechanical response of these films. Moving from one side to the other side for electrons via these fibrous chains is easier if there are more PEDOT:PSS nanoparticles in the material rather than insulating polymers like hydrogels. This belief is clearly shown in Fig.2.a through increasing the percentage of Alginate in the film. 1:3 PEDOT:Alg in control films demonstrate more nano particles rather than 1:1 and 1:1 more than 3:1. This also has been shown for the same films after treating with DMSO overnight.

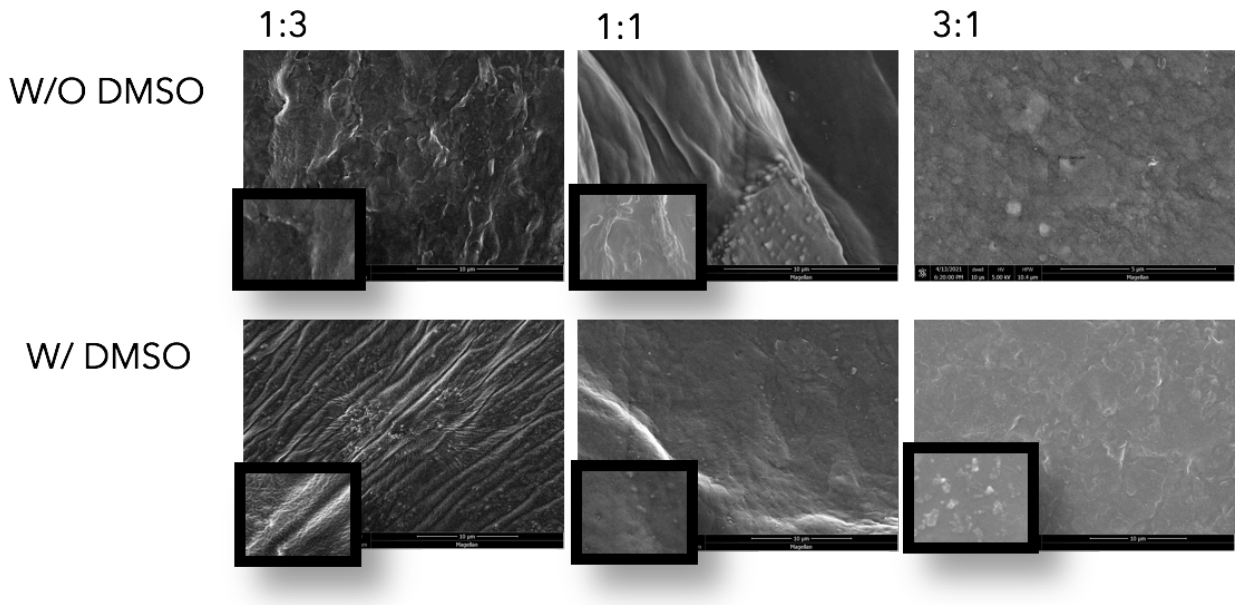


**Figure 29. SEM results of all PEDOT:PSS samples with and without DMSO.**

Atomic Force Microscopy (AFM)

Additionally, Figure 2.b. provides the corresponding AFM topography images of PEDOT:PSS/Alg 1:3, 1:1 and 3:1 before and after submerging them into DMSO. The roughness and the height of the 1:3 PEDOT:PSS/Alg samples clearly shows the composition of the samples are different and exposing the samples to DMSO creates stronger chains and therefore non-uniform and more stable films. By adding more PEDOT:PSS the roughness increases as well as the average height.

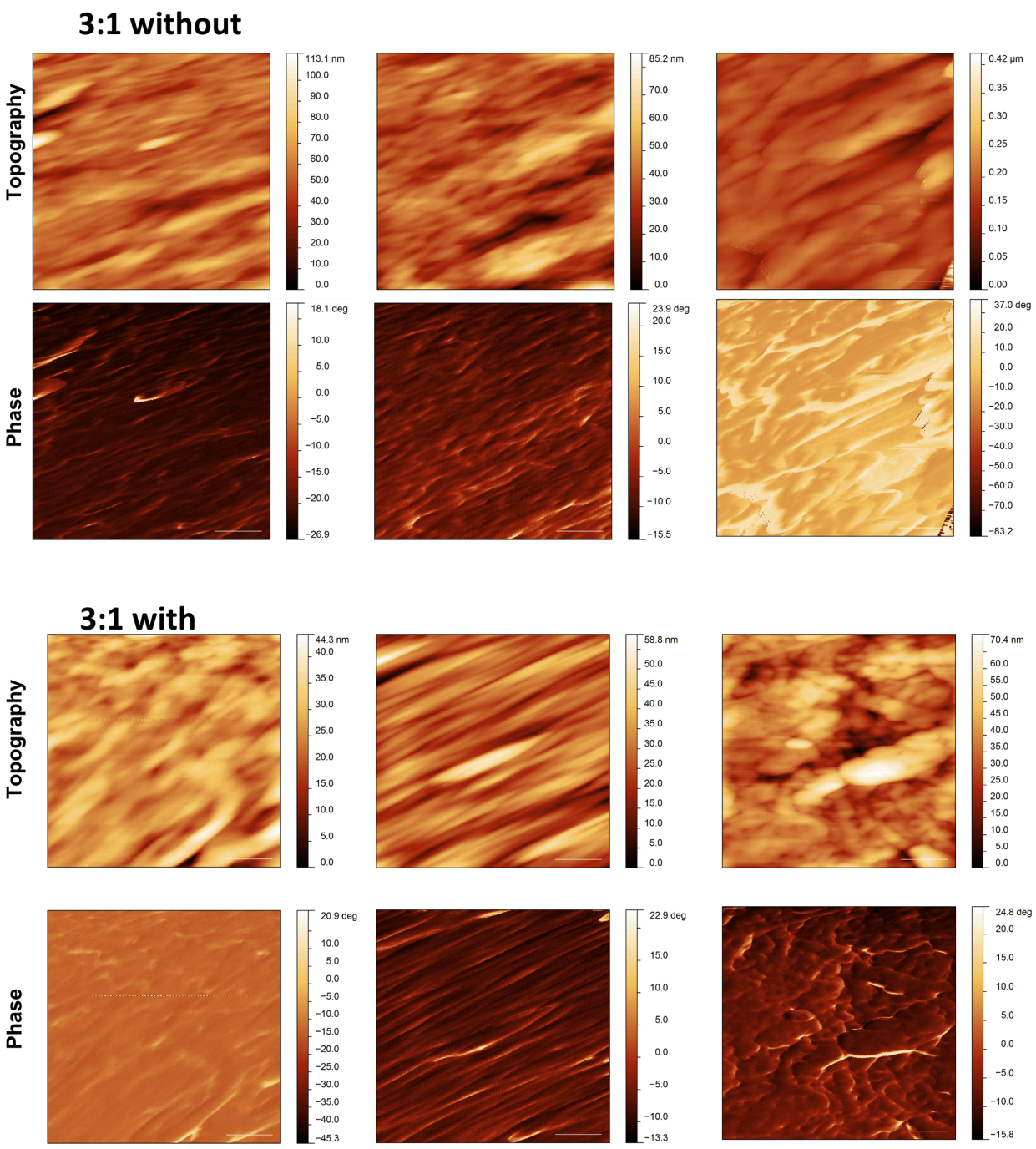
3:1 without
Topography
Phase
113.1 nm
100.0
90.0
80.0
70.0
60.0
50.0
40.0
30.0
20.0
10.0
0.0
85.2 nm
70.0
60.0
50.0
40.0
30.0
20.0
10.0
0.0
0.42 µm
0.35
0.30
0.25
0.20
0.15
0.10
0.05
0.00
18.1 deg
10.0
5.0
0.0
−5.0
−10.0
−15.0
−20.0
−26.9
23.9 deg
20.0
15.0
10.0
5.0
0.0
−5.0
−10.0
−15.5
37.0 deg
20.0
10.0
0.0
−10.0
−20.0
−30.0
−40.0
−50.0
−60.0
−70.0
−83.2
3:1 with
Topography
Phase
44.3 nm
40.0
35.0
30.0
25.0
20.0
15.0
10.0
5.0
0.0
58.8 nm
50.0
45.0
40.0
35.0
30.0
25.0
20.0
15.0
10.0
5.0
0.0
70.4 nm
60.0
55.0
50.0
45.0
40.0
35.0
30.0
25.0
20.0
15.0
10.0
5.0
0.0
20.9 deg
10.0
5.0
0.0
−5.0
−10.0
−15.0
−20.0
−25.0
−30.0
−35.0
−40.0
−45.3
22.9 deg
15.0
10.0
5.0
0.0
−5.0
−10.0
−13.3
24.8 deg
20.0
15.0
10.0
5.0
0.0
−5.0
−10.0
−15.8

## 1:1 without

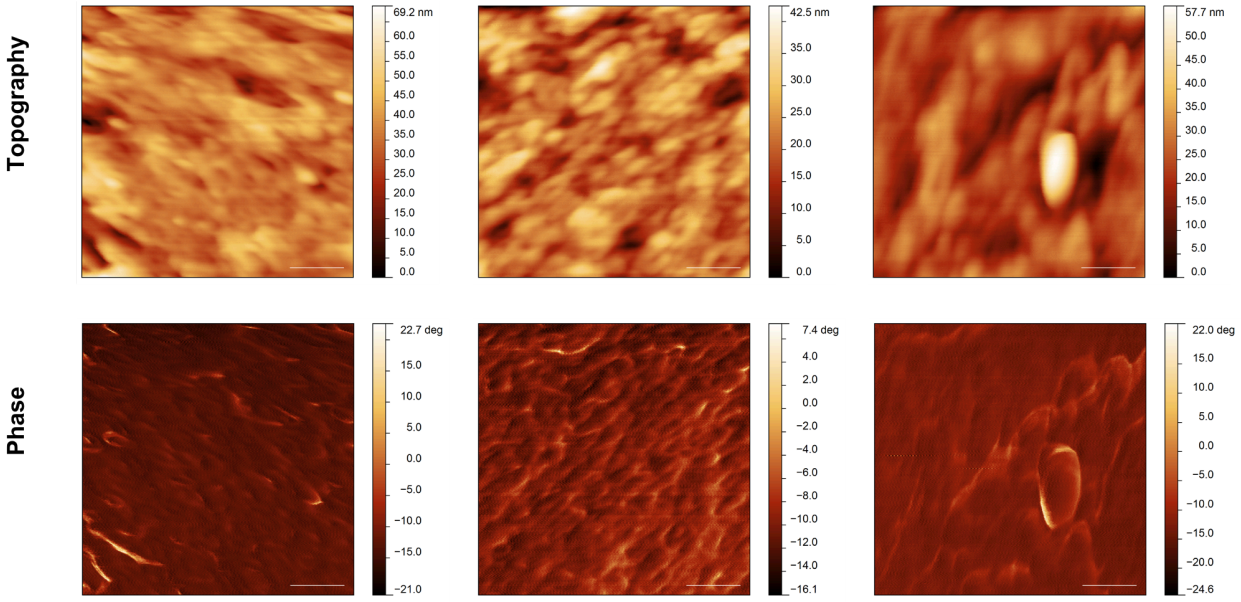


## 1:1 with

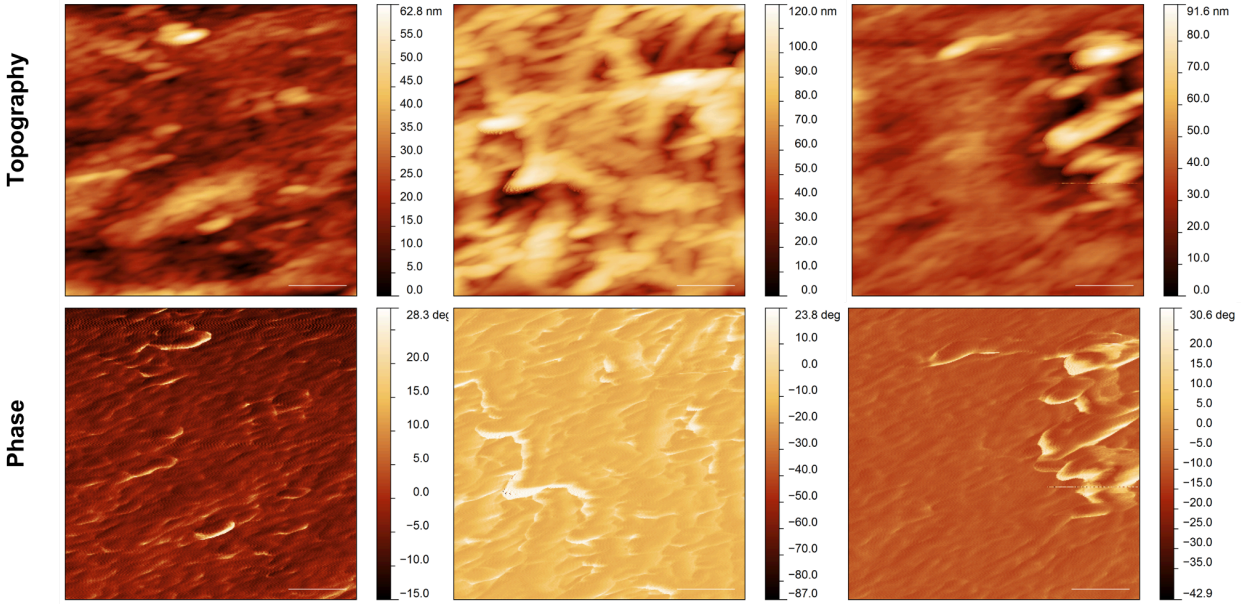

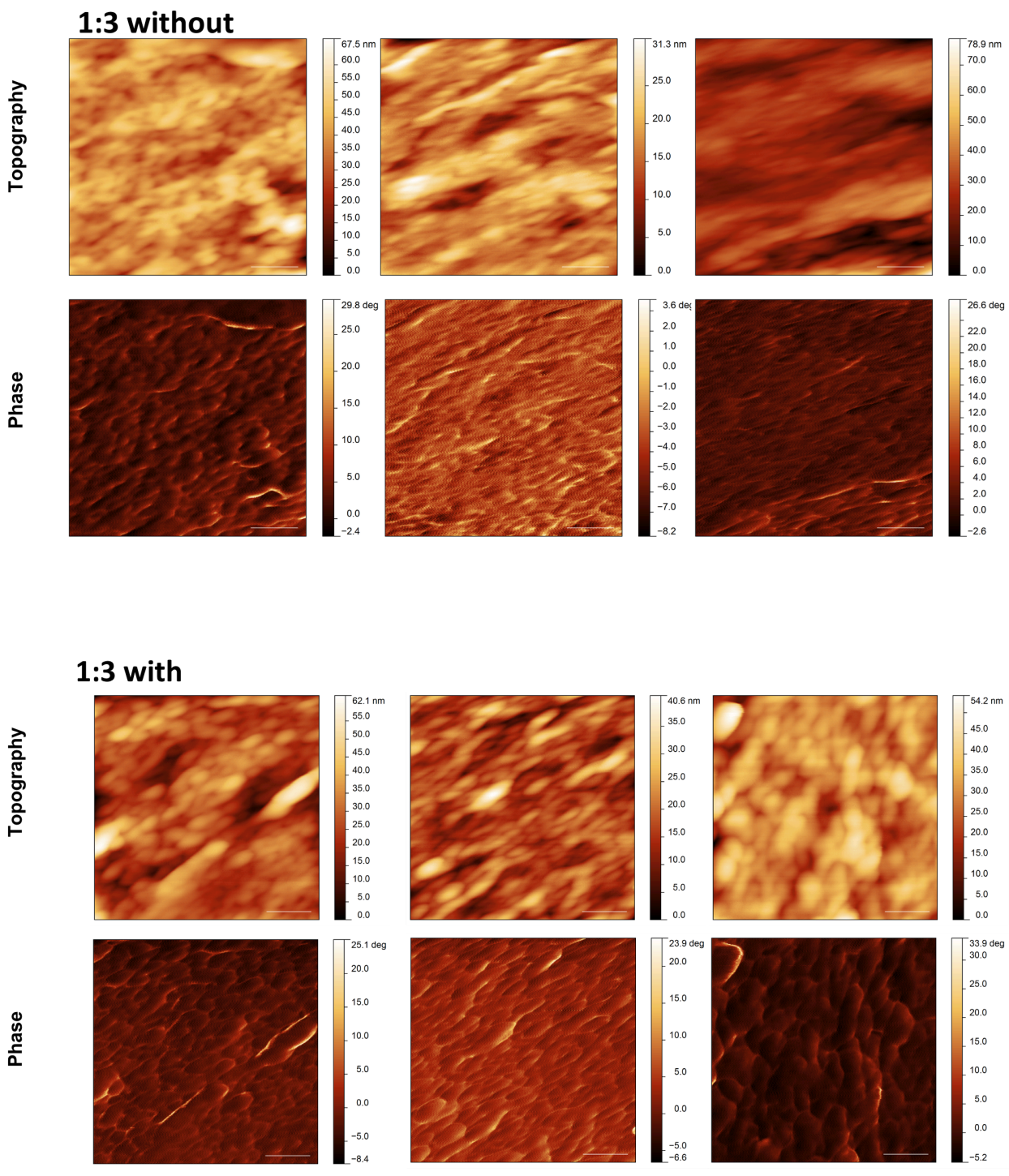


**Figure 30. AFM results of all PEDOT:PSS samples with and without DMSO.**

**Table 4. Roughness of 1:1 PEdOT:Alg samples with and without PDMS**

| Region | 1:1 without | 1:1 with |
|---|---|---|
| 1 | 6.63 | 7.451 |
| 2 | 5.3 | 16.47 |
| 3 | 6.762 | 10.364 |
| **Average (nm)** | **6.23** | **11.43** |

Resistance Measurements

The addition of PEDOT:PSS into alginate-based hydrogel films imparts the films with conductive properties, enabling them to function as substrates for biosensing applications.

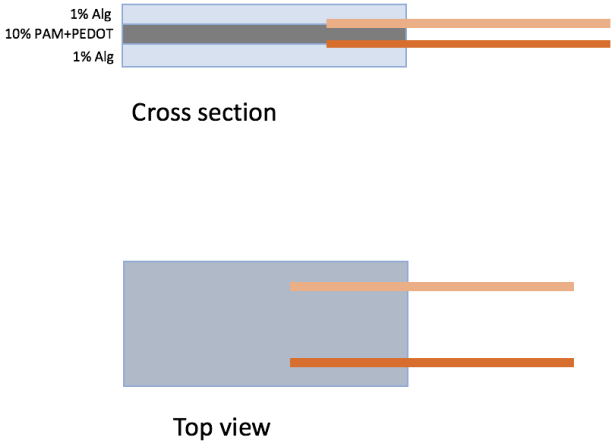


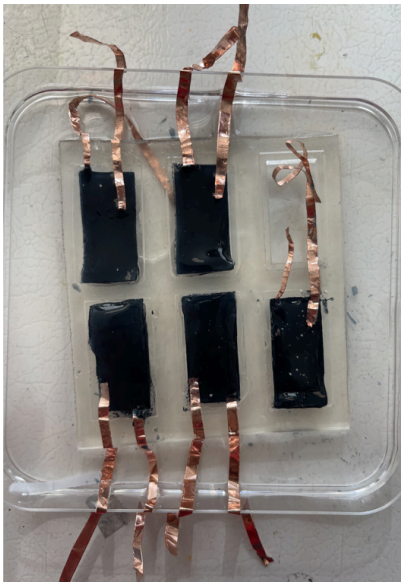

Upon the addition of PEDOT:PSS, a notable decrease in resistance was observed in the control samples, corresponding to an increase in the film's conductivity (Figure 3a). Furthermore, it was observed that films with a higher ratio of PEDOT:PSS exhibited increased conductivity, implying a correlation between the concentration of PEDOT:PSS and the enhancement of electrical conductivity in the films.

DMSO increase the conductivity (0.1 to1000 Scm-1 ) by extending PEDOT:PSS microgel particles from a trapped state into linear long chains.

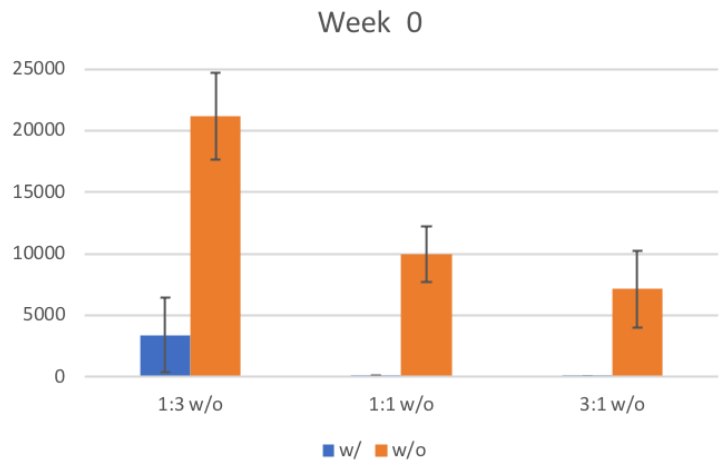


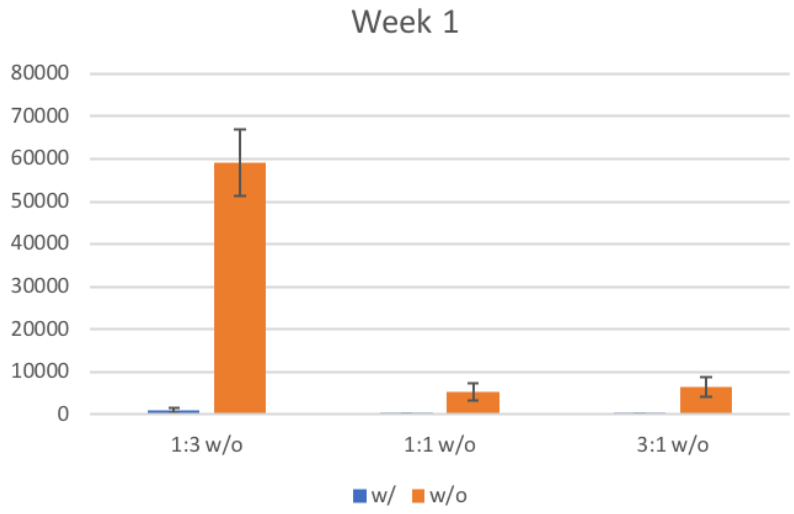

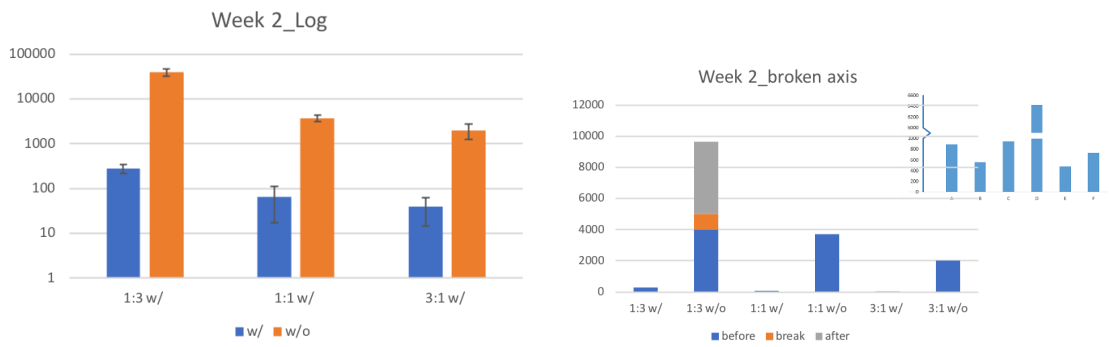


**Figure 31. Resistance of all PEDOT:PSS samples with and without DMSO over time.**

Exposure to DMSO further increases the conductivity of the PEDOT/ALG films due to X. Initially, the DMSO-treated samples exhibit higher resistance compared to the control samples, suggesting a less conductive nature induced by the solvent. The conductivity of the films after DMSO exposure increases by an order of magnitude for 1:3 PEDOT/ALG, two orders of magnitude for 1:1 PEDOT/ALG, and almost three orders of magnitude for 3:1 PEDOT/ALG. DMSO-treated PEDOT/ALG films retain this improvement over the course of two weeks and exhibit a similar slight increase in conductivity, corresponding to the decrease in resistance shown in Figure 3b, as the non-treated films.

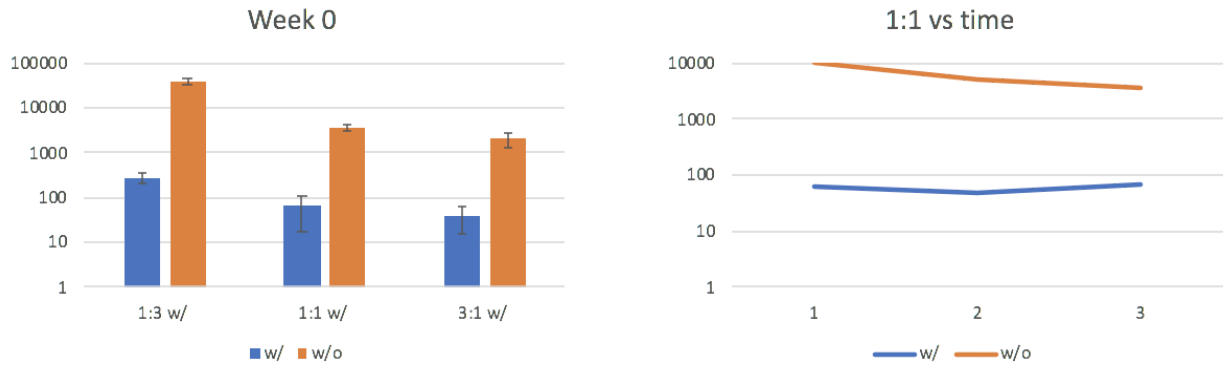

The observed decrease in resistance could be attributed to various factors such as increased intermolecular interactions, improved polymer chain alignment, or enhanced charge carrier mobility within the film structures. These findings suggest that while DMSO treatment initially impacts conductivity adversely, the long-term trend reflects an overall enhancement in electrical properties for both control and treated samples. These films can be stored at room temperature for up to two months without significant change in their conductivity. Further analysis is warranted to elucidate the underlying mechanisms driving this phenomenon and to optimize the fabrication process for desired conductivity outcomes.

Dynamic Mechanical Analysis (DMA)

Tensile tests were performed on rectangular sections of PEDOT/ALG films with varying ratios of PEDOT:PSS to alginate ratios (1:3, 1:1, 3:1) to assess the impact of DMSO on their mechanical properties. The DMSO-treated samples exhibited an increase in stretchability, as shown by their increased strain-to-break relative to the dry control samples, in exchange for a decrease in stiffness (Figure 3c-d).

This is likely attributed to lateral association of alginate chains caused by exposure to DMSO and additional solvent-induced gelation within the alginate network. Long-term, the PEDOT/ALG films show minimal mechanical degradation within a week of synthesis followed by consistent mechanical behavior afterwards (Figure 3e-f).

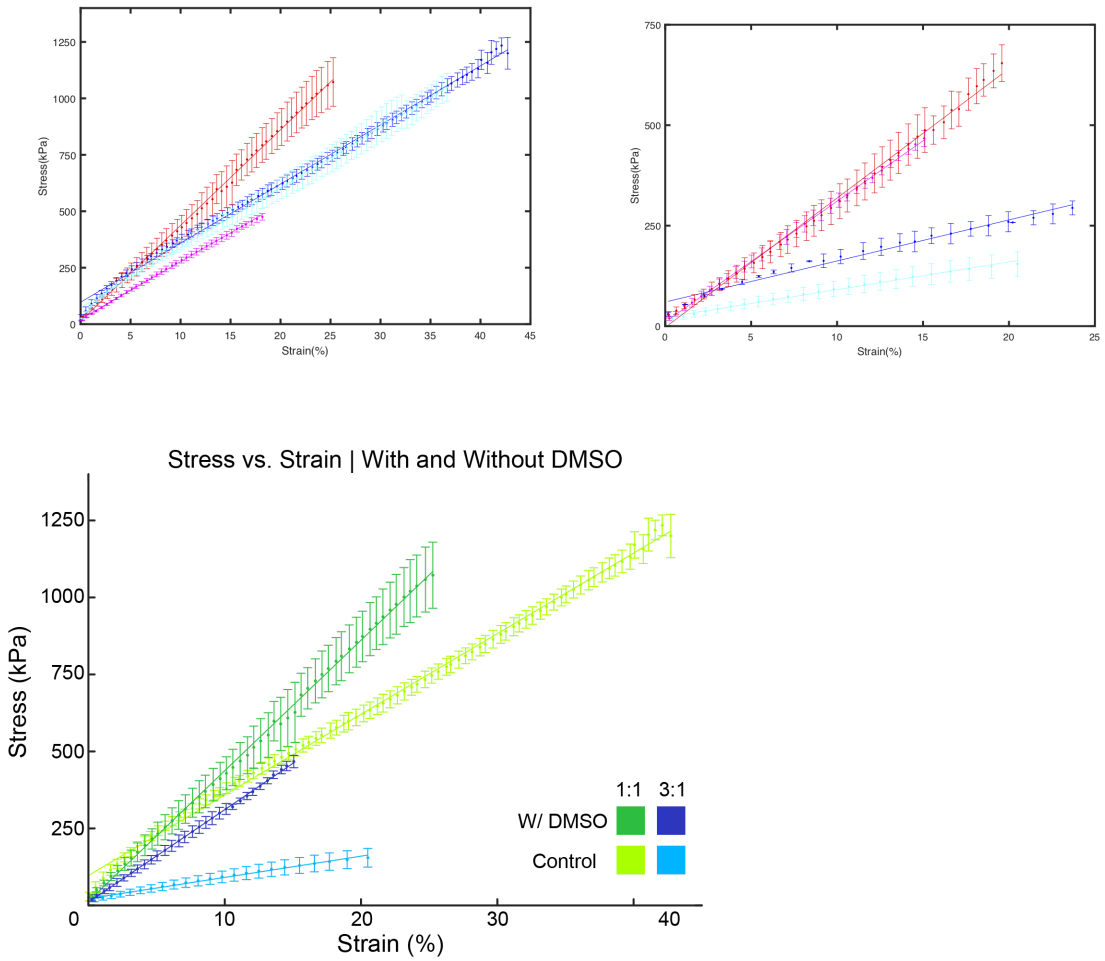


**Figure 32. Mechanical properties of all PEDOT:PSS samples with and without DMSO.**

And tensile results are as below:

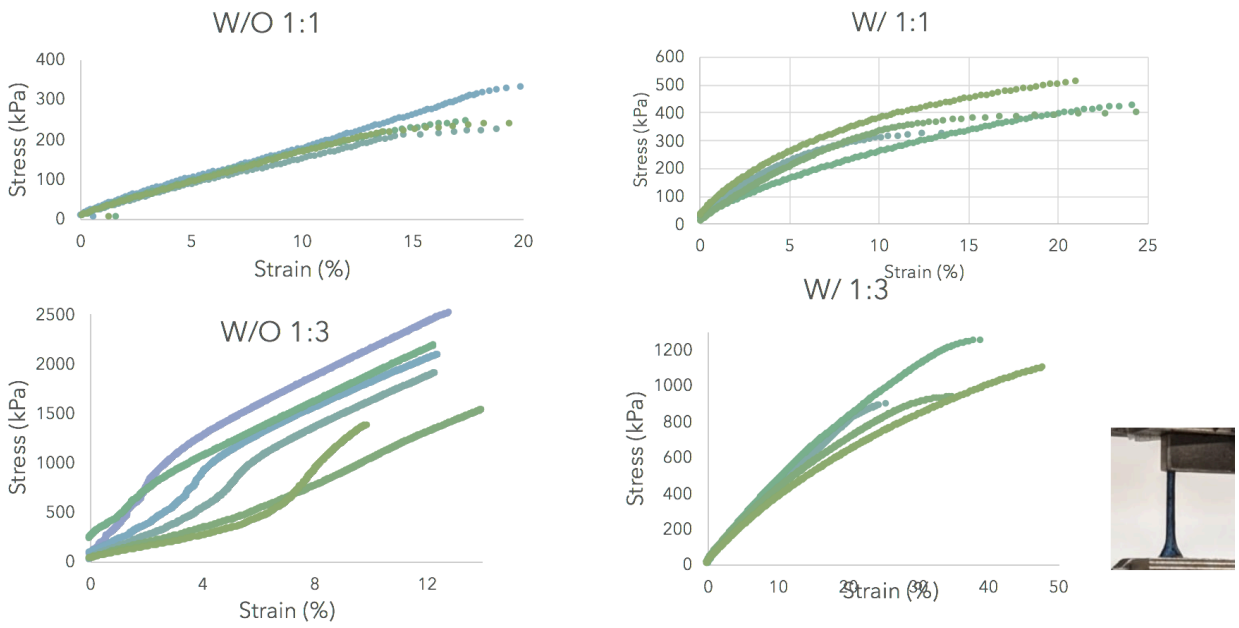


Electromyography (EMG)

Figure 4.b and 4.c show real time recording voltage signals for control and DMSO treated samples, respectively. The PEDOT:PSS conductive electrodes were prepared and then commercial three leads were connected to a portable Arduino microcontroller to collect the data indicating the potential of PEDOT:Alg films in wearable healthcare devices. The electrodes were placed on hand (Figure 4.d.) and upon closing or opening a spike will happen on the output signal. By comparing these two diagrams, we show that the PEDOT:PSS films that are treated with DMSO are more sensitive to motion than those without DMSO post treatment and they are considered better motion sensors, benefiting many applications.

EMG signals collected from the bicep are shown in figure .

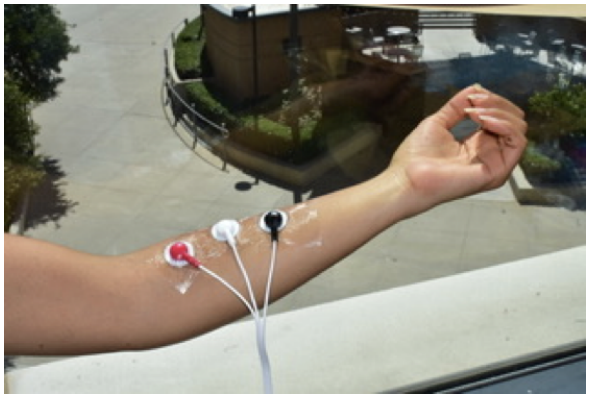


1200
1000
800
600
400
200
0
1 137 273 409 545 681 817 953 1089 1225 1361 1497 1633 1769 1905 2041 2177 2313 2449 2585 2721 2857 2993 3129 3265 3401 3537 3673

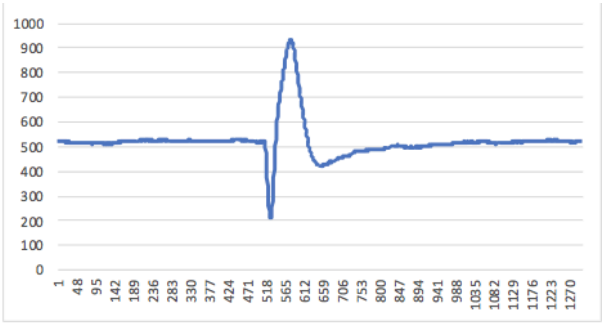
1000
900
800
700
600
500
400
300
200
100
0
1 48 95 142 189 236 283 330 377 424 471 518 565 612 659 706 753 800 847 894 941 988 1035 1082 1129 1176 1223 1270

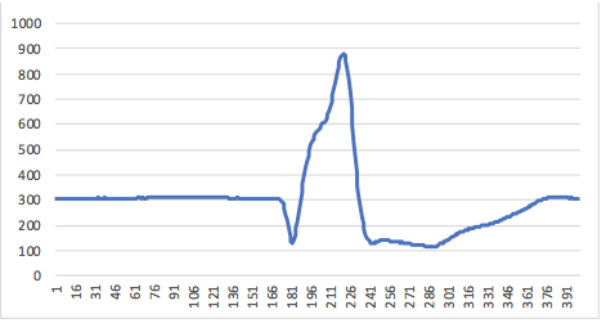
1000
900
800
700
600
500
400
300
200
100
0
1 16 31 46 61 76 91 106 121 136 151 166 181 196 211 226 241 256 271 286 301 316 331 346 361 376 391

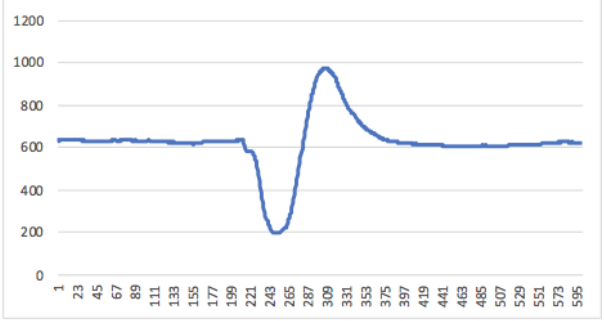
1200
1000
800
600
400
200
0
1 23 45 67 89 111 133 155 177 199 221 243 265 287 309 331 353 375 397 419 441 463 485 507 529 551 573 595

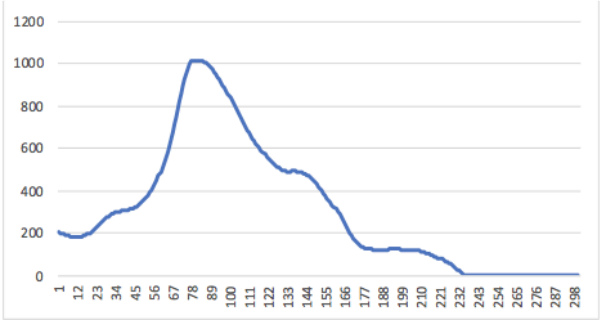
1200
1000
800
600
400
200
0
1 12 23 34 45 56 67 78 89 100 111 122 133 144 155 166 177 188 199 210 221 232 243 254 265 276 287 298


900
800
700
600
500
400
300
200
100
0
1 34 67 100 133 166 199 232 265 298 331 364 397 430 463 496 529 562 595 628 661 694 727 760 793 826 859 892

**Figure 33. EMG signals collected from the bicep**

Likewise signals from the forehead are shown in Figure .

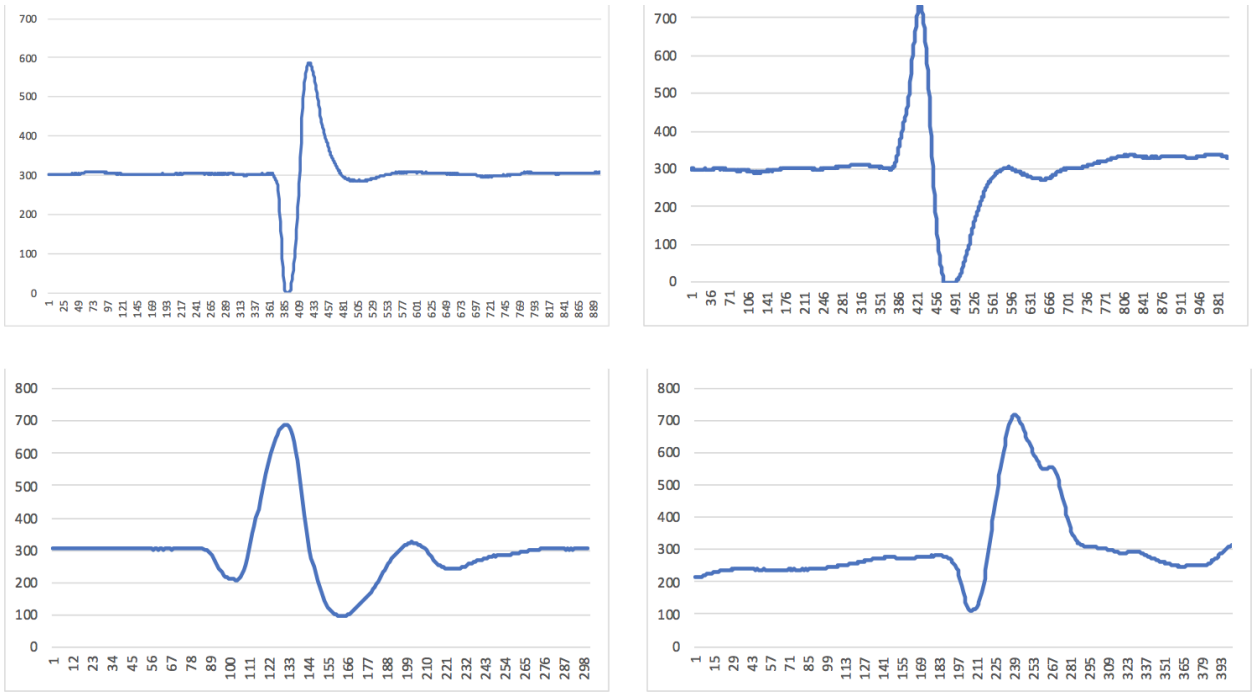


Figure 34 display EMG signals acquired from arm.

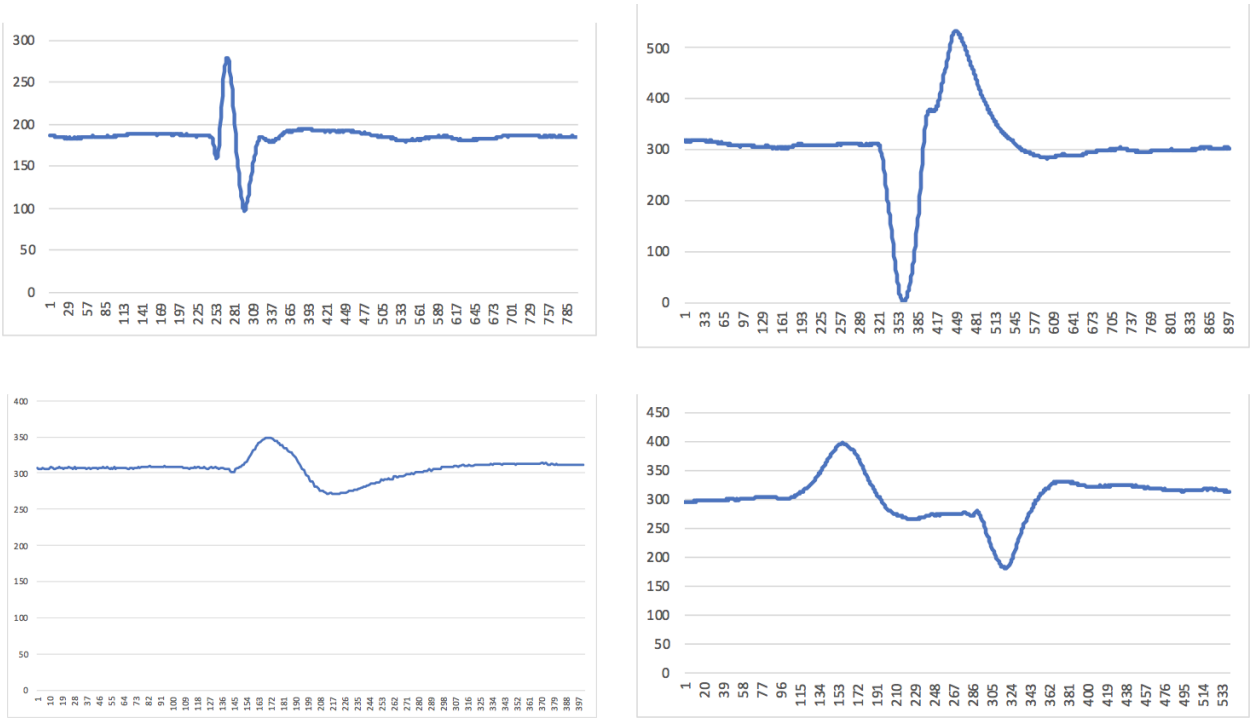

**Figure 34. EMG signals collected from the arm**

Showcases of EMG signals for different areas highlight the adaptability and reliability of PEDOT:Alg films in physiological monitoring applications. Overall, these findings underscore the promising prospects of PEDOT:Alg films in the field of flexible electronics and biomedical engineering.

## References

[1] Choi, C., Choi, J., & Oh, H. (2019). Recent advances in flexible and stretchable bio-electronic devices integrated with nanomaterials. Advanced Materials, 31(48), 1807888.

[2] Guex, A. G., Puetzer, J. L., & Armgarth, A. (2018). Conductive hydrogels: mechanically robust hybrids for use as biomaterials. Macromolecular Bioscience, 18(11), 1800109.

[3] Li, G., & Mooney, D. J. (2016). Designing hydrogels for controlled drug delivery. Nature Reviews Materials, 1(12), 16071.

[4] Sun, J. Y., Zhao, X., & Illeperuma, W. R. K. (2012). Highly stretchable and tough hydrogels. Nature, 489(7414), 133-136.

[5] Caló, E., & Khutoryanskiy, V. V. (2015). Biomedical applications of hydrogels: a review of patents and commercial products. European Polymer Journal, 65, 252-267.

[6] Hoffman, A. S. (2012). Hydrogels for biomedical applications. Advanced Drug Delivery Reviews, 64, 18-23.

[7] Wu, Z. L., & Moshe, M. (2017). Three-dimensional shape transformations of hydrogel sheets induced by small-scale modulation of internal stresses. Nature Communications, 8(1), 15800.

[8] Zhao, X., & Kim, J. (2016). Stretchable conductive hydrogels for wearable electronics and flexible energy storage. Journal of Materials Chemistry A, 4(12), 4466-4479.

[9] Hoffman, Allan S., and Laura E. Schoen. "Biomaterials for tissue engineering." Circulation research 95.1 (2004): 111-121.

[10] Annabi, Nasim, et al. "Engineering a highly elastic human protein–based sealant for surgical applications." Science translational medicine 9.410 (2017).

[11] Lee, Kuen Yong, et al. "Hydrogels for biomedical applications: their characteristics and the mechanisms behind them." Tissue Engineering and Regenerative Medicine 17.3 (2020): 313-325.

[12] Caló, Enrica, and Vincenzo V. Khutoryanskiy. "Biomedical applications of hydrogels: A review of patents and commercial products." European Polymer Journal 65 (2015): 252-267.

[13] Annabi, Nasim, et al. "Engineering complex tissues." Regenerative Biomaterials 3.2 (2016): 99-107.

[14] Peppas, Nicholas A., and Ali S. Hoffman. "Hydrogels as dynamic biomaterials." Biomaterials science: an introduction to materials in medicine. Academic Press, 2013. 137-151.

[15] Wang, Quan, and Yi Hong. "Thermoresponsive hydrogels for biomedical applications." Chemical Society Reviews 42.17 (2013): 7335-7372.

[16] Hoffman, Allan S., and Laura E. Schoen. "Biomaterials for tissue engineering." Circulation research 95.1 (2004): 111-121.

[17] Langer, Robert. "Drug delivery and targeting." Nature 392.6679_suppl (1998): 5-10.

[18] Boateng, Joshua S., and Kofi O. Auffret. "Wound healing dressings and drug delivery systems: A review." Journal of pharmaceutical sciences 97.8 (2008): 2892-2923.

[19] Lee, Kuen Yong, et al. "Hydrogels for biomedical applications: their characteristics and the mechanisms behind them." Tissue Engineering and Regenerative Medicine 17.3 (2020): 313-325.

[20] Duan, Xiaonan, et al. "Hydrogel-based biosensors for in vitro diagnostics." Analytical chemistry 89.1 (2016): 102-123.

[21] Yao, Haixin, et al. "Biosensors based on DNA-functionalized hydrogels." Chemical Society Reviews 48.14 (2019): 3771-3796.

[22] Son, Donghee, et al. "Hydrogel electronics with tunable mechanical properties." Advanced Materials 25.36 (2013): 5078-5084.

[23] Yuk, Hyunwoo, et al. "Hydrogel bioelectronics." Chemical Society Reviews 48.6 (2019): 1642-1667.

[24] Bandodkar, Amay J., and Joseph Wang. "Non-invasive wearable electrochemical sensors: a review." Trends in biotechnology 32.7 (2014): 363-371.

[25] Kim, Jang-Ung, et al. "Epidermal electronics." Science 333.6044 (2011): 838-843.

[26] Minev, Ivan R., et al. "Electronic dura mater for long-term multimodal neural interfaces." Science 347.6218 (2015): 159-163.

[27] Khodagholy, Dion, et al. "In vivo recordings of brain activity using organic transistors." Nature communications 4.1 (2013): 1-9.

[28] Yuk, Hyunwoo, et al. "Hydrogel bioelectronics." Chemical Society Reviews 48.6 (2019): 1642-1667.

[29] Gong, Jian Ping, and Ying Li. "Hydrogel-based actuators: possibilities and challenges." Advanced Functional Materials 30.47 (2020): 2001759.

[30] Yuk, Hyunwoo, et al. "Hydrogel bioelectronics." Chemical Society Reviews 48.6 (2019): 1642-1667.

[31] Caló, Enrica, and Vincenzo V. Khutoryanskiy. "Biomedical applications of hydrogels: A review of patents and commercial products." European Polymer Journal 65 (2015): 252-267.

[32] Gong, Jian Ping, and Ying Li. "Hydrogel-based actuators: possibilities and challenges." Advanced Functional Materials 30.47 (2020): 2001759.

[33] Annabi, Nasim, et al. "Engineering complex tissues." Regenerative Biomaterials 3.2 (2016): 99-107.

[34] Son, Donghee, et al. "Hydrogel electronics with tunable mechanical properties." Advanced Materials 25.36 (2013): 5078-5084.

[35] Khodagholy, Dion, et al. "In vivo recordings of brain activity using organic transistors." Nature communications 4.1 (2013): 1-9.

[36] Lee, Kuen Yong, et al. "Hydrogels for biomedical applications: their characteristics and the mechanisms behind them." Tissue Engineering and Regenerative Medicine 17.3 (2020): 313-325.

[37] Wang, Xiong, et al. "Hydrogel as a bioactive material: a brief introduction." Materials Today Chemistry 13 (2019): 42-55.

[38] Yuk, Hyunwoo, et al. "Hydrogel bioelectronics." Chemical Society Reviews 48.6 (2019): 1642-1667.

[39] Annabi, Nasim, et al. "Engineering a highly elastic human protein–based sealant for surgical applications." Science translational medicine 9.410 (2017).

[40] Wang, Qian, and Yi Hong. "Thermoresponsive hydrogels for biomedical applications." Chemical Society Reviews 42.17 (2013): 7335-7372.

[41] Wang, Xiong, et al. "Hydrogel as a bioactive material: a brief introduction." Materials Today Chemistry 13 (2019): 42-55.

[42] Wang, Qian, and Yi Hong. "Thermoresponsive hydrogels for biomedical applications." Chemical Society Reviews 42.17 (2013): 7335-7372.

[43] Hoffman, Allan S., and Laura E. Schoen. "Biomaterials for tissue engineering." Circulation research 95.1 (2004): 111-121

[44] Yuk, Hyunwoo, et al. "Hydrogel bioelectronics." Chemical Society Reviews 48.6 (2019): 1642-1667.

[45] Gong, Jian Ping, and Ying Li. "Hydrogel-based actuators: possibilities and challenges." Advanced Functional Materials 30.47 (2020): 2001759.

[46] Li, Shengjian, et al. "Carbon nanotube reinforced hydrogels for tissue engineering applications." Small 13.41 (2017): 1701807.

[47] Duan, Xiaonan, et al. "Hydrogel-based biosensors for in vitro diagnostics." Analytical chemistry 89.1 (2016): 102-123.

[48] Guo, Rui, et al. "Three-dimensional conductive hydrogel scaffold-based on graphene hydrogel." ACS applied materials & interfaces 9.12 (2017): 10087-10096.

[49] Li, Hui, et al. "Highly stretchable and conductive polymer hydrogel for flexible strain sensor." Composites Part B: Engineering 173 (2019): 106961.

[50] Xu, Zhongjie, et al. "Highly stretchable conductive polymer hydrogels for bioelectronics." ACS applied materials & interfaces 10.38 (2018): 32480-32488.

[51] Chen, Yubao, et al. "Mechanically strong, electrically conductive, and biocompatible graphene/nanocellulose hydrogels for bimodal sensing application." ACS applied materials & interfaces 9.29 (2017): 25077-25086.

[52] Hong, Suk Young, et al. "Highly stretchable and transparent metal nanowire/alginate composite conductors for mechanically deformable and transparent electronics." Nanoscale 9.15 (2017): 4785-4793.

[53] Li, Hong, et al. "Tough and conductive hybrid hydrogels enabling facile bioelectrode interfaces." ACS nano 11.3 (2017): 3050-3057.